OBSERVATIONS OF PHYSICAL PROPERTIES AND CURRENTS IN THE NORTHERN GULF OF MEXICO DURING SUMMER, 2002-2004, AND CURRENTS FROM JANUARY TO JULY 2006

A Thesis

by

MICHAEL ALAN LALIME

Submitted to the Office of Graduate Studies of
Texas A&M University
in partial fulfillment of the requirements for the degree of

MASTER OF SCIENCE

May 2010

Major Subject: Oceanography

OBSERVATIONS OF PHYSICAL PROPERTIES AND CURRENTS IN THE NORTHERN GULF OF MEXICO DURING SUMMER, 2002-2004, AND CURRENTS FROM JANUARY TO JULY 2006

A Thesis

by

MICHAEL ALAN LALIME

Submitted to the Office of Graduate Studies of
Texas A&M University
in partial fulfillment of the requirements for the degree of

MASTER OF SCIENCE

Approved by:

Co-Chairs of Committee,	Steven F. DiMarco
	Ann E. Jochens
Committee Members,	John W. Nielsen-Gammon
Head of Department,	Piers Chapman

May 2010

Major Subject: Oceanography

ABSTRACT

Observations of Physical Properties and Currents in the Northern Gulf of Mexico during Summer, 2002-2004, and Currents from January to July 2006. (May 2010)

Michael Alan Lalime, B.S., Hawaii Pacific University

Chair of Advisory Committee: Dr. Steven F. DiMarco

Many processes in the ocean are interrelated. The direction with which an eddy rotates will determine if nutrients are moved closer to the surface where they can be utilized by plankton to increase the base of the food chain, or it can restrict growth by causing the surface layer of nutrient poor water to deepen below the photic layer. The direction of current flow will also affect the temperature structure, which is a contributing factor in the density of water. A change in density can act as a barrier between the surface and deeper waters, effectively isolating the surface from deep waters. It is important to understand the physical properties in a study area in order to understand the dynamics controlling the distributions of nutrients, which influence the distribution of plankton, which influences the distribution of predator species like squid and whales. The Sperm Whale Seismic Study (SWSS) tracked the locations of sperm whales in the Gulf of Mexico. This study seeks to describe the physical environment in which they live.

To that end, various physical properties observed during the SWSS cruises were processed and used in conjunction with sea surface height (SSH) fields from satellite altimetry data. The data from different years and from the same years are used to provide descriptions of the physical environment present during the SWSS cruises and how that environment changed between cruises. A time-series of currents, collected over a six month time period in 2006, is included to document how the currents are influenced by different processes found along the continental slope in the northern Gulf of Mexico.

The findings indicate the observed currents are related to local SSH features. Temperature structure can be influenced throughout the upper 1000 m by these SSH features. The temperature structure is stable over time but depends on local SSH features. Properties nearer to the surface are more variable than at depth. Although the overlying wind field most likely influences the currents at 51 m no correlation between winds observed at the *Brutus* platform and currents observed at 51 m at the *Ocean Star* platform was found.

DEDICATION

To my beautiful wife and perseverance.

ACKNOWLEDGEMENTS

I would like to thank my committee co-chairs, Dr. DiMarco and Dr. Jochens, and my committee member, Dr. Nielson-Gammon, for their guidance and support throughout the course of this research.

Thanks also go to my friends and colleagues and the department faculty and staff for making my time at Texas A&M University an interesting experience.

Finally, thanks to my mother and father for their encouragement and most of all to my wife for her extreme and infinite patience and love.

TABLE OF CONTENTS

Page

ABSTRACT iii

DEDICATION v

ACKNOWLEDGEMENTS vi

TABLE OF CONTENTS vii

LIST OF FIGURES viii

LIST OF TABLES xiii

1. INTRODUCTION 1

    1.1 Physical Oceanography of the Gulf of Mexico 1
    1.2 Inflow and Outflow of the Gulf of Mexico 3
    1.3 General Circulation of the Gulf of Mexico 5
    1.4 Water Masses in the Gulf of Mexico 7
    1.5 Observational Area 8
    1.6 Overview of the SWSS Program 9
    1.7 Objectives 11

2. DATA AND METHODS 12

    2.1 SWSS Program Synopsis 12
    2.2 Description of the SWSS Data Sets 13
    2.3 Platform-Mounted Data 24

3. RESULTS 28

    3.1 SWSS Cruises 28
    3.2 Platform-Mounted Data 92

4. SUMMARY AND CONCLUSIONS 122

REFERENCES 129

VITA 135

LIST OF FIGURES

FIGURE		Page
1.1	Gulf of Mexico bathymetry and selected geographical locations	3
2.1	*Ocean Star* (left) and *Brutus* (right) platforms	24
3.1	Weekly intervals of SSH during the SWSS S-tag cruise in 2002	30
3.2	Velocity vectors during 2002 for the near surface 150-kHz (11m) depth bin	31
3.3	Vertical sections from the ADCP data for the initial transit south from Galveston to 27ºN where the *R/V Gyre* turned eastward	33
3.4	Location of transect for vertical section shown in Figure 3.5 showing the near surface velocity vectors in cm/s	34
3.5	Vertical sections from the ADCP data for the segment shown in Figure 3.4	35
3.6	Location of transect for vertical section shown in Figure 3.7 showing the near surface velocity vectors in cm/s	36
3.7	Vertical sections from the 150-kHz ADCP data for the segment shown in Figure 3.6	37
3.8	Locations of XBT and CTD stations for cruise 02G08	38
3.9	Vertical section of temperatures created from selected XBT stations shown in Figure 3.8	39
3.10	Vertical profiles of all XBT stations deployed during cruise 02G08	40
3.11	Vertical profile showing XBT EOF vertical mode amplitudes during summer 2002 cruise 02G08	42
3.12	Modal amplitudes for XBT EOF calculation for 2002 cruise 02G08	43
3.13	Weekly intervals of SSH during the SWSS habitat Survey cruise in 2003	45

FIGURE Page

3.14 Velocity vectors during first cruise of 2003 for the near surface 38-kHz (41 m) depth bin 46

3.15 Location of transect for 38-kHz vertical section shown in Figure 3.16 showing velocity vectors in cm/s at 41 m 47

3.16 Vertical sections from the 38-kHz ADCP data for the segment shown in Figure 3.15 48

3.17 Location of transect for 38-kHz vertical section shown in Figure 3.18 showing velocity vectors in cm/s at 41 m 49

3.18 Vertical sections from the 38-kHz ADCP data for the segment shown in Figure 3.17 50

3.19 Locations of XBT and CTD stations for cruise 03G06..... 51

3.20 Temperature – Salinity plots for each of the four cruises during the SWSS program..... 53

3.21 Vertical section of temperatures created from selected XBT stations shown in Figure 3.19..... 54

3.22 Comparison of temperatures using selected XBT stations between 89ºW and 91ºW on outbound and return legs of the cruise 56

3.23 Cruise 03G06 vertical profiles of all XBT stations..... 57

3.24 Vertical profile showing XBT EOF vertical mode amplitudes during 2003 cruise 03G06 58

3.25 Modal amplitudes for XBT EOF calculation for 2003 cruise 03G06 59

3.26 Weekly intervals of SSH during the SWSS S-tag cruise in 2003 61

3.27 Velocity vectors during the second cruise of 2003 for the near surface (41 m) depth bin 62

3.28 Vertical sections from the 38-kHz ADCP data for the segment straddling 94ºW in Figure 3.27 63

FIGURE Page

3.29 Velocity vectors after transiting across the shelf..... 64

3.30 Vertical sections from the 38-kHz ADCP for the cruise track shown in Figure 3.29 65

3.31 Locations of XBT and CTD stations during cruise 03G07..... 67

3.32 Geostrophic velocity profile for two stations during cruise 03G07..... 68

3.33 Vertical section of temperatures created from selected XBT stations shown in Figure 3.31..... 69

3.34 Cruise 03G07 vertical profiles of all XBT stations..... 70

3.35 Vertical profile showing XBT EOF vertical mode amplitudes during 2003 cruise 03G07 71

3.36 Modal amplitudes for XBT EOF calculation for 2003 cruise 03G07..... 72

3.37 Weekly intervals of SSH during the SWSS S-tag cruise in 2004..... 74

3.38 Velocity vectors during 2004 for the near surface 150-kHz (11m) depth bin..... 75

3.39 Velocity vectors during 2004 for the near surface 38-kHz (41m) depth bin..... 76

3.40 Location of transect for 150-kHz vertical section shown in Figure 3.41 showing velocity vectors m in cm/s at 10 m..... 77

3.41 Vertical sections from the 150-kHz ADCP data for the segment shown in Figure 3.40 78

3.42 Location of transect for 38-kHz vertical section shown in Figure 3.43 showing vector velocity vectors in cm/s at 41 m..... 79

3.43 Vertical sections from the 38-kHz ADCP data for the segment shown in Figure 3.42 80

3.44 Location of transect for 150-kHz vertical section shown in Figure 3.45 showing velocity vectors in cm/s at 10 m..... 81

FIGURE Page

3.45 Vertical sections from the 150-kHz ADCP data for the segment shown in Figure 3.43 82

3.46 Location of transect for 150-kHz vertical section shown in Figure 3.47 showing velocity vectors in cm/s at 10 m 83

3.47 Vertical sections from the 150-kHz ADCP data for the segment shown in Figure 3.46 84

3.48 Location of transect for 38-kHz vertical section shown in Figure 3.49 showing velocity vectors in cm/s at 41 m 85

3.49 Vertical sections from the 38-kHz ADCP data for the segment shown in Figure 3.48 86

3.50 Locations of XBT and CTD stations during cruise 04G05 88

3.51 Vertical section of temperatures created from selected XBT stations shown in Figure 3.50 89

3.52 Cruise 04G05 vertical profiles of all XBT stations 90

3.53 Vertical profile showing XBT EOF vertical mode amplitudes during 2004 cruise 04G05 91

3.54 Modal amplitudes for XBT EOF calculation for 2004 cruise 04G05 92

3.55 Record length velocity vectors of wind and the near-surface (51 m) 38-kHz ADCP depth bin 93

3.56 Results of the coherency analysis between the wind and near-surface 38-kHz ADCP velocity vectors 94

3.57 Record length statistics of 38-kHz ADCP velocity components and speed 95

3.58 Gap-filled record length 38-kHz ADCP time-series showing the velocity components at six depths between 51 m and 803 m 96

3.59 Gap-filled record length 38-kHz ADCP time-series showing the speed at six depths between 51 m and 803 m 97

FIGURE Page

3.60 SSH field for late January, 2006 99

3.61 SSH field for mid February, 2006 100

3.62 Hovmöller plot of speed (in cm/s) for the *Ocean Star* platform 102

3.63 SSH field for mid March, 2006 104

3.64 SSH field for early April, 2006 105

3.65 SSH field for early May, 2006 106

3.66 SSH field for early June, 2006 108

3.67 SSH field for the third week of June, 2006 111

3.68 SSH field for the third week of July, 2006 112

3.69 Power spectral densities for each velocity component computed at each of the depths used in the horizontal velocity time-series presented in log-log format 115

3.70 Vertical profiles of the u-component EOF vertical mode amplitudes 117

3.71 Time-series showing the u-component modal amplitudes 118

3.72 Vertical profiles of the v-component EOF vertical mode amplitudes 119

3.73 Time-series showing the v-component modal amplitudes 120

4.1 Mean temperatures for all XBT stations and depths for each cruise 124

LIST OF TABLES

TABLE		Page
2.1	SWSS cruise summary	15
2.2	SWSS instrument deployment	16
2.3	ADCP alignment (Joyce) parameters	17
3.1	U-component tidal constituent amplitudes (cm/s) for the eight constituents removed from each time-series depth shown in Figure 3.58 .	113

1. INTRODUCTION

The northern Gulf of Mexico is bordered by five states, which share in the abundant natural and economic resources provided by the Gulf. From the shrimp fishery and sport fishing, to the production of oil and gas, the shelf and slope of the northern Gulf are rich. The twenty-nine marine mammal species living in the Gulf could be impacted by human activities. The continental margin of the Texas-Louisiana slope is one of the most complex margins in the world and is now crisscrossed by a network of oil and gas pipelines, which run for thousands of miles across the northern Gulf.

A short description of the Gulf of Mexico covering general aspects of circulation, regional water masses, and the Loop Current are presented in this section. A succinct depiction of the Sperm Whale Seismic Study program goals is provided because the majority of data used in this project were collected during that program. Thesis objectives are described at the end of this section.

1.1 Physical Oceanography of the Gulf of Mexico

1.1.1 Description of Gulf of Mexico

The Gulf of Mexico is a semi-enclosed basin attached to the North Atlantic Ocean. This subtropical sea is bordered by the United States, Mexico, and Cuba. The

---

This thesis follows the style and format of the *Journal of Physical Oceanography*.

Gulf is directly connected to the North Atlantic Ocean through the Florida Straits, and indirectly connected to it through the Caribbean Sea, with which it forms the American Mediterranean Sea (Figure 1.1).

At 24°N, the Gulf of Mexico is about 1700 km long, extending from 80.5°W to 97.5°W. The maximum meridional extent is found in the western Gulf along 94.5°W, and is 1200 km wide, extending from about 18.25°N to 29.25°N. In the eastern Gulf between 22°N and 30°N, at 86°W, the maximum meridional distance is close to 900 km.

The Mississippi and Atchafalaya Rivers contribute most of the river-supplied freshwater to the Gulf of Mexico. The discharge from these two rivers is about equal to the discharge of freshwater from all the other rivers emptying into the Gulf combined (Dinnel and Wiseman 1986; Etter et al. 2004).

It is important to understand the physical properties that describe the oceanographic environment, because the distributions of these properties determine the biological habitat in the northern Gulf of Mexico. The physical environment is determined by a host of properties, such as the direction of flow, which can cause upwelling of nutrient-rich water closer to the surface where it will stimulate biological production, or which can cause downwelling of nutrient poor water, effectively limiting biological production (Jochens and DiMarco 2008).

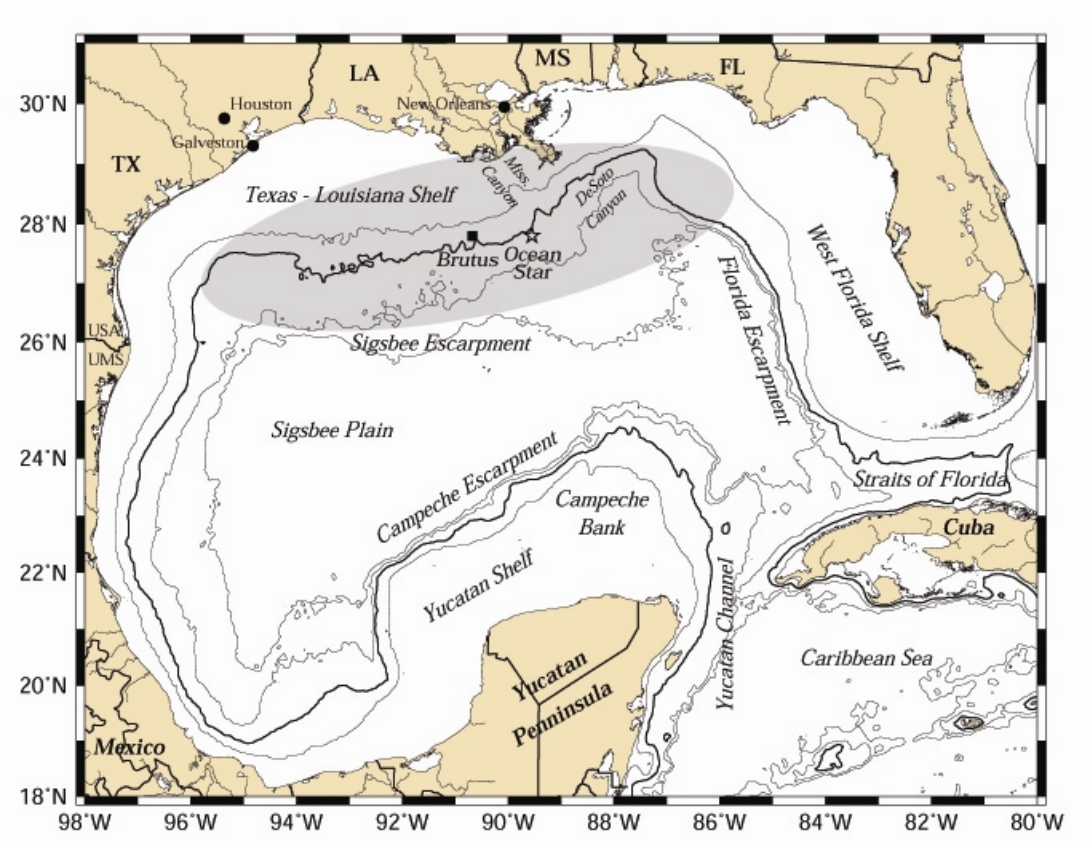

Figure 1.1 Gulf of Mexico bathymetry and selected geographical locations. The gray oval along the Texas-Louisiana slope represents the approximate observational area for the Sperm Whale Seismic Study and was the region of interest described in this thesis. The study area was centered about the 1000 m isobath. Shown are the 200 m, 1000 m (bold), 2000 m, and 3000 m depth contours.

1.2 Inflow and Outflow of the Gulf of Mexico

Water exchange occurs with the Caribbean Sea through the Yucatan Channel, between Mexico and Cuba, and with the North Atlantic Ocean through the Straits of Florida, between Florida and Cuba (Figure 1.1). According to previous work, the

Yucatan Channel has a maximum depth of 2040 m and the Straits of Florida 730 m near Miami Florida (Sheinbaum et al. 2002; Bunge et al. 2002).

Due to the difference in the depths of the two channels, deep flows can only occur through the Yucatan Channel (Sheinbaum et al. 2002). Southward flowing countercurrents transport water out of the deep Gulf of Mexico at an average rate of 1.8 cm/s (Sheinbaum et al. 2002; Maul et al. 1985).

These southward flowing countercurrents were speculated to be related to Loop Current volume transport (Maul 1977). This was not confirmed by the data collected from a single mooring that was placed in the Yucatan Channel for a period of three years (Maul et al. 1985). In that study, the authors suggest a minimum of three moorings arrayed across the Yucatan Channel would be needed to properly understand the dynamics of the deeper flows within the channel (Maul et al. 1985). An expanded study, using 8 moorings spanning the Yucatan Channel, was conducted. That study was performed from September 1999 through June 2000, when the instruments were recovered and then redeployed for another eleven months. Using the expanded observations, Bunge et al. (2002), discovered a link between Loop Current volume transport and the deep southward flowing countercurrents, below 500m within the Yucatan Channel.

1.3 General Circulation of the Gulf of Mexico

Low-frequency (days to weeks) wind forcing, such as local wind stress curl, has been proposed as a mechanism for driving the dynamics of the upper ocean of the Gulf of Mexico (Molinari 1978; Sturges 1993). High-frequency energetic atmospheric events such as storms can also affect the velocity structure in the surface ocean (Shay et al. 1998). The mean circulation of the western Gulf of Mexico has been accepted to be that of an anticyclonic gyre (Molinari et al. 1978; Sturges 1993). This anticyclonic gyre is primarily driven by the curl of local wind stress with occasional enhancement by westward moving Loop Current Eddies (LCEs) (Molinari 1978; Sturges 1993). Seasonal changes occur on the Texas-Louisiana shelf with down-coast flow (cyclonic) from September to June and up-coast flow (anticyclonic) from June to August (Cochrane and Kelly 1986; Nowlin et al. 2005). The circulation on the Florida Shelf does not have seasonal variability (Ohlman and Niiler 2005).

The Mississippi River can strongly influence the stratification of the upper ocean. These waters are also rich in nutrients that, if advected offshore, might serve to increase the food supply of large predators, such as sperm whales (Jochens et al. 2006). Water from the Mississippi River and over the shelf has been shown to be transported offshore and water from offshore transported onto the shelf by the actions of eddies or eddy pairs (Hamilton et al. 2002; Ohlmann et al. 2001).

The eastern half of the Gulf of Mexico is mainly dominated by the Loop Current, which is the Gulf of Mexico section of the current system connecting the Yucatan

Current to the Gulf Stream (Leipper 1970). The Loop Current causes the formation of smaller cyclonic eddies and sheds large anticyclonic rings (LCEs), which have diameters of 200 km – 400 km, and water properties similar to those of the Loop Current. The frequency with which these LCEs are shed from the Loop Current has been documented to be every six to seventeen months (Sturges and Leben 2000).

The Yucatan Current is renamed the Loop Current when it crosses into the Gulf of Mexico. Leipper (1970) reported the Loop Current has a lateral extent of 90 km – 150 km and maintains a speed between 50 cm/s – 200 cm/s, while Elliot (1982) demonstrated that Loop Current influence can extend to 1200 m depth, or more, as illustrated by the depression of the 5ºC isotherm. Estimates of transport volumes for the Loop Current system have ranged from 24 Sv (Sheinbaum et al. 2002) to 30 Sv (Morrison and Nowlin 1977). One Sverdrup (Sv) is defined as 10^6 m^3/s.

The Loop Current can strongly influence currents on the shelf in the northern Gulf of Mexico when it has penetrated close to the shelf edge (Wiseman and Dinnel 1988). Due to the many eddies often present within the Gulf of Mexico, the mesoscale circulation has been shown to change dramatically over short times (Elliott 1982).

The formation of cyclonic eddies associated with the Loop Current has been well documented and shown to contribute to the separation of Loop Current eddies (Zavala-Hidalgo et al. 2003; Vukovich 1986; Vukovich and Maul 1985). These eddies typically have diameters of 100-150 km, velocities up to 50 cm s^{-1}, and rotational periods of about two weeks (Hamilton 1992). These cyclones can persist up to 15 months and are strong enough to influence thermal structure to 800 m, but only have a surface temperature

differential with surrounding waters of a couple degrees Celsius (Hamilton 1992; Zavala-Hidalgo et al. 2003).

Past work has shown the water properties below 1500 m or the 17ºC isotherm are highly homogeneous (Nowlin et al. 1969). There is evidence showing the circulation displays bottom intensification, with characteristics of topographic Rossby waves that are generated by fluctuations associated with the Loop Current and which can propagate to within 300m of the surface (Hamilton 1990; Hamilton 2007). However, there are insufficient quantities of data to fully describe the circulation within the deep Gulf of Mexico at this time (Nowlin et al. 2001), although new observations since 2002 are beginning to shed light on the deep circulation (Donohue et al. 2006; Cox et al. 2010).

1.4 Water Masses in the Gulf of Mexico

Water mass analysis performed across the Loop Current, in the Caribbean Sea, and in the western Gulf of Mexico indicates that Loop Current waters are similar to Caribbean Sea waters and different from waters in the western Gulf of Mexico, or from waters outside the boundaries of the Loop Current (Morrison and Nowlin 1977; Morrison et al. 1983).

Water in the Gulf of Mexico comes from either the Caribbean Sea via the Yucatan Channel, the Atlantic Ocean through the Straits of Florida, or inflow into the Caribbean Sea and then into the Gulf of Mexico, or from rainfall, rivers and streams for freshwater (Sheinbaum et al. 2002; Morrison and Nowlin 1977).

The Gulf of Mexico can be separated into two layers, a deep layer and a surface layer. The deep water layer can be defined as that below 1500 m (Nowlin et al. 1969) due to the homogeneity of the water properties; the surface layer is above 1500 m. The surface water layer can be influenced by winds or other atmospheric interactions, such as hurricanes (Shay et al. 1998). Changes in salinity caused by evaporation or precipitation, or changes in temperature caused by heating and cooling, also affect the surface waters (Etter 1983; Dinnel and Wiseman 1986; and Etter et al. 2004).

There are two main types of water found within the Gulf of Mexico, Gulf-type and Caribbean-type, which is sometimes called Loop Water. The water masses located in the study area are primarily Gulf-type waters occasionally influenced by the Loop Current or Loop Current Eddies (Morrison and Nowlin 1977). Because the study area is located along the 1000 m isobath, the important water masses expected to be found in this region will not include water masses discussed by Nowlin et al. (1969) at depths greater than 1000 m.

1.5 Observational Area

The study area for the Sperm Whale Seismic Study (SWSS) program was mainly located between the 800 m and 1200 m isobaths primarily between the Mississippi and DeSoto Canyons (Jochens et al. 2006). However, most of the SWSS survey cruises began in Galveston, TX, and commenced operations in the western Gulf, then transited northeastward along the 1000 m isobath. The gray oval in Figure 1.1 shows the

approximate limits of the observational region. Time-series data were collected by a 38-kHz Acoustic Doppler Current Profiler (ADCP) located on the mobile offshore drilling rig, *Ocean Star*, and wind data were collected on *Brutus*; a fixed offshore production platform. The locations of these two platforms are shown in Figure 1.1.

The close proximity of the SWSS program study area and the location of the *Ocean Star*, to the largest freshwater river discharging into the Gulf of Mexico, suggest the study area will occasionally be impacted by river outflow (Dinnel and Wiseman 1986; Etter et al. 2004; Jochens et al. 2006). Offshore transport of low-salinity river discharge waters or onshore transport of high salinity Gulf waters is strongly influenced by the presence and location of eddies (Molinari and Mayer 1982; Wiseman and Dinnel 1988; Ohlmann et al. 2001; Hamilton et al. 2002; Ohlmann and Niiler 2005). Offshore transport of low-salinity water near DeSoto Canyon occurs primarily during the summer months along the eastern edge of the Loop Current and can extend to the Florida Keys (Morey et al. 2003).

1.6 Overview of the SWSS Program

The SWSS program was a multi-year program funded by the U.S. Minerals Management Service (MMS) from 2002 through 2007. It examined the sperm whale population of the northern Gulf of Mexico. The SWSS program had three objectives: 1) to determine the baseline or normal behavior of sperm whales in the northern Gulf of Mexico; 2) to characterize their habitat; and 3) to identify plausible behavioral changes

caused by man-made noise with specific detection of behavioral changes brought about by the use of seismic air-gun arrays (Jochens et al. 2006).

The SWSS program field work was conducted from May 2002 through fall 2006 and consisted of six components. These included two types of tagging studies. One cruise applied short-term (hours) digital acoustic recording tags (D-tags), attached using suction cups, to the whales; these monitored diving behavior and vocalizations, and examined whale response to air-gun sounds. The other used satellite-tracked radio tags (S-tags) that were used for long duration (seasonal) studies of sperm whale distribution.

These tags, along with data collected from several conductivity-temperature-depth (CTD) stations and expendable bathythermograph (XBT) probes, 153 kHz and 38-kHz ADCP profiles, and flow-through fluorometer analysis of chlorophyll from near-surface waters, provided information for the habitat characterization facet of the SWSS program. The locations of whales were compared to sea surface height fields derived from satellite altimetry, ocean color from the Sea-viewing Wide Field-of-view Sensor (SeaWiFS), and sea surface temperature fields collected from Advanced Very High Resolution Radiometer (AVHRR) satellites as part of the habitat characterization. Sperm whale locations underwater were determined by 3-D passive acoustics, which also provided some tracking capabilities. Finally, identification of individual whales and relatedness of groups of whales was accomplished through the photo identification and genetic analysis elements of the SWSS program. These elements allow the quantification of the observed sperm whale population within the Gulf of Mexico (Jochens et al. 2006).

1.7. Objectives

It was the goal of this thesis to describe the physical environment encountered during the SWSS program. This will be accomplished by examining and describing the physical oceanographic data, collected along the northern continental slope, on five SWSS cruises, which were spread over three summers (2002-2004), and one moored dataset that was collected from a platform-mounted 38-kHz ADCP from January through July 2006. After the data were processed the next step was to analyze and interpret these data, together with ancillary data sets collected concurrently by other organizations. The ancillary data include historical sea surface height data from the Colorado Center for Astrodynamics Research (CCAR) and wind data collected from the National Data Buoy Center (NDBC) buoys or platforms. This analysis includes comparisons between the summers 2002-2004, comparisons between two cruises in the same year, during the summer of 2003, and comparisons among various depth levels within each dataset. The platform-mounted data was investigated for the spectral character of currents and for coherency analysis with wind data. The major physical oceanographic features and associated processes present on the continental slope during the SWSS cruises will be characterized. The currents in the upper water column will be described.

2. DATA AND METHODS

This section describes the shipboard and time-series data and data collection procedures and processing methods used in this thesis. Data sets include ADCP, XBT, and CTD data from the SWSS program, ADCP data from the *Ocean Star*, wind data from the *Brutus* platform, and sea surface height altimetry data.

Graphical representation software used to produce many of the figures for this analysis includes MATLAB versions 7.1.0.124 (R14) and 7.7.0.471 (R2008b) and the Generic Mapping Tools (GMT) version 3.4.6 (Wessel and Smith 1998).

2.1 SWSS Program Synopsis

To achieve its objectives, the SWSS program utilized a research vessel to provide observations of the physical environment while other vessels were used for behavioral studies and seismic observations. They used satellite-tracked tags that remained attached for several months to monitor the location of the tagged whales. Short-term digital tags that remained attached for several hours were used to analyze the diving behavior and record sperm whale vocalizations. Genetic analysis was performed on skin samples to establish how related different groups of sperm whales were to each other. The habitat characterization component used information from numerous ship-based instruments. Ship-based instruments included ADCP, CTD sensors, and XBT probes. These were combined with other data, such as, wind data and satellite derived sea surface height and temperature fields, to provide a description of the physical

environment in which the sperm whales were found. Passive acoustic studies were also used to observe sperm whale location and behaviors. Finally, direct surface observations by large binoculars and photographs were used to identify individual whales under study.

2.2 Description of the SWSS Data Sets

The SWSS cruise type, start and end dates, and duration are listed in Table 2.1. Because of limitations encountered with the quantity of physical oceanographic data collected, a subset of cruises was selected for further study (bold). Each cruise lasted about 3 weeks. Cruises used for this study are S-tag cruises and habitat survey cruise. The D-tag cruises were not used for this study. Of the cruises considered here, one cruise took place during 2002, two during 2003, and one during 2004.

2.2.1 Shipboard Current Velocity Data

Two frequencies of ADCP were used during the SWSS program: 150-kHz narrowband and 150-kHz broadband instruments. This depended on functional status and availability. In addition, a long-range 38-kHz broadband ADCP was installed. The different frequencies allowed for different depth ranges to be observed. The upper 200 – 300 m was observed with 4 m vertical resolution using the 150-kHz ADCP; the 38-kHz ADCP profiled the upper 800 – 1000 m with 16 m resolution.

Due to the instrument depth below the ship's hull and the blank after transmission of an acoustic pulse (called a ping), the center of the near-surface bin of data was about 10 – 12 m below surface for the 150-kHz and about 35 m for the 38-kHz instrument. The operational depths observed depend on a few factors including but not limited to sea state and the backscattering properties of the water column.

The sea state causes the ship to heave and roll as waves pass under the hull. The ADCP uses depth cell mapping during the velocity calculations to make sure the horizontal velocity observations from each beam are taken at the same depth (Gordon 1996). This means that if the ADCP is tilted, the bin number used for a horizontal velocity observation can be different for each acoustic beam in a beam pair. That is, one acoustic beam is oriented more vertical than the opposite beam which would be angled out to the side. So the more vertical beam might take 55 bins to reach a certain depth, while the outwardly slanted beam might need 60 bins to reach the same water depth. Therefore, as the ship rolls the maximum bin number for a beam pair that can be observed is reduced as one beam might reach its maximum bin before the other beam. This is possible because the ADCP has an internally recording tilt sensor, which automatically compensates for pitch and roll.

The backscattering properties of the water depend on water clarity. If the number of particulates in the water is too low, the signal strength of the returning acoustic echoes will be too weak to accurately estimate velocity. If there are too many particles in the water, the depth of observations will be attenuated and the range reduced.

The returning echoes from all the particulates in the water are collectively referred to as the echo.

Table 2.1. SWSS cruise summary

Cruise	Ship Name	Starting Date	Ending Date	Year	Type
02G08	***R/V Gyre***	**19 June**	**9 July**	**2002**	**S-tag**
02G11	*R/V Gyre*	19 August	15 Sept.	2002	D-tag
03G06	***R/V Gyre***	**31 May**	**21 June**	**2003**	**Habitat Survey**
EW0303	R/V Maurice Ewing	3 June	24 June	2003	D-tag
03G07	***R/V Gyre***	**26 June**	**14 July**	**2003**	**S-tag**
04G05	***R/V Gyre***	**25 May**	**18 June**	**2004**	**S-tag**
Sailboat	Summer Breeze	20 June	15 August	2004	Photo-ID

2.2.2 Observational Data

Table 2.2 shows the various types and amounts of data collected for each of the SWSS cruises. The numbers in the CTD and XBT columns refers to the number of CTD casts performed or XBT probes deployed during the cruise. The “T” and “S,” in the flow-through column, indicate temperature and salinity data were collected during the cruise. The flow-through system observed near-surface (3.5 m) temperature and salinity and collected data using a thermosalinograph while chlorophyll data was obtained with a flow-through fluorometer.

Deployment of the CTD and of XBT probes occurred on all cruises by the *R/V Gyre*. The habitat survey cruise (03G06), which was the first cruise of 2003, carried out the largest number of XBT (89) and CTD (8) casts.

Table 2.2. SWSS instrument deployment

Cruise	150-kHz	38-kHz	CTD	XBT	Flow-Through
02G08	Y	--	5	35	T,S
03G06	Y	Y	8	89	T,S
03G07	Y	Y	5	51	T,S
04G05	Y	Y	5	70	T,S

2.2.3 ADCP Data

All cruises conducted on the *R/V Gyre* used one of the 150-kHz ADCP instruments. The two cruises conducted during 2003 and the 2004 cruise also utilized the 38-kHz ADCP. A "Y" in Table 2.2 indicates the ADCP instrument was present on the cruise.

ADCP configuration information was provided in Table 4.5.1 on page number 78 of the SWSS Annual Report: Year 1 (Jochens and Biggs 2003). The 150-kHz current meter was configured to collect a maximum of 75 bins of data, while the 38-kHz current meter was configured to collect a maximum of 80 bins of data. Bin sizes were 4 m for the 150-kHz ADCP and 16 m for the 38-kHz. Time delays between pings were 1-second for the 150-kHz and 3-seconds for the 38-kHz. The corresponding transmit and blank after transmit lengths were also 4 m and 16 m.

Table 2.3 lists the calculated ADCP alignment parameters for the project cruises (Joyce 1989). Because the instruments were removed at the conclusion of each cruise and remounted prior to each subsequent cruise, these parameters are different for each cruise. The Joyce parameters are used to adjust the data. Correction for the alignment difference between the instrument frame of reference and that of the ship involves rotating the data clockwise by the alignment error angle. Correction for the sensitivity error occurs by scaling up the data by the calculated error.

Table 2.3. ADCP alignment (Joyce) parameters

Dataset	Cruise	ADCP Frequency (kHz)	Alignment Error (degrees)	Sensitivity Error	Variance Squared
STAG02_150	02G08	150	-0.6695	1.00514	0.99680
WSHC03_038	03G06	38	0.0241	1.00059	0.99999
STAG03_038	03G07	38	-0.0095	1.00130	0.99999
STAG04_038	04G05	38	0.0150	1.00080	0.99999
STAG04_150	04G05	150	-1.7555	1.00871	0.99493

The ADCP data collected during the SWSS program were collected in either broadband or narrowband format. The 38-kHz ADCP collected in the broadband format; however, this instrument did not collect reliable data during 2002. The problems with the 38-kHz ADCP during the 2002 season are described in the SWSS Annual Report: Year 1 (Jochens and Biggs 2003).

For each cruise either the 150-kHz narrowband ADCP or 150-kHz broadband ADCP was mounted in a through-hull transducer well. A description of the ADCP

mounting and calibration procedures is provided in Murphy et al. (1992). The 38-kHz phased-array ADCP was mounted in a sea chest that was attached 15 m aft of the transducer well in which the 150-kHz was mounted (John Walpert, GERG, personal communication).

The navigation data collected from an AshTech ADU2 3DF differential global positioning system (DGPS) antenna array was used to estimate ship velocity. If the water depth was less than about 1.5 times the 150-kHz ADCP water profiling range, then bottom-tracking could be used by the ADCP to estimate how fast the ADCP was moving over the bottom. This provides an estimate of ship velocity. Bottom-tracking uses longer duration acoustic pulses than the water profiling acoustic pulses. This enables the acoustic beam to ensonify the entire beam footprint at the same time, which allows the ADCP to calculate an accurate estimate of the ship velocity. In addition to the position information, the antenna array supplied the most accurate heading, pitch, and roll attitude information available, once per second. This information provided important corrections to the ADCP measurements.

A thorough description of the collection of ADCP and navigation data along with merging and quality assurance and control steps for these data are provided in the SWSS annual reports (Jochens and Biggs 2003; Jochens and Biggs 2004; and Jochens and Biggs 2006); only an abridgement is provided here. The processing of data from these ADCP instruments varied slightly because of the differences in the broadband and narrowband formats. The data from both 150-kHz and 38-kHz instruments were used to

produce five-minute average ensembles for each instrument, which were then post-processed for analysis.

The steps necessary to convert raw ADCP data into usable images begin by converting the data from raw binary format into ASCII format using the RDI programs NBPLBK (narrow-band play back), for the narrow-band data, and BBPLBK (broad-band play back), for the broad-band data formats. There are then three quality control steps which identify and remove erroneous data. Steps two and three in the quality control process involve using the output from the previous step as input.

The first quality control step checks the data for instances of bad bottom-tracking in deep water, where the water depth is too great to allow for bottom-tracking. If there are good data present this step corrects the bad bottom-tracking by setting the depth to 500 m. It also removes those data that were flagged as bad by the NBPLBK or BBPLBK programs, which are listed in the data as -32768. If the water depth was too shallow to allow for data to be collected to the maximum number of bins then the unused bins are flagged as bad since they contain no data. During this step if one data bin is identified as bad, or falls below the percent good threshold, then any bins deeper than it are also flagged as bad.

The 5-minute ensemble data were rejected for the following cases: if no navigation data were recorded during the 5-minute interval, if the bottom-tracking was shallower than the first bin depth, if the ship speed was less than 100 cm/s or greater than 650 cm/s, if the thirty percent-good threshold was not met for the first bin, or if

there were less than three beams of good data. Any data with less than a thirty percent-good beam echo-intensity were flagged as bad.

The data that passed the first step of quality assurance and quality control (QA/QC) were then merged with the navigational data, in step two, by matching the timestamp in the processed data with the timestamp in the navigational data. Since the timestamps of the navigational data rarely correspond exactly with a timestamp in the processed data, the closest available navigational time was used. In step three, the processed datasets were plotted using GMT for viewing to subjectively determine any other data to exclude as outliers or other obvious bad data points.

When data quality control was complete, vertical sections of velocity were created, and vector stick plots of the near surface bin were overlaid upon sea surface height (SSH) fields. The SSH fields were downloaded from the Colorado Center for Astrodynamics Research (http://argo.colorado.edu/~realtime/gsfc_gom-real-time_ssh).

2.2.4 Ancillary Data

The SSH product was created at CCAR from TOPEX/Poseidon, Jason, GEOSAT Follow-On, ERS-2 and ENVISAT satellite altimeter data. The SSH fields were downloaded for dates at the beginning, middle, and end of each cruise. These data have a spatial decorrelation scale of 100 km and a temporal decorrelation scale of 12 days (Leben et al. 2002).

2.2.5 Continuous Profiling Data

A Sea-Bird SBE-19 SeaCat Profiler CTD was used to collect data to 1000 m. The CTD was manufacturer-calibrated prior to the summer cruises each year. The temperature sensor was accurate to 0.01ºC with a resolution of 0.001ºC over the range 5ºC to 35ºC. The conductivity sensor was accurate to 0.001 S/m and had a 0.0001 S/m resolution from 0 to 7 S/m. The pressure sensor was calibrated across the 0 to 6000 m range.

There were three models of expendable bathythermograph (XBT) probes deployed during the SWSS cruises. Model T-7 sampled to 760 m and was the primary model deployed. Model T-10 sampled to 200 m, and the Deep Blue model, which also sampled to 760 m.

The probes were deployed using a hand-held launcher that was placed into a launch tube. This launch tube extended from inside the electronics lab through the floor where it extended over the port side hull of the *R/V Gyre*. From the end of the tube, the XBT probe dropped about 1.5 m into the water. The data from the probe was recorded on a computer, which had a Sippican Mark-12 data acquisition board installed. Vertical resolution for all three XBT models was 65 cm and temperature accuracy was 0.1ºC.

The CTD and XBT data were processed by SWSS personnel and stored in files according to the QA/QC procedures documented in the SWSS year-one annual report

(Jochens and Biggs 2003). These XBT and CTD data files were converted by the text processing programming language, AWK, into a format readable by MATLAB. Empirical orthogonal function (EOF) analysis was performed on the XBT files. Vertical profiles and temperature-salinity property plots of the CTD files were created.

Temperature-salinity property plots containing all the CTD profiles for each cruise were created for water mass analysis. Geostrophic velocity profiles were calculated for selected CTD station pairs for each cruise (Pond and Pickard 2000).

Empirical orthogonal function (EOF) analysis (Emery and Thompson 2001) was chosen to examine the variance contained within the XBT data because EOF analysis will take large amounts of data and distill the information into modes of variance, which are few in number, and easy to work with. The original data are also recoverable for each station of data by simple multiplication.

XBT stations that extended deeper than 700 m were used to construct vertical sections of temperature along the 1000 m isobath. Because most XBTs sampled beyond 700 m, XBT records less than 700 m were excluded from the EOF analysis. Because the EOF analysis requires all the datasets to be of equal length, all XBT records used in the EOF analysis were cropped to the shallowest common depth.

Prior to station selection, the metadata were analyzed to determine the number of any repeated XBT stations. A station was repeated if, during the descent of the probe, the communication wire prematurely broke resulting in incomplete sampling of the water column. Determination of a repeated station involved performing verification tests on the metadata, using date, time, and position information.

For the purposes of these tests, the spatial separation of the XBT stations was assumed to be at least 5 km, and at least 10 minutes was assumed to have elapsed between stations. The planned distance between the XBT stations was 10 nautical miles (M), about 18 km (Jochens and Biggs 2004). A separation between two consecutive stations of less than 5 km was assumed to indicate a repeat station. The descent time of the probe was calculated to be about 2 minutes. Therefore, any XBT stations that were sampled within 10 minutes of each other were flagged as possible repeat stations. This test identified 6 repeated stations during the 02G08 cruise and 1 repeated station during the 04G05 cruise.

The analysis of the 04G05 stations led to the development of a verification test to confirm that the listed date and times of each XBT station were during the cruise. It was found that 51 of the 68 stations during the 04G05 cruise had inaccurate year information, which was corrected manually.

Once the final data set to be analyzed was determined, the data were prepared for the EOF analysis. The depth of 700 m was chosen as the cutoff for the EOF analysis. Then, an initial vertical section plot was created and the data contoured. In the figures that include SSH fields, the selected XBT stations used in the vertical sections are represented by filled black circles and unused (repeated, suspect, or disregarded because of shallow depths) stations by red inverted triangles. CTD stations are shown as white squares.

2.3 Platform-Mounted Data

Moored instrumentation deployed from offshore oil and gas platforms were used to provide data for investigation during this study. The *Ocean Star* provided ADCP data and the *Brutus* platform provided hourly wind data (Figure 2.1). The locations of these stations are shown in Figure 1.1.

Figure 2.1 *Ocean Star* (left) and *Brutus* (right) platforms. The image of the *Ocean Star* was taken from Rigzone (2010) and the image of *Brutus* was taken from the National Data Buoy Center (NDBC 2010).

The *Ocean Star*, a mobile offshore drilling unit operated by Kerr-McGee Oil and Gas Corporation, was used to collect a time-series of current velocity profiles in the

upper 1000 m of the water column. The profiles were estimated using a 38-kHz ADCP deployed over the side of the rig by a hydraulic boom-skid.

To install the ADCP, the boom-skid was welded to the deck and the hydraulics lines and power hooked up and tested. Then the ADCP was hoisted by crane onto the boom-skid and connected to two ¼" stainless steel support cables connected to two hydraulic winches that were welded to the boom-skid. The ADCP was connected to a computer using a data cable that was attached to one of the support cables using large cable-ties. The cable-ties were spaced 18 – 24 inches apart.

Prior to shipping to the offshore platform, the ADCP was fastened within a stainless-steel shroud for protection and calibrated according to manufacturer guidelines. The transducer face was coated with a layer of Desitin™ diaper rash cream as a cheap but effective means to provide anti-fouling protection. Both the boom-skid and ADCP were shipped on a flatbed trailer to the shipping facilities in port Fourchon Louisiana, where they were loaded onto a rig boat and transported to the *Ocean Star*.

The deployment parameters for the ADCP set it to ping every 3 seconds. These pings were averaged into ensembles of 20 minute duration, each collecting 400 pings of data. There were 60, 16 m long, bins of data collected per ensemble with a 16 m blanking distance. The first collected bin was centered 33 m from the instrument, and the ADCP was deployed at a depth of 18 m, which was just below the hull, thus the first bin was centered 51 meters below the surface. The data were collected with Earth coordinates using the instrument tilts, bin mapping, and 3 beam solutions.

The ADCP on the *Ocean Star* collected data from 16:30 (local time) on 01/19/06 through 22:30 on 08/23/06. The dataset was truncated to midnight on 07/18/06 because the data collected after that time appears to become chaotic and erroneous. During this deployment the *Ocean Star* was positioned in Atwater Valley lease block 140 at 27.81ºN, 89.55ºW. The water depth at this location was 1140 m.

The data were automatically sent to the NDBC where they were subjected to the NDBC quality assurance and control checks. The NDBC first performed a time continuity test to make sure the time of each measurement was reasonable. If a measurement did not fail this test, then the range limit test was performed on each velocity measurement, rejecting any data more than 3 standard deviations from the climatological mean. Finally, a test was performed on the vertical velocity and any data for which the vertical velocity was found to be "too high to be physically reasonable" failed this test. The horizontal velocity measurements are then deleted (NDBC technical document 09-02).

In this study, the data were first loaded into the RD Instruments program WinADCP version 1.13 for viewing. The velocity components, error velocity and direction were exported as separate files readable by MATLAB, which was used for quality control and analysis. Several steps were performed in which the separate files were combined into a single composite file and outliers greater than 3 standard deviations from the mean were removed. The missing data gaps were filled by linear interpolation because none of the gaps spanned more than a few hours of time. The data sets were decimated to hourly data from the 20 minute data by selecting every third

point. Date and time strings were combined into a Julian day value and represented as a number in decimal days.

Wind data were collected from another platform, named *Brutus*, which was operated by Shell International E&P. The *Brutus* platform, a fixed drilling platform, was located at 27.8ºN, 90.67ºW; it had an anemometer 122.0 m above site elevation which recorded wind data for most of the 6 months for which the *Ocean Star* ADCP collected data.

The same time continuity and range limit checks were performed on the wind data as were performed on the ADCP data at the NDBC. After downloading the data from the NDBC, the wind data were converted into component velocities and then interpolated to the same time scale as the *Ocean Star* data by linear interpolation. A coherency analysis was performed using the mscohere function in MATLAB between the wind data and the surface-most (51 m depth) bin of the ADCP data from the *Ocean Star* platform.

3. RESULTS

In this section, I describe the principal findings from each SWSS cruise. First, I describe the general circulation features using altimeter data. The general oceanographic conditions at the beginning, middle, and end of each cruise are discussed. Then, subsets of each cruise were detailed and the vertical velocity structure was examined and compared to features observed in the altimeter fields. CTD stations were used to identify the presence or absence of subtropical underwater (SUW), which can be used as an indicator of water masses associated with the Loop Current. The CTD stations were used for geostrophic velocity calculations. For most CTD station pairs, geostrophic velocities were very small. Then, the temperature structure along the 1000 m isobath was described using selected XBT stations. Vertical profiles from the XBT stations were presented and compared between cruises. Finally, the variability in the temperature structure was expressed using empirical orthogonal function (EOF) analysis. It will be shown that nearly 100% of the temperature structure was explained by the first mode of variability.

3.1 SWSS Cruises

3.1.1 Summer 2002

For the duration of cruise 02G08, the Loop Current was located southeast of 26ºN, 87ºW, and therefore did not directly influence the study area. However, a warm

slope eddy (WSE) that extended northwestward from the Loop Current was located partly within the study area between 87ºW and 91.5ºW. The dimensions of the WSE were about 250 km east-to-west and 125 km north-to-south. This WSE was bordered by two small cold slope eddy (CSE) features to the north and west that were centered at about 28.5ºN, 90ºW and 27ºN, 94ºW. During the cruise the CSE north of the WSE strengthened as the SSH became more negative (Figure 3.1, Panel c). Meanwhile the SSH sequence shows that the CSE to the west diminishes in size from about 300 km to about 200 km by the end of the cruise (Figure 3.1).

There was a large oblong Loop Current Eddy (LCE) in the western Gulf (Figure 3.1). The northern limb was close to the point where the *R/V Gyre* made its eastward turn near 27ºN, but only appeared in the extreme lower left of the SSH field as the green area near 95ºW (Figure 3.2). The SSH series in Figure 3.1 shows that this LCE was in the process of encroaching on the western edge of the Gulf of Mexico and spinning down. At the start of the cruise, the LCE was elongated in the northwest-southeast direction. During the cruise, the eddy rotated clockwise so the orientation of the long axis was more northeast-southwest by the end of the cruise.

From the progression of SSH plots shown in Figure 3.1, it appears that, as this LCE encroached on the western boundary, a part of the LCE extended northeastward toward the WSE by the end of the cruise. As we will see this WSE was located in the study area and presumably influenced the horizontal velocity structure.

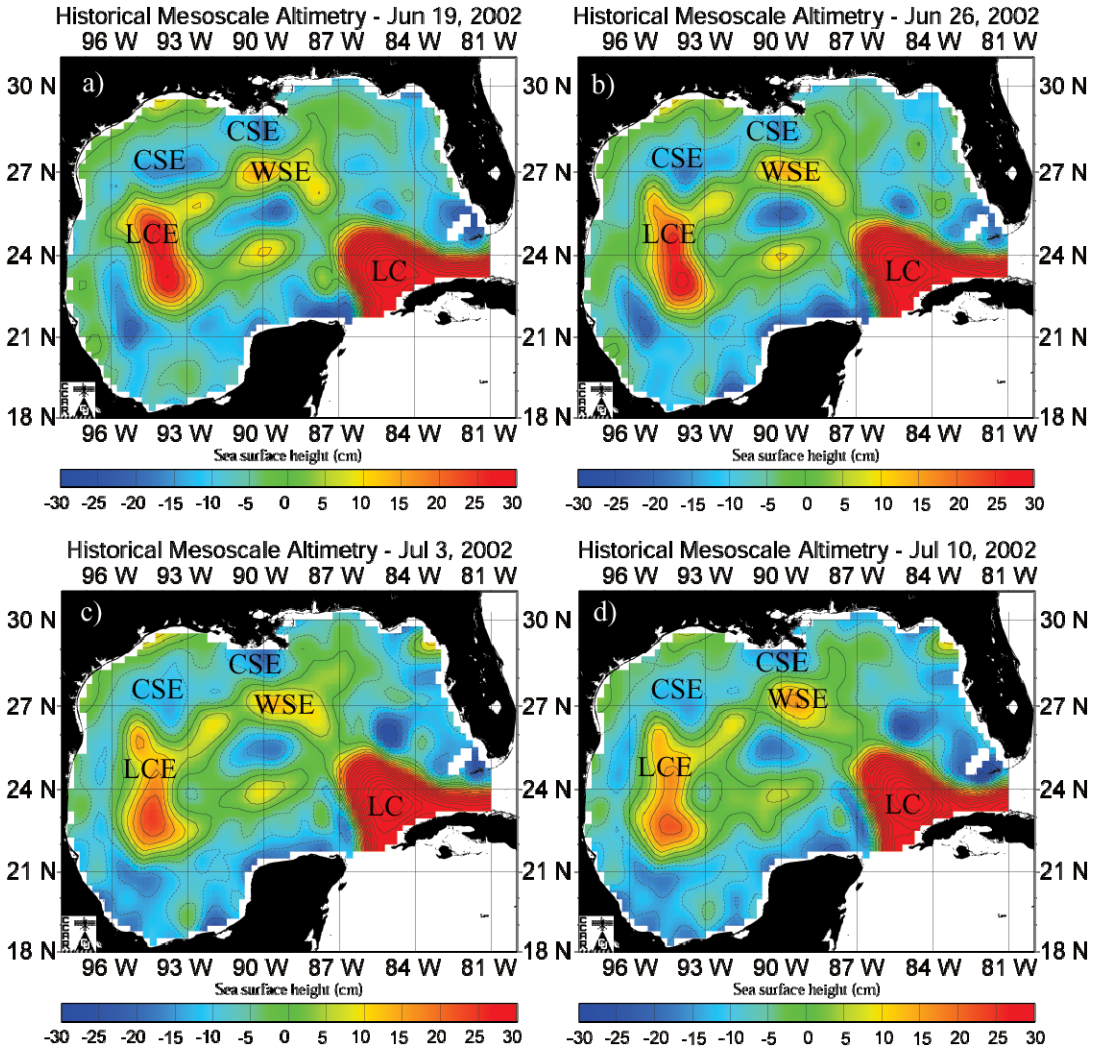

Figure 3.1 Weekly intervals of SSH during the SWSS S-tag cruise in 2002. Images downloaded from the Colorado Center for Astrodynamics Research. The contour interval is 5 cm. (SSH Source: R. Leben, CCAR, Univ. of Colorado).

The *R/V Gyre* initially transited south from Galveston, Texas, to near 27ºN before turning northeast and following the 1000 m isobath. During this part of the cruise, the western part of the study area was primarily filled by a small CSE that was

less than 100 km in diameter and was centered at 27ºN, 93.75ºW at the edge of the Sigsbee Escarpment (Figure 3.2). During this cruise, the CSE appears to diminish in the SSH field and by the end of the cruise was centered near 27ºN, 94ºW.

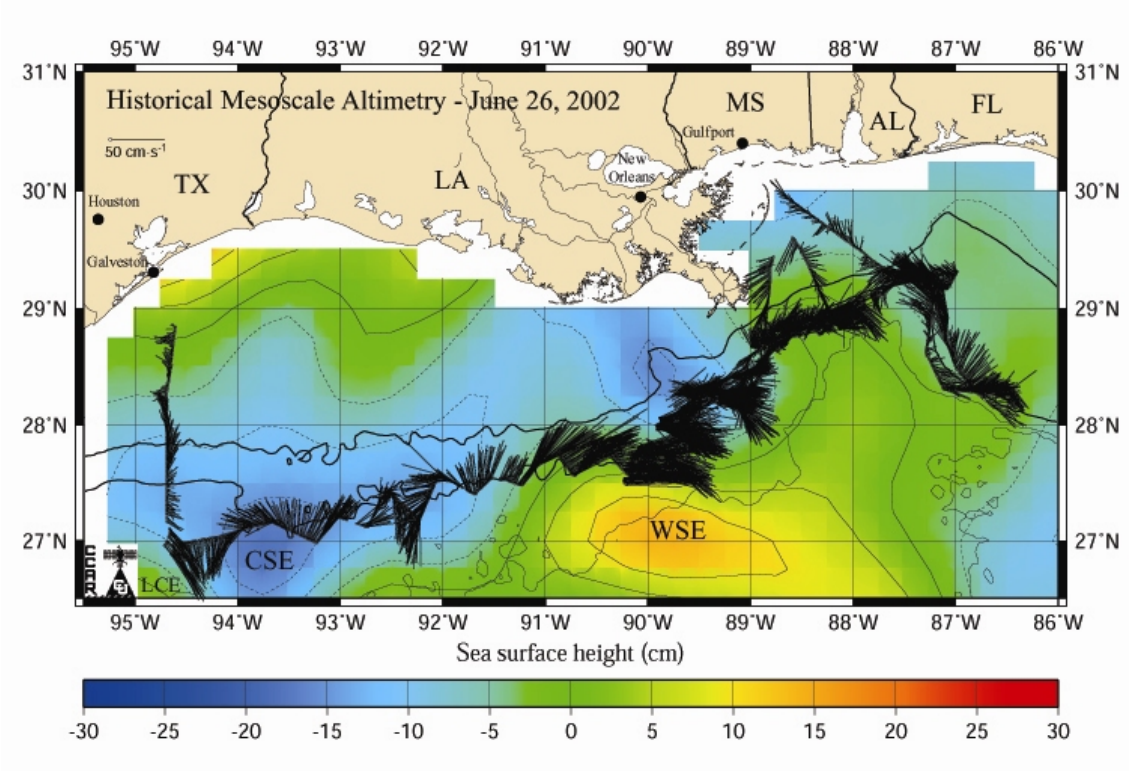

Figure 3.2 Velocity vectors during 2002 for the near surface 150-kHz (11m) depth bin. Shown are the 200 m, 1000 m (in bold), 2000 m, and 3000 m depth contours. The SSH contour interval is 5 cm. (SSH Source: R. Leben, CCAR, Univ. of Colorado).

From Galveston south to 27ºN, the current was variable in speed and direction. South of 27.5ºN the flow became southeasterly throughout the observed part of the water column between the LCE and CSE. Near 27ºN there was a marked increase in horizontal velocities to the southeast in the upper 100 m with the speed close to 50 cm/s,

as the ship approached the northern tip of the LCE that occupied most of the western Gulf (Figure 3.3).

The transit across the small CSE between 94ºW and 93ºW shows how the SSH field influences the direction of current flow (Figure 3.4). The velocity vectors in Figure 3.4 illustrate the counterclockwise flow of the CSE. Figure 3.5 shows that the flow was barotropic to at least the depth limit (~200 m) observed by the ADCP as the flow was southeast to the west of 94ºW, then the direction of flow changed to northwest, and finally to the northeast at 93.5ºW, the eastern edge of the CSE.

Between 92.5ºW and 91.5ºW, the ship appears to have passed through a relatively weak CSE that was less apparent in the SSH field, but which does appear in the velocity field in Figure 3.4. East of 91.5ºW, as the ship passed along the northern edge of the WSE centered near 27.5ºN, 89.5ºW, the flow was strongly to the east throughout the upper 250 m.

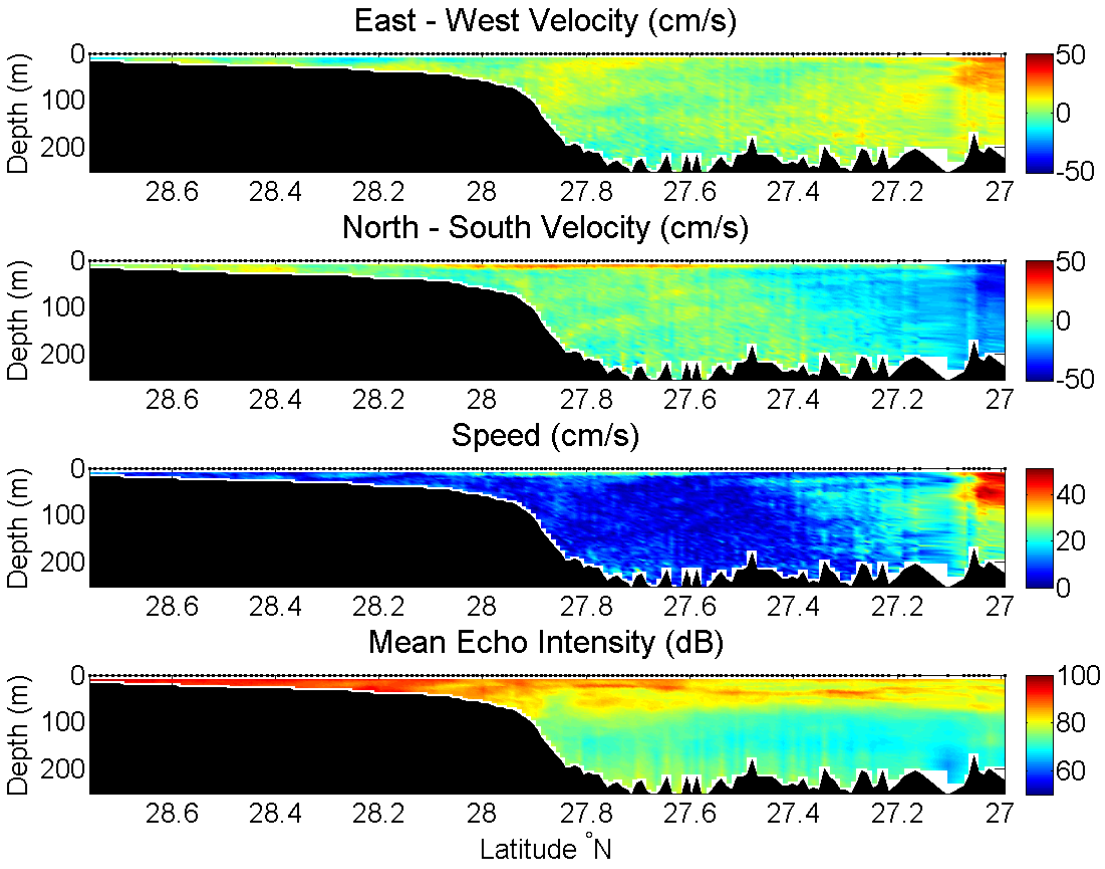

Figure 3.3 Vertical sections from the ADCP data for the initial transit south from Galveston to 27ºN where the *R/V Gyre* turned eastward. The black filled area represents the bottom tracking depth which is not equivalent to the actual water depth in water deeper than about 250 m. East and north component velocities are positive while west and south are negative in the upper two panels.

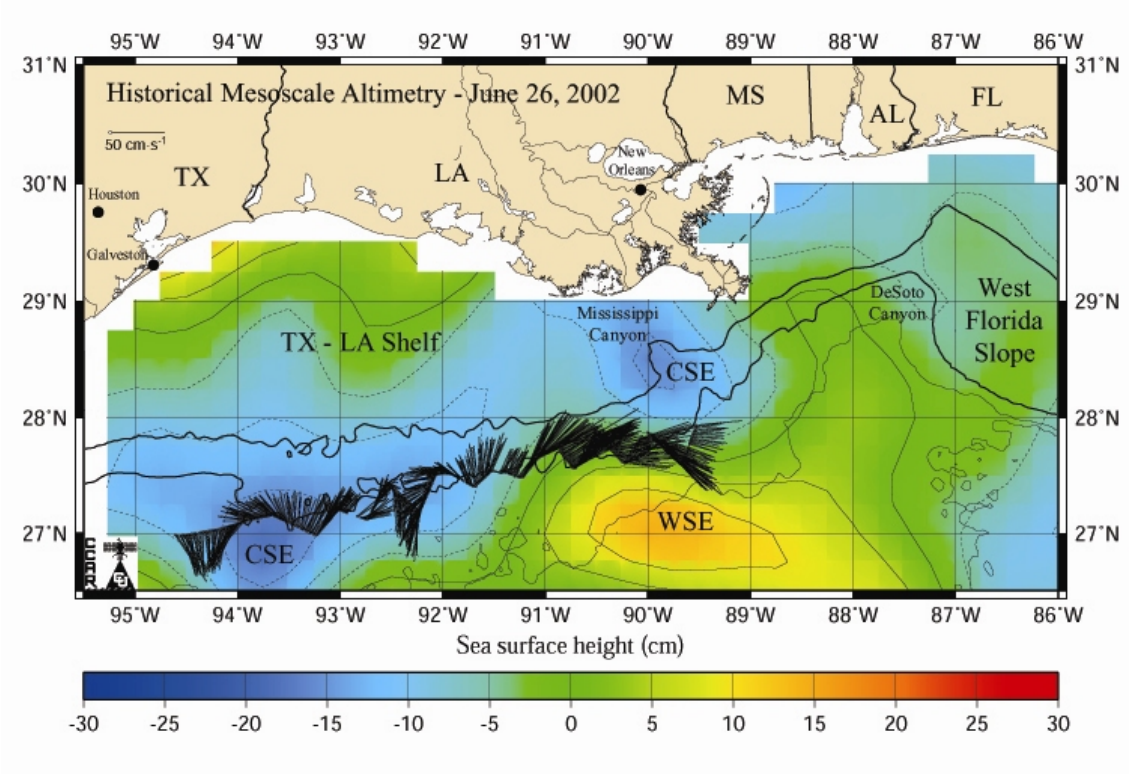

Figure 3.4 Location of transect for vertical section shown in Figure 3.5 showing the near surface velocity vectors in cm/s. Shown are the 200 m, 1000 m (in bold), 2000 m, and 3000 m depth contours. The SSH contour interval is 5 cm. (SSH Source: R. Leben, CCAR, Univ. of Colorado).

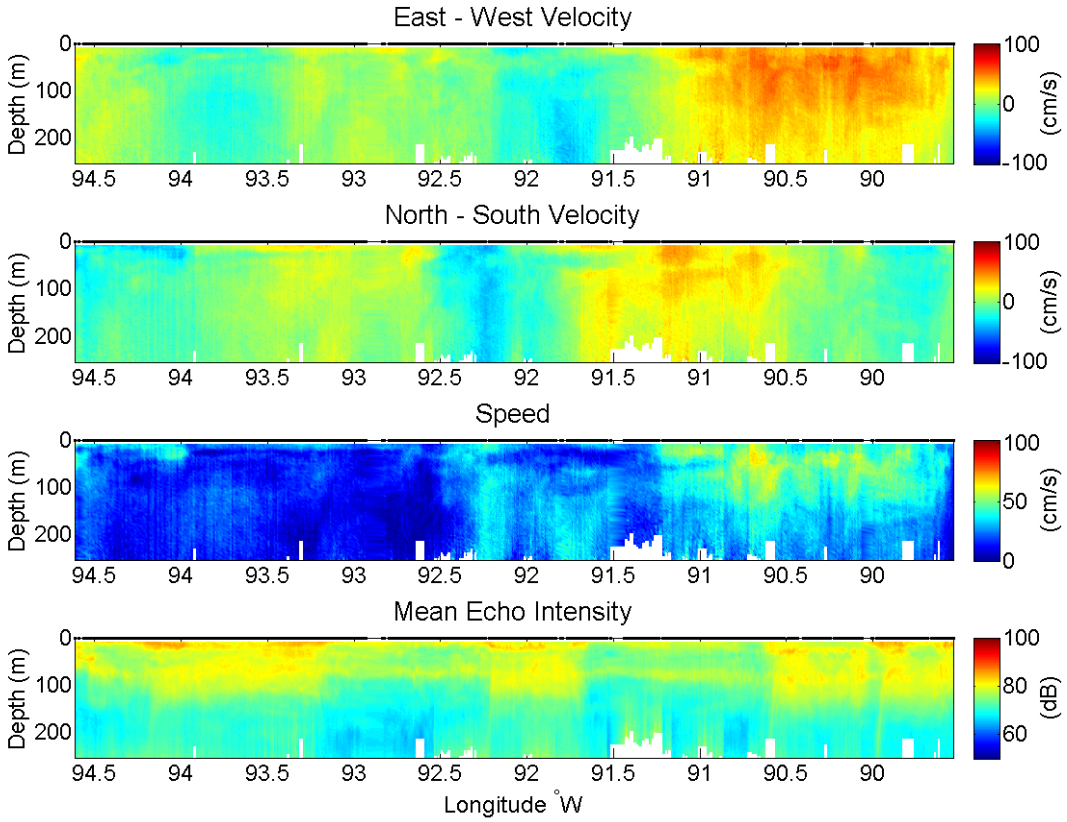

Figure 3.5 Vertical sections from the ADCP data for the segment shown in Figure 3.4. East and north component velocities are positive while west and south are negative in the upper two panels. The white space near the bottom of each panel indicates that no ADCP data are available. Note the change of velocity scale from Figure 3.3.

At the time of the cruise, the CSE at 27ºN, 94ºW was weakening and dissipating while the WSE in the east was concentrating and strengthening. During the cruise, the WSE may have extended to the northeast and into DeSoto Canyon. By the end of the cruise, the WSE did not extend eastward past 87ºW (Figure 3.1).

East of 90ºW and along the 1000m isobath, the dominant horizontal flow was northward due to the WSE extending into DeSoto Canyon. There was a weak cyclonic

feature at the base of DeSoto Canyon at 29ºN, 87.3ºW, where the nearby currents were considerably variable, rotating from the northwest to the northeast along the 1000 m isobath of the West Florida Slope (Figure 3.6).

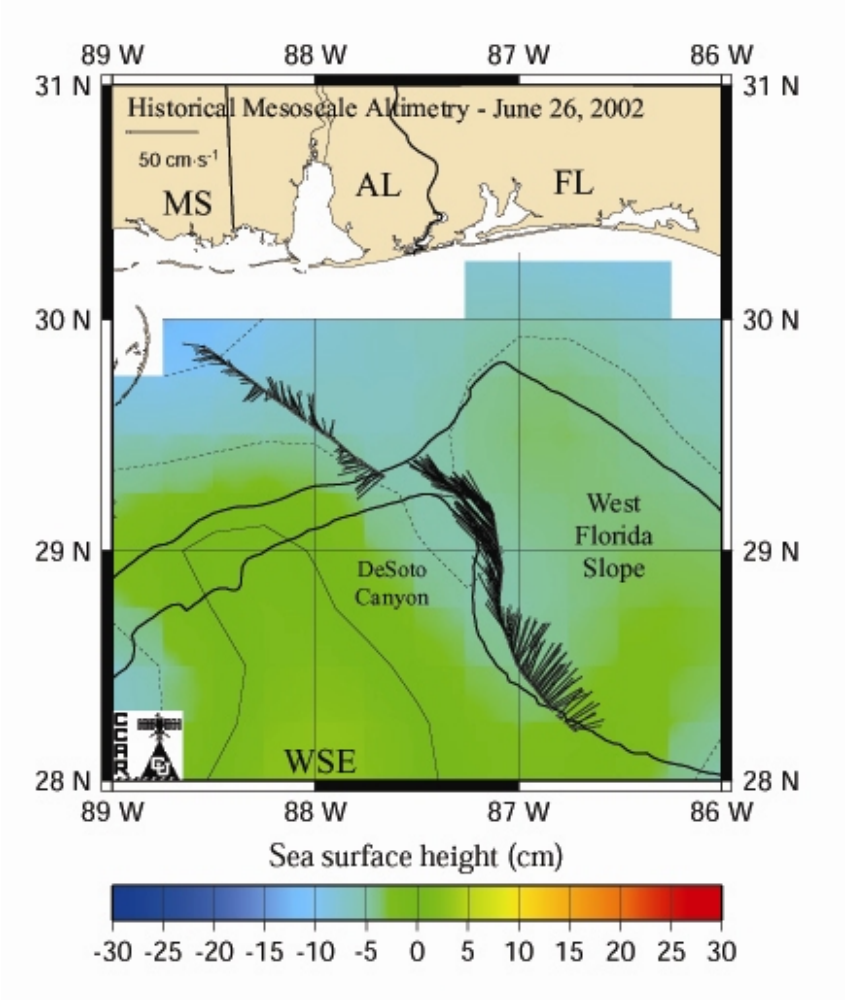

Figure 3.6 Location of transect for vertical section shown in Figure 3.7 showing the near surface velocity vectors in cm/s. Shown are the 200 m, 1000 m (in bold), 2000 m, and 3000 m contour lines. The SSH contour interval is 5 cm. (SSH Source: R. Leben, CCAR, Univ. of Colorado).

A vertical section along the easternmost transect shown in Figure 3.6 shows that velocities were close to 50 cm/s in the upper 100 m near the periphery while near the center of the cyclonic feature velocities were weak (Figure 3.7). This illustrates the degree of influence on the flow that even a weak feature in the SSH field can have on the currents.

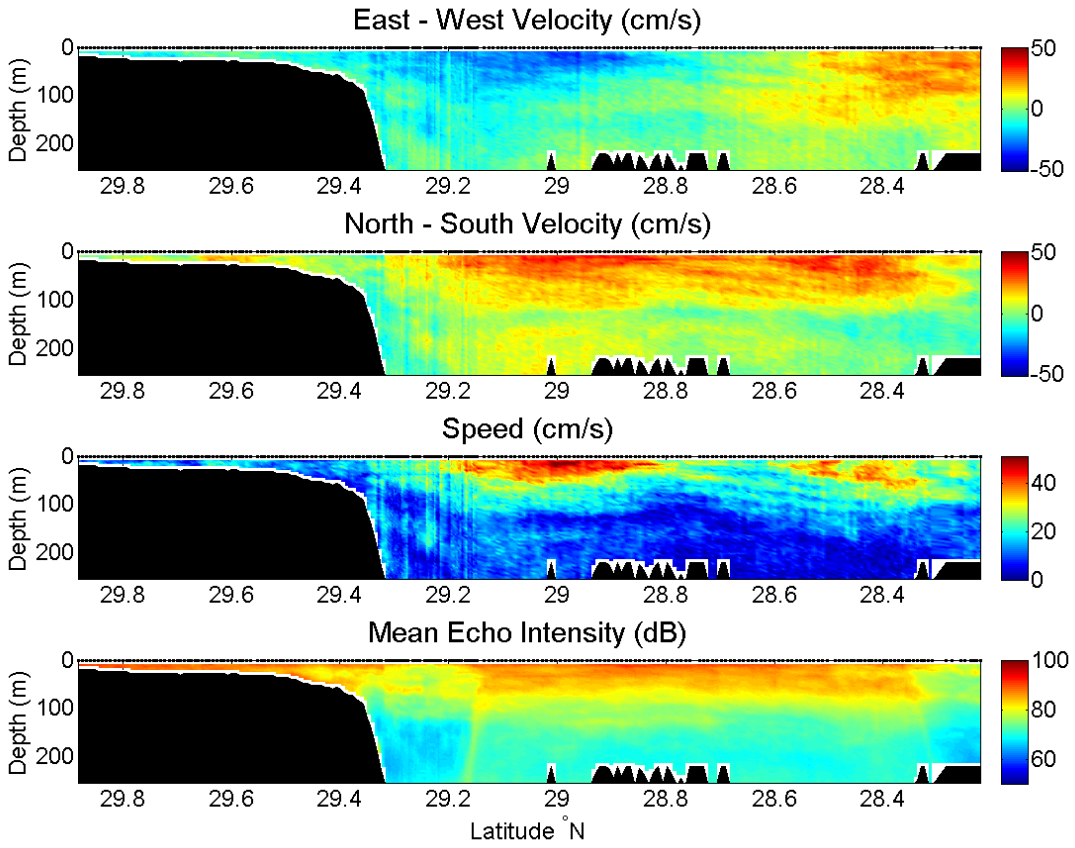

Figure 3.7 Vertical sections from the 150-kHz ADCP data for the segment shown in Figure 3.6. East and north component velocities are positive while west and south are negative in the upper two panels. The black filled area represents the bottom tracking depth which is not equivalent to the actual water depth in water deeper than about 250 m.

The locations of the XBT and CTD stations conducted during the cruise were shown in Figure 3.8. Subtropical Underwater was an indicator of Loop Current water and was identified by salinity in excess of 36.70 between 150 m – 200 m. The CTD stations for this cruise did not reveal the presence of any subtropical underwater (SUW). Geostrophic calculations show weak velocities between CTD stations, however this results because the mesoscale circulation features were smaller than the station spacing.

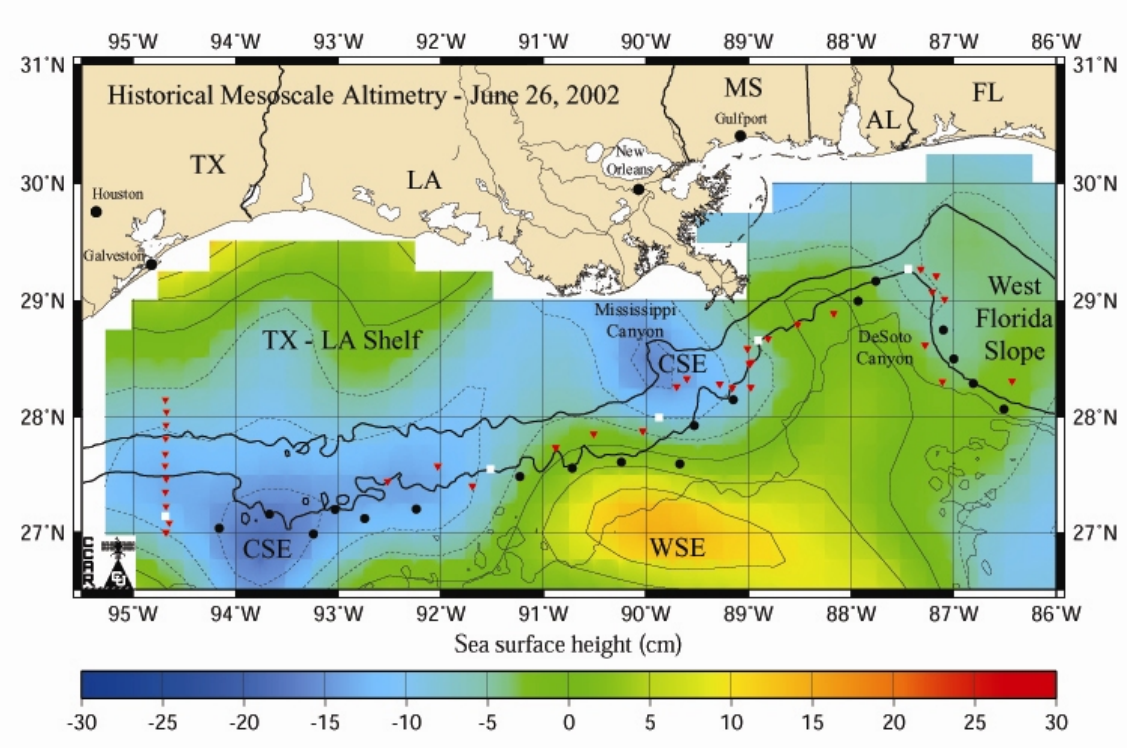

Figure 3.8 Locations of XBT and CTD stations for cruise 02G08. Black circles represent XBT stations used to create the vertical section. Red inverted triangles represent XBT stations not selected for use in the vertical section. White squares represent locations of CTD stations. Shown are the 200 m, 1000 m (in bold), 2000 m, and 3000 m contour lines. The SSH contour interval is 5 cm. (SSH Source: R. Leben, CCAR, Univ. of Colorado).

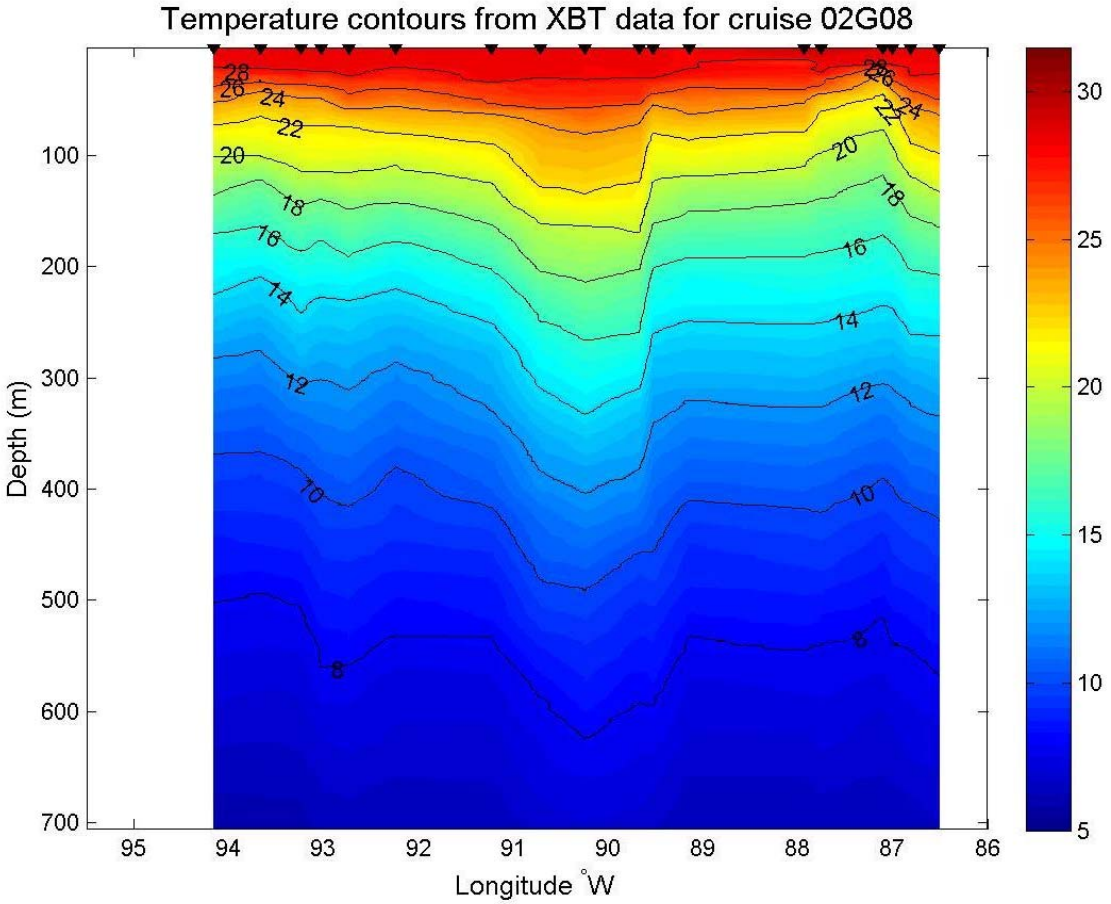

Figure 3.9 Vertical section of temperatures created from selected XBT stations shown in Figure 3.8. Black inverted triangles across the top edge represent the longitude of the XBT stations used. Temperatures are shown in Celsius. The white space on each side depicts the part of the study area that is not represented in the vertical section.

Figure 3.9 shows temperatures to 700 m along the 1000 m isobath at the locations of the black circles shown in Figure 3.8. The isotherms were closer together near the surface and farther apart at depth. The isotherms were deflected upwards near 94ºW, 92ºW, and 87ºW due to the CSEs present at those locations. The downward

deflection of the isotherms from 89.5ºW to 91ºW corresponds to the edge of the WSE. The downward deflection at 86.5ºW was caused by the northern part of the WSE at this location.

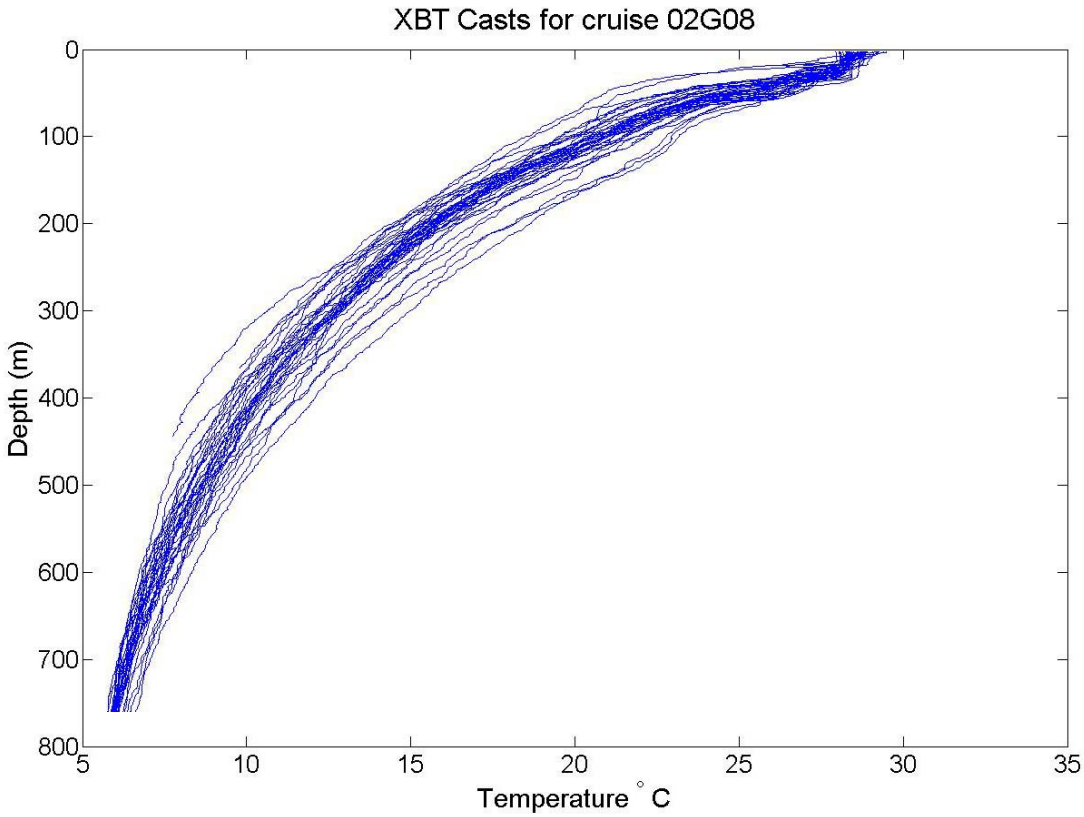

Figure 3.10 Vertical profiles of all XBT stations deployed during cruise 02G08.

The vertical profiles of all XBT stations (Figure 3.10) show the relationship between temperature and depth. They show the greater change of temperature near the surface than at depth as seen in the isobaths in the vertical section in Figure 3.9. They also indicate some variability between stations located at depths between 100 m and

450 m. The upper 25 m was fairly well mixed. Below 450 m, the data reveal the increasing homogenization with depth as the variability between profiles decreases.

The results of the EOF analysis on the XBT data from this cruise were shown in Figures 3.11 and 3.12. Almost all the variance in temperature was associated with mode 1 (> 99.6%). This mode has the greatest amplitude near the surface and decays with depth (Figure 3.11). The vertical profiles show that temperature was higher near the surface and decreases with depth; therefore, mode 1 represents the depth dependency of temperature.

Mode 2 contains much less variance than mode 1. This mode has considerably more vertical structure in the depth range of 100 m to about 450 m. The spatial pattern of the modal amplitudes was shown in Figure 3.12. Mode 2 was believed to represent the variability of temperature with a change in location, and therefore represents the different processes (CSE, WSE, or LCE) that were occurring on the slope. For example, the WSE was associated with positive amplitudes in Mode 2 while the CSEs were negative (Figure 3.12).

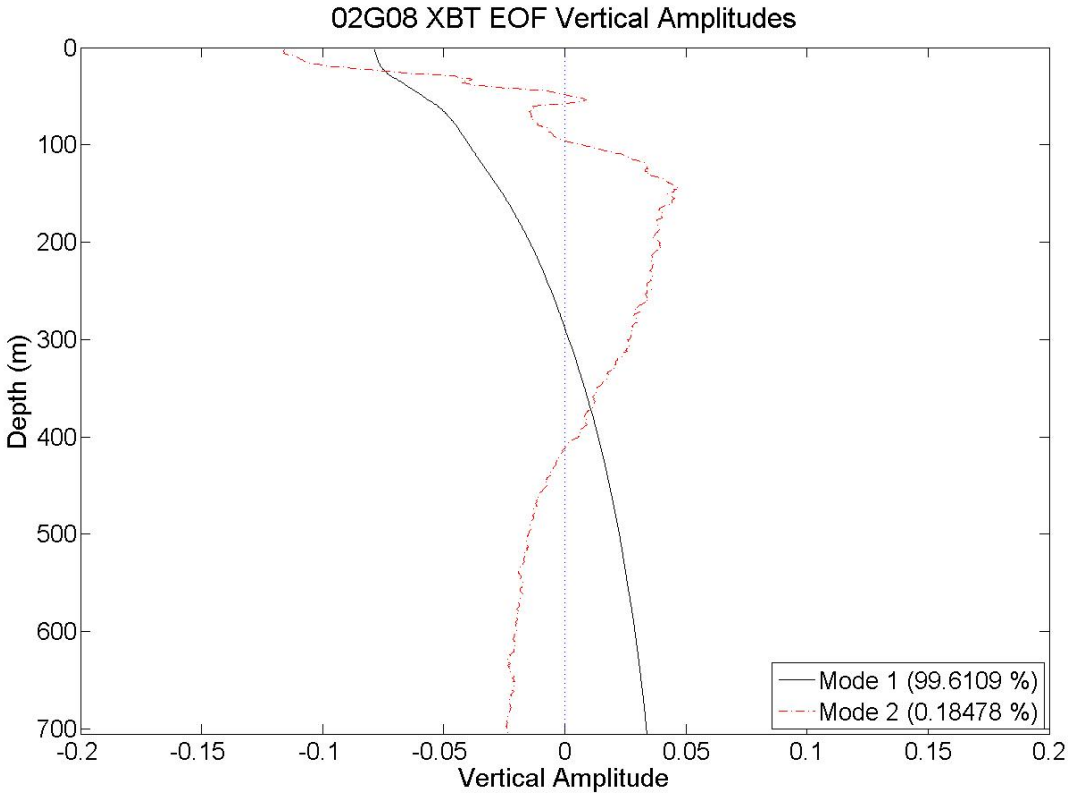

Figure 3.11 Vertical profile showing XBT EOF vertical mode amplitudes during 2002 cruise 02G08.

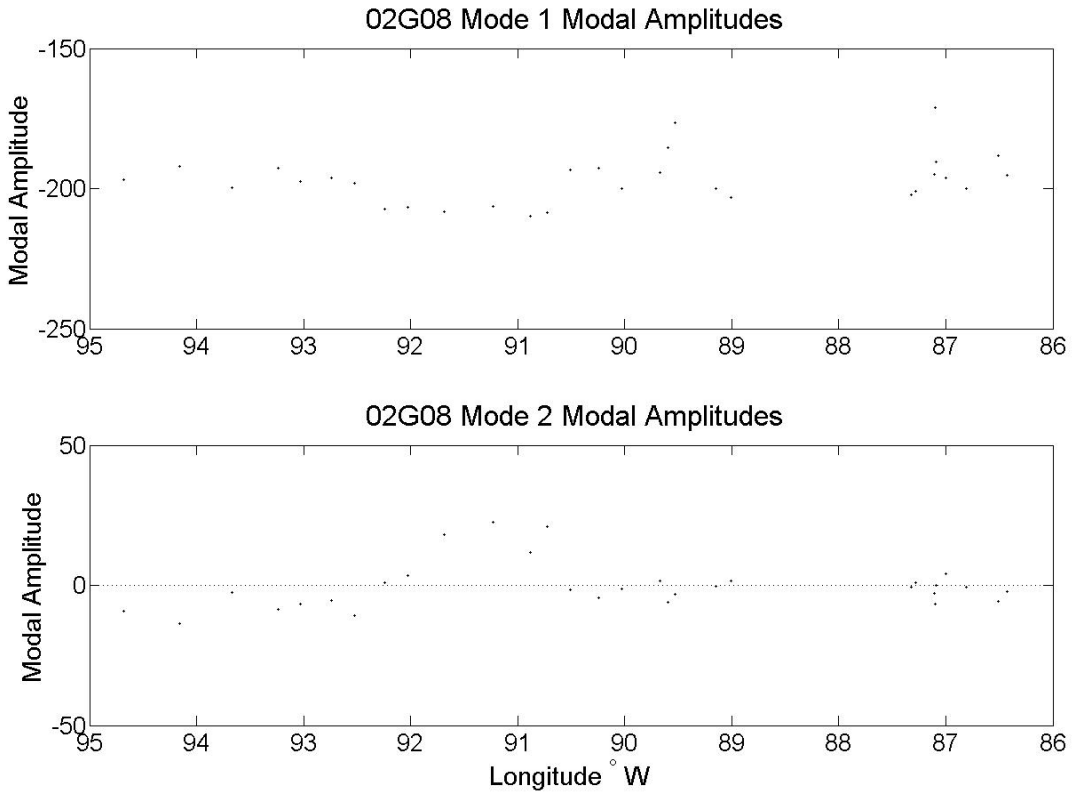

Figure 3.12 Modal amplitudes for XBT EOF calculation for 2002 cruise 02G08.

3.1.2 Summer 2003

The series of SSH images depicted in Figure 3.13 shows the Loop Current was the dominant feature in the eastern (east of 91ºW) Gulf of Mexico during the summer of 2003. The western Gulf was populated by various cyclones and a large anticyclonic feature centered at 24ºN, 93ºW.

In late May, a nearly separated Loop Current circulated about a hub near 26.5ºN, 88ºW. Two CSEs were located on either side of the Loop Current; one centered 25ºN, 89ºW, and the other at 25.5ºN, 85ºW. The CSE on the eastern side of the Loop Current moved southeast during the cruise. When this occurred the pinched part of the Loop Current widens and an LCE separation event no longer seems likely. During this time the Loop Current expands further north and west into the Gulf of Mexico. The Loop Current impinged on the slope and then extended westward along it for a short distance (Figure 3.13, Panels b-d).

The western edge of the Loop Current extended from 89ºW to near 91ºW at about 27.5ºN. This was the farthest west the Loop Current would reach during the two 2003 cruises. North of the Loop Current between 88.5ºW and 89ºW was an area of cyclonic circulation, centered on the Mississippi River balize delta (Figure 3.13, Panel a).

West of 90ºW a mixture of weak cyclonic and anticyclonic features occupied the slope. A weak anticyclone centered near 27ºN, 95ºW extended southeastward, where it

connected with the larger LCE (Figure 3.13) during the first week of the cruise. This LCE dominated the Gulf west of 90ºW, as seen in all four panels of Figure 3.13.

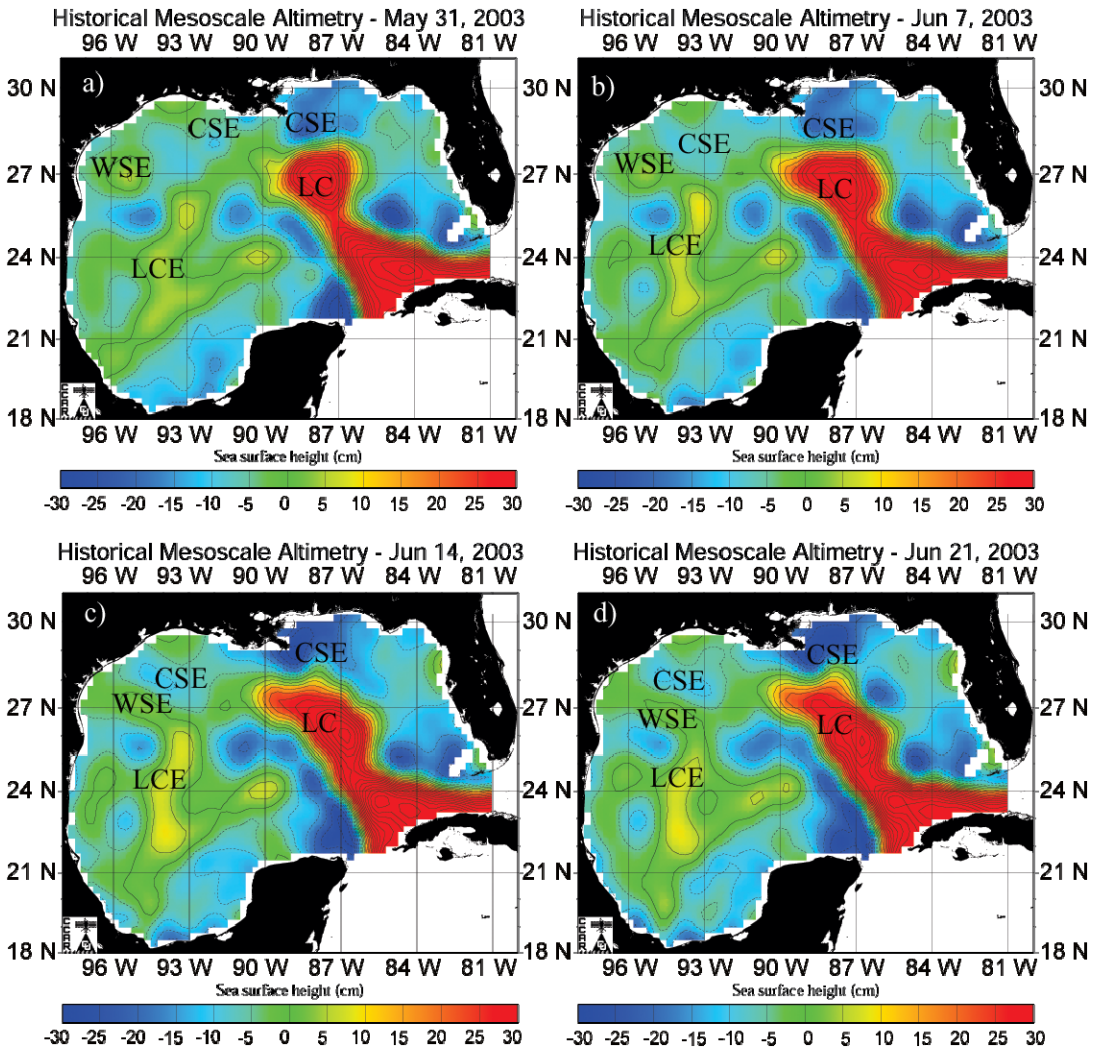

Figure 3.13 Weekly intervals of SSH during the SWSS habitat survey cruise in 2003. Images downloaded from the Colorado Center for Astrodynamics Research. The SSH contour interval is 5 cm. (SSH Source: R. Leben, CCAR, Univ. of Colorado).

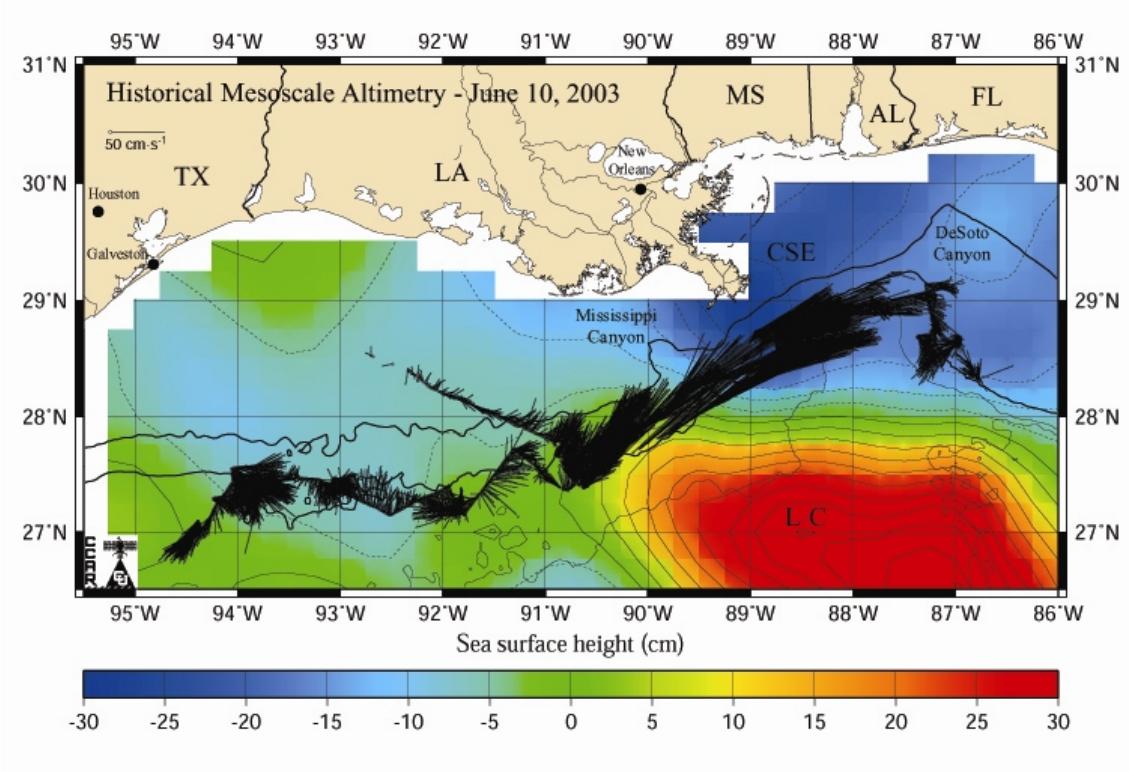

Figure 3.14 Velocity vectors during first cruise of 2003 for the near surface 38-kHz (41m) depth bin. Shown are the 200 m, 1000 m (in bold), 2000 m, and 3000 m contour lines. The SSH contour interval is 5 cm. (SSH Source: R. Leben, CCAR, Univ. of Colorado).

A transect along the 1000 m isobath, between 95º - 87ºW from June 2nd through June 13th, shows that there were two different current regimes in the study area divided at 91ºW (Figure 3.14). To the west of 91ºW, currents were variable in direction and weaker in magnitude than the vectors observed east of 91ºW. The magnitude and direction of near-surface velocity vectors were related to the proximity to the slope features. East of 91ºW, the Loop Current dominated the velocities. The velocity vectors show the flow can be somewhat inferred from the SSH features.

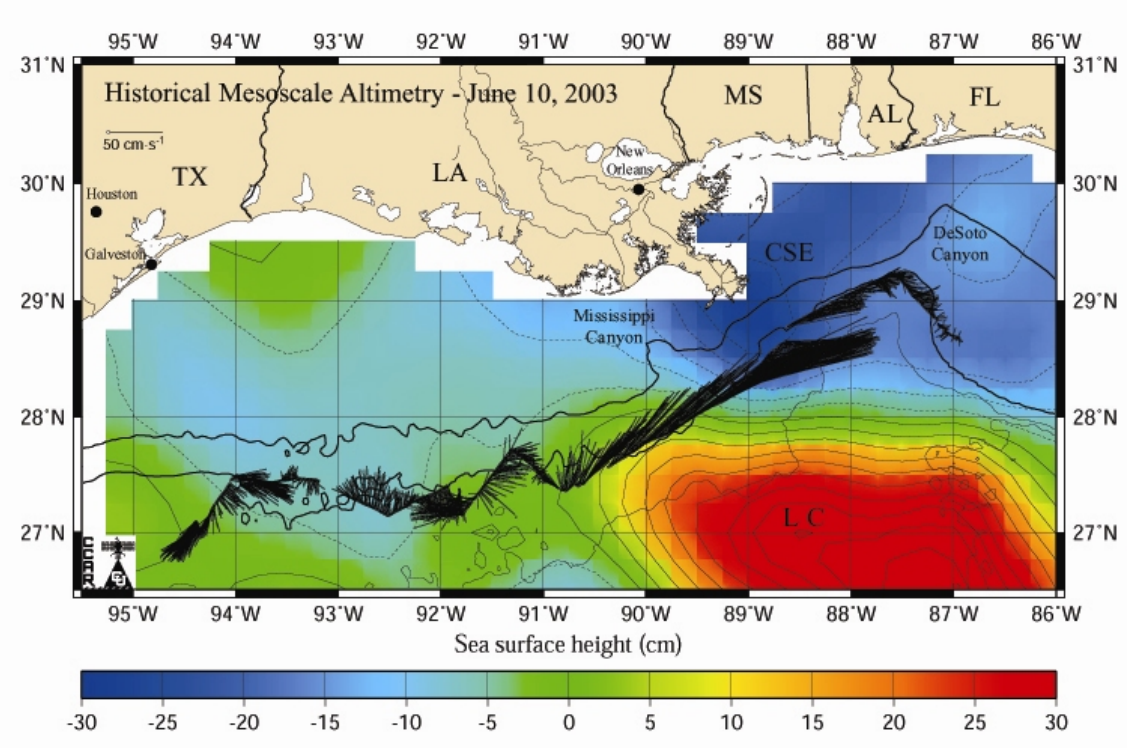

Figure 3.15 Location of transect for 38-kHz vertical section shown in Figure 3.16 showing velocity vectors in cm/s at 41 m. Shown are the 200 m, 1000 m (in bold), 2000 m, and 3000 m contour lines. The SSH contour interval is 5 cm. (SSH Source: R. Leben, CCAR, Univ. of Colorado).

The corresponding vertical section for the cruise segment in Figure 3.15 gives an example of the control of the Loop Current on vertical velocity structure (Figure 3.16). West of 91ºW the speed was weak and generally around 25-40 cm/s while to the east of 91ºW and west of 88.5ºW, the speed increases to more than 100 cm/s. The velocities were surface intensified. Speeds on the order of 50 cm/s can be found as deep as 400 m in the region around the Loop Current. The east to west component velocity was about twice that of the north to south component velocity. Away from the Loop Current the velocities and speeds were about half those along the Loop Current.

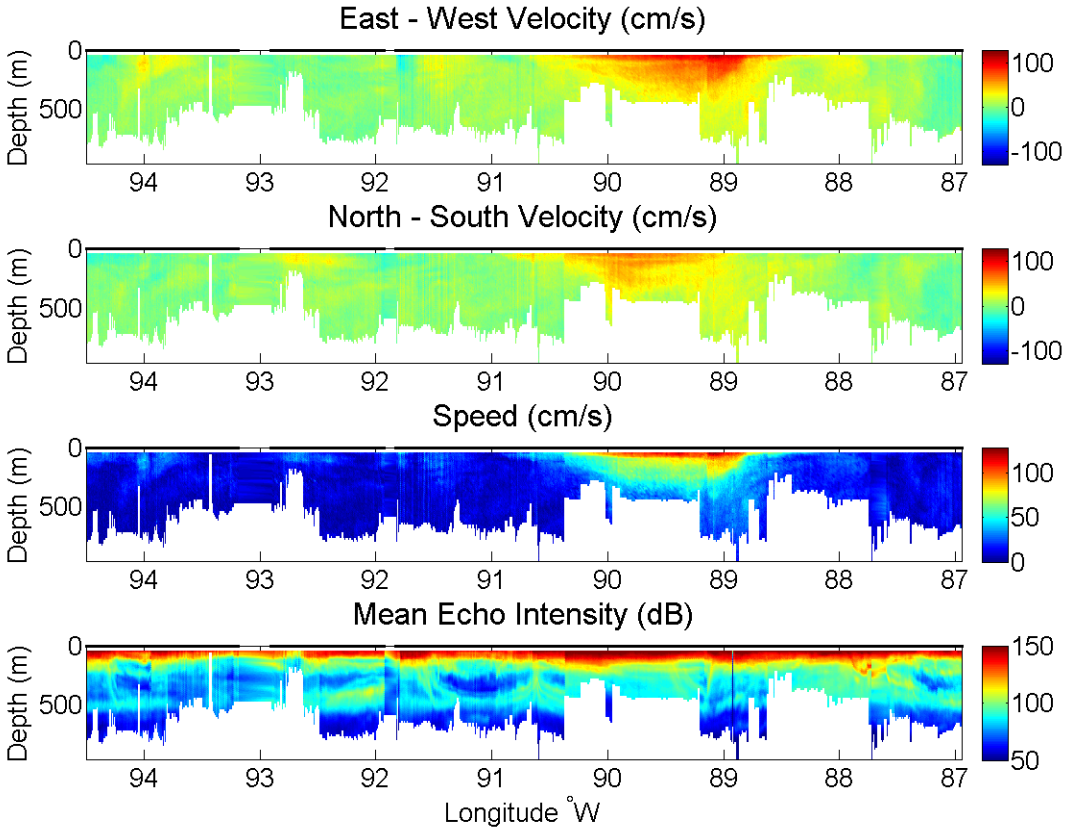

Figure 3.16 Vertical sections from the 38-kHz ADCP data for the segment shown in Figure 3.15. East and north component velocities are positive while west and south are negative in the upper two panels. The white space near the bottom of each panel indicates the bottom of the usable ADCP data.

In the last week of the cruise, the ship revisited the northern limb of the LC between 87ºW and 92ºW (Figure 3.17). By this time the Loop Current had started to retreat towards the southeast. The velocity vectors show that the magnitude and direction of the flow in this region was similar to what it was on the outward leg of the cruise a week earlier.

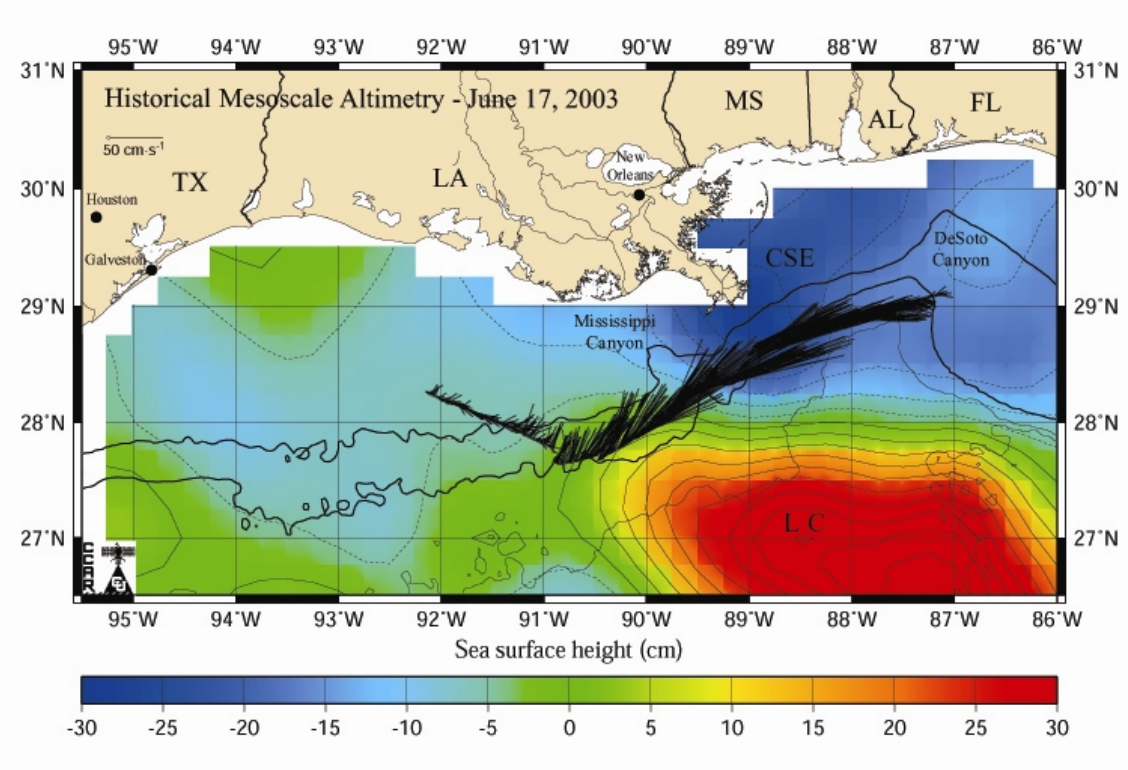

Figure 3.17 Location of transect for 38-kHz vertical section shown in Figure 3.18 showing velocity vectors in cm/s at 41 m. Shown are the 200 m, 1000 m (in bold), 2000 m, and 3000 m contour lines. The SSH contour interval is 5 cm. (SSH Source: R. Leben, CCAR, Univ. of Colorado).

The vertical sections of velocity and speed show current speeds on the order of 50 cm/s to a depth of about 400 m. The cross-section of water displaying the strong surface intensified flow was similar to what it was during the previous week (Figures 3.16 and 3.18). Maximum near-surface speeds remain near 100 cm/s. Component velocities in the east to west direction were again approximately double the north to south direction (Figure 3.18).

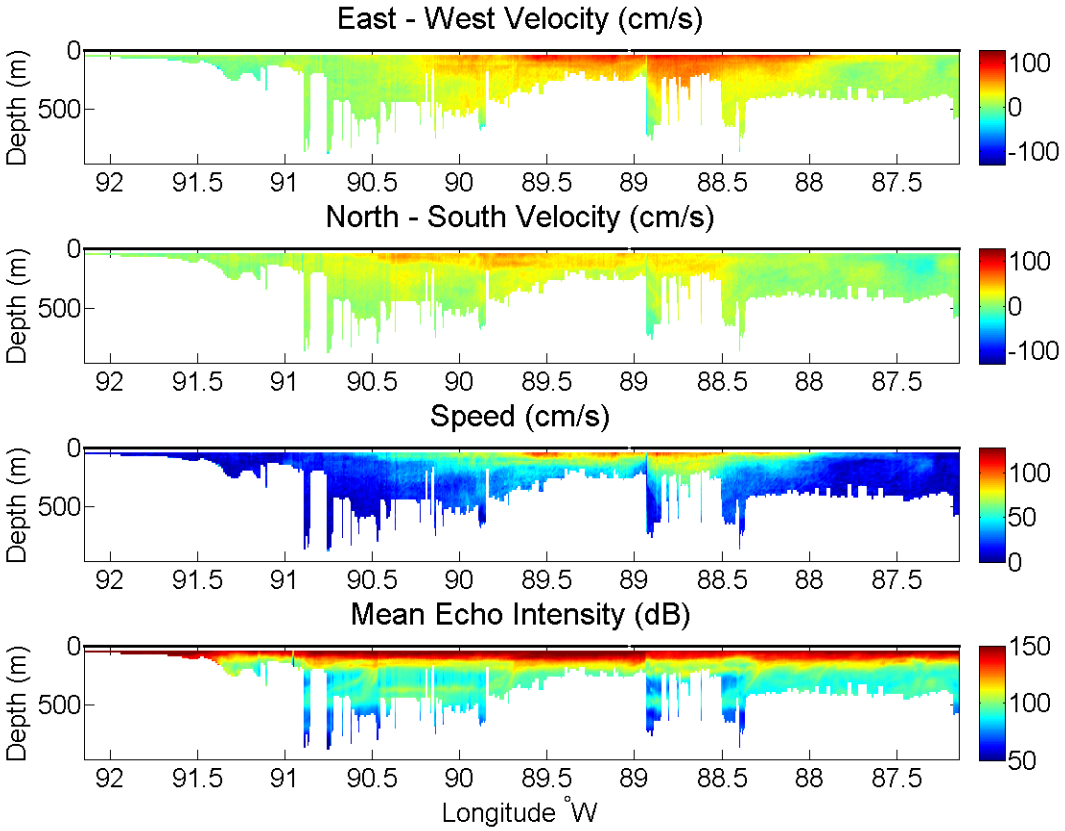

Figure 3.18 Vertical sections from the 38-kHz ADCP data for the segment shown in Figure 3.17. East and north component velocities are positive while west and south are negative in the upper two panels. The white space near the bottom of each panel indicates the bottom of the usable ADCP data.

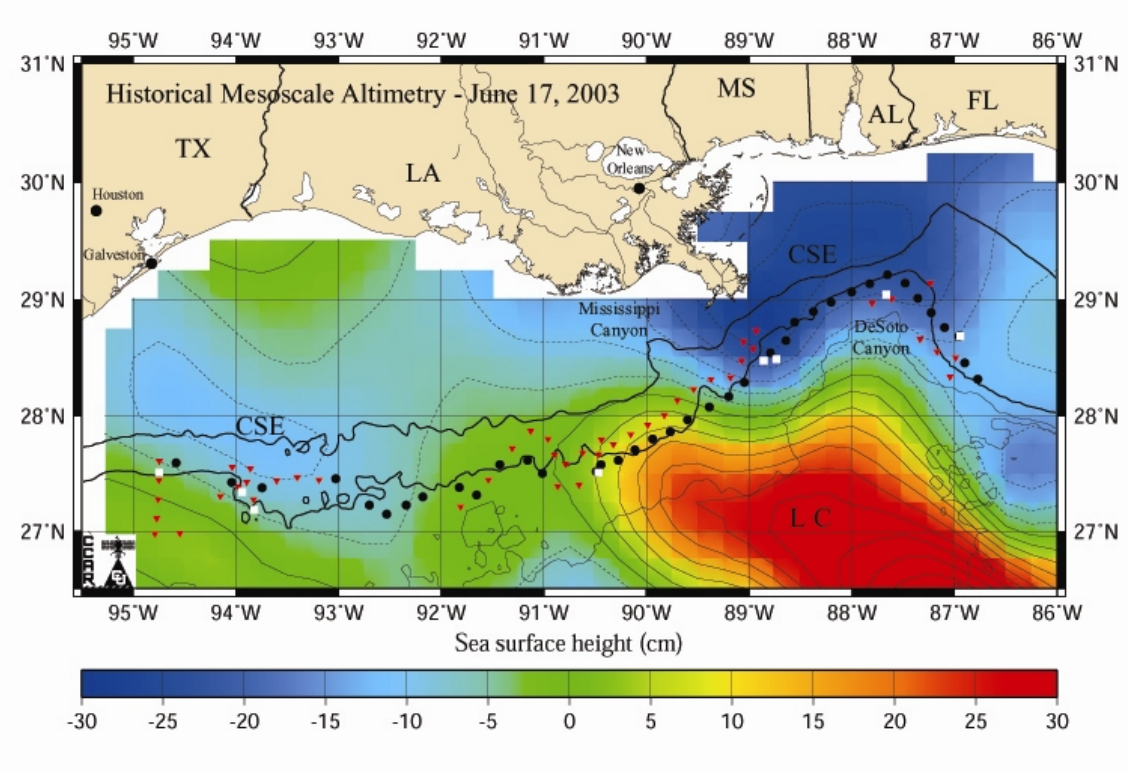

Figure 3.19 Locations of XBT and CTD stations for cruise 03G06. Black circles represent XBT stations used to create the vertical section. Red inverted triangles represent XBT stations not selected for use in the vertical section. White squares represent locations of CTD stations. Shown are the 200 m, 1000 m (in bold), 2000 m, and 3000 m contour lines. The SSH contour interval is 5 cm. (SSH Source: R. Leben, CCAR, Univ. of Colorado).

The locations of the XBT and CTD stations performed during the cruise were shown in Figure 3.19. The temperature-salinity property diagram for this cruise showed salinity values exceeding 36.7 (Figure 3.20). This could indicate the presence of subtropical underwater (SUW). This means the cruise likely sampled water from the Loop Current since SUW was found in the Loop Current water but was much less common in the Gulf water outside the Loop Current. Geostrophic analysis performed on a couple of CTD stations did not provide useful information. The stations were either too far apart or located in areas of similar SSH. The velocities calculated were on the order of 5 cm/s or less instead of the 100 cm/s or more seen in the ADCP data in the same vicinity. This results because the CTD stations do not span the SSH feature but rather only provide the relative velocity between the two CTD stations used in the calculation.

The temperature structure along the 1000 m isobath during the cruise was shown in Figure 3.21. The structure was more complicated than that for the 2002 cruise shown in Figure 3.9. In the west, a region of weak SSH gradients was reflected as relatively flat isotherms. Near 93ºW, the edge of the CSE to the northwest caused the uplift in the isotherms. Near 92ºW, the diminutive WSE, that appeared to be moving to the southwest (Figure 3.13) as the Loop Current pushed westward, caused the isotherms to become deeper.

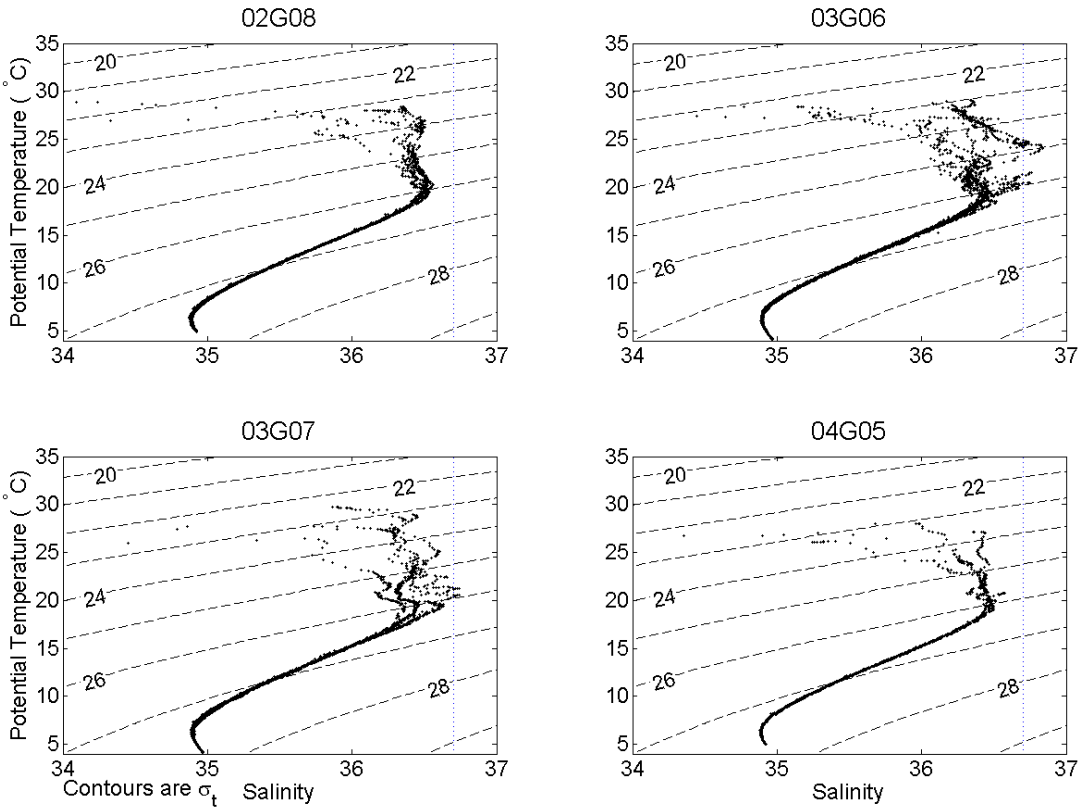

Figure 3.20 Temperature – Salinity plots for each of the four cruises during the SWSS program. The vertical dotted line represents a salinity of 36.7.

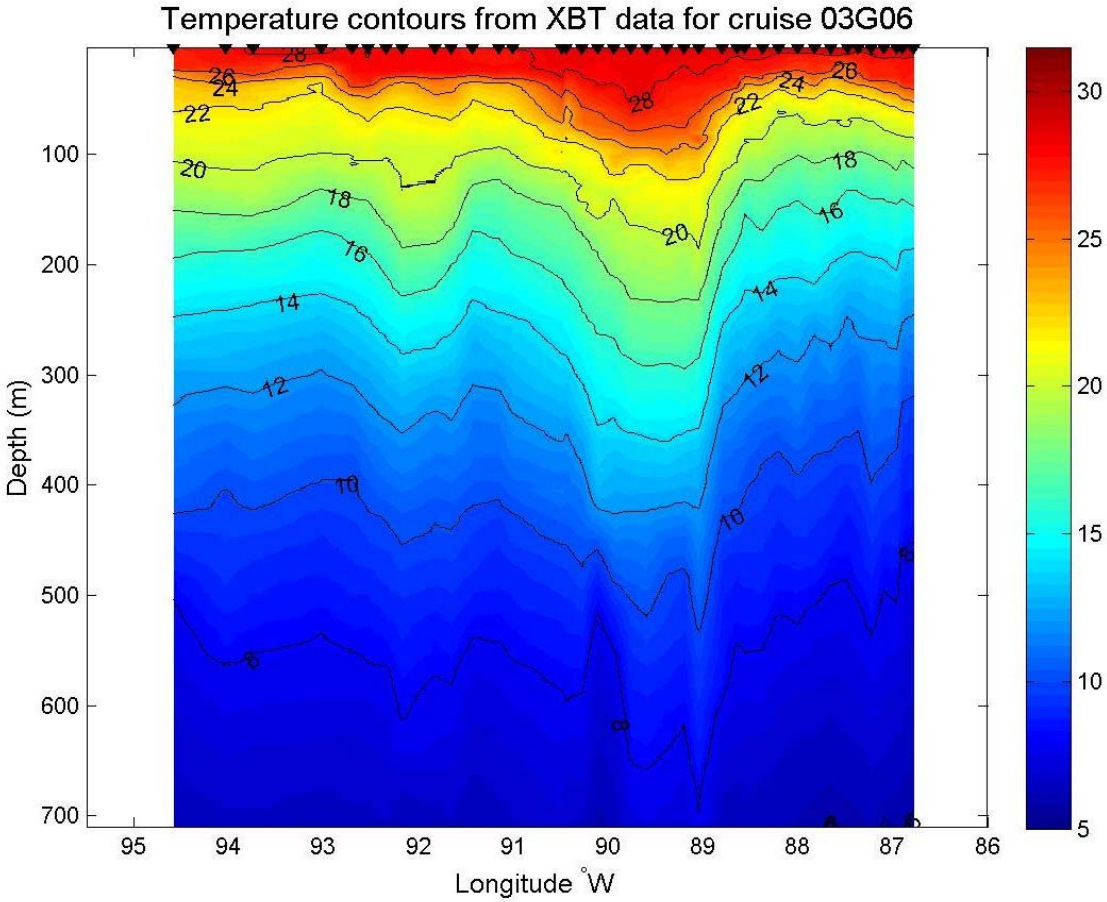

Figure 3.21 Vertical section of temperatures created from selected XBT stations shown in Figure 3.19. Black inverted triangles across the top edge represent the longitude of the XBT stations used. Temperatures are shown in Celsius. The white space on each side depicts that part of the study area not represented in the vertical section.

Between the small positive SSH anomaly located near 92ºW and the Loop Current, the shallowing of the isotherms was suggestive of a relative minimum SSH anomaly there that was poorly resolved in the altimetry data. Between 91ºW and 89ºW, downwelling or horizontal advection of warm water associated with the anticyclonic flow of the Loop Current was suggested by the downward sloping isotherms. For example, the Loop Current has deflected the 16ºC isotherm about 100 m deeper than to the west of 93ºW, where the change in SSH was small and the isotherms were nearly horizontal. From 89ºW to 87ºW, the cruise track passed through a cyclonic feature.

A comparison of XBT stations performed about a week apart and at about the same locations, illustrates the change in temperature structure as the Loop Current retreated from the area (Figure 3.22). The XBT stations used in the second profile were those between 89ºW and 91ºW on the northern line depicted by the inverted red triangles in Figure 3.19. The earlier (and slightly farther south) temperature structure showed deeper isotherms compared to the later temperature structure. Using the 16ºC isotherm as an indicator, there was about a 50 m change of depth during the week.

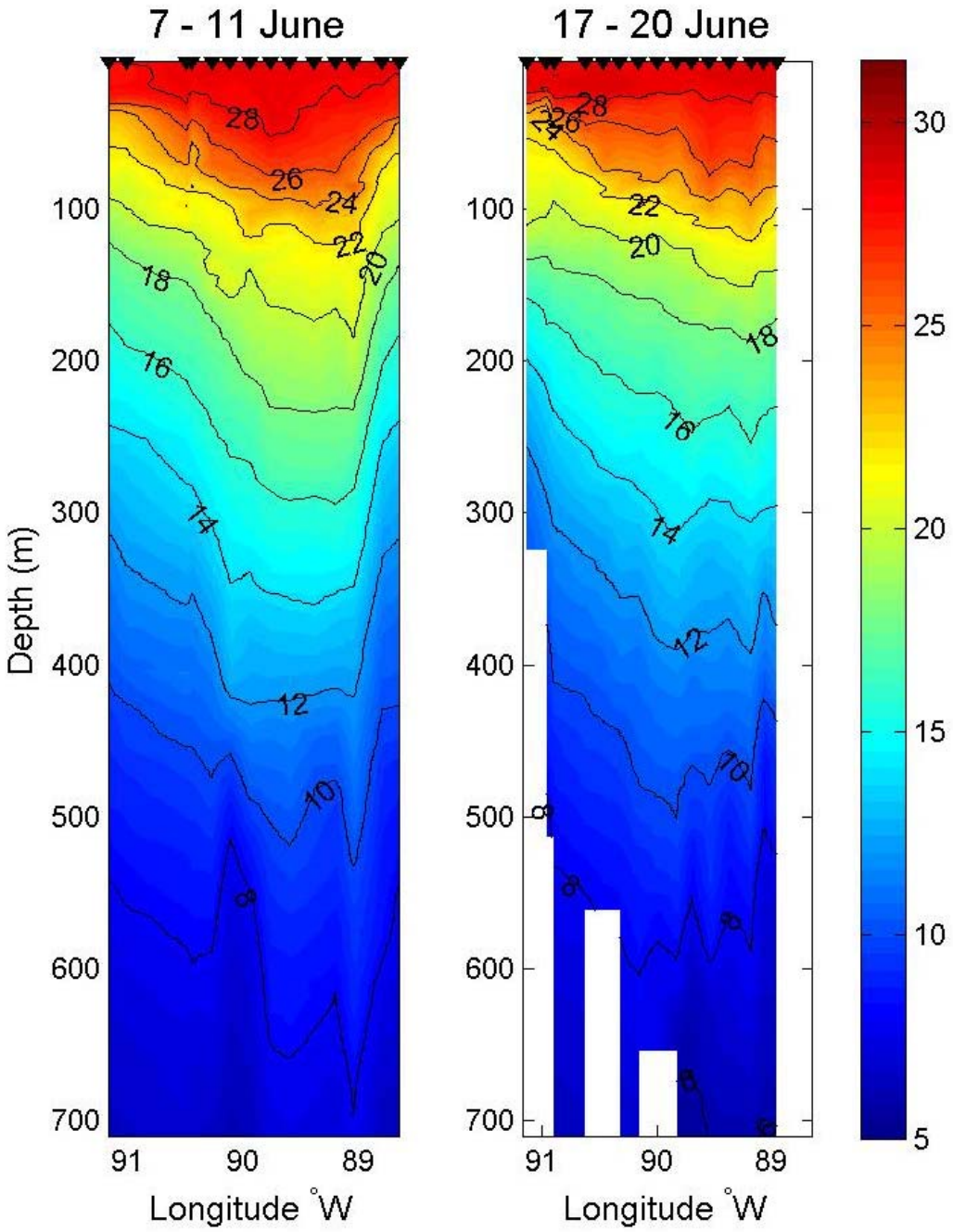

Figure 3.22 Comparison of temperatures using selected XBT stations between 89ºW and 91ºW on outbound and return legs of the cruise. Black inverted triangles across the top edge represent the longitude of the XBT stations used. Temperatures are shown in Celsius.

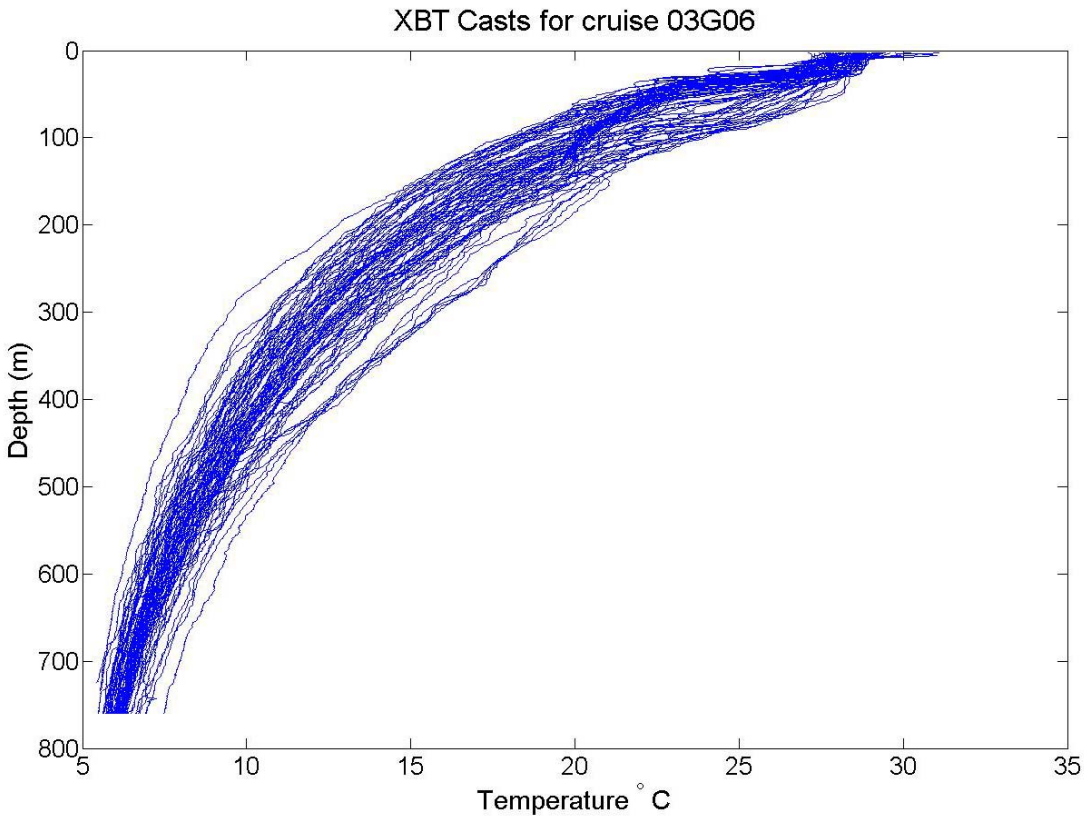

Figure 3.23 Cruise 03G06 vertical profiles of all XBT stations.

The vertical profiles of all XBTs resemble those from 2002 in several ways. They reflect the depth dependence of temperature. Summer surface mixing equalizes the temperatures in the upper 25 m of the profiles. The homogenization of temperature with depth below 450 m was responsible for the similarity between profiles at those depths. The profiles show some variability across the study area occurs between 100 m and 450 m. Temperatures in the surface waters observed during this cruise were about 5ºC warmer than during cruise 02G08 (Figure 3.23).

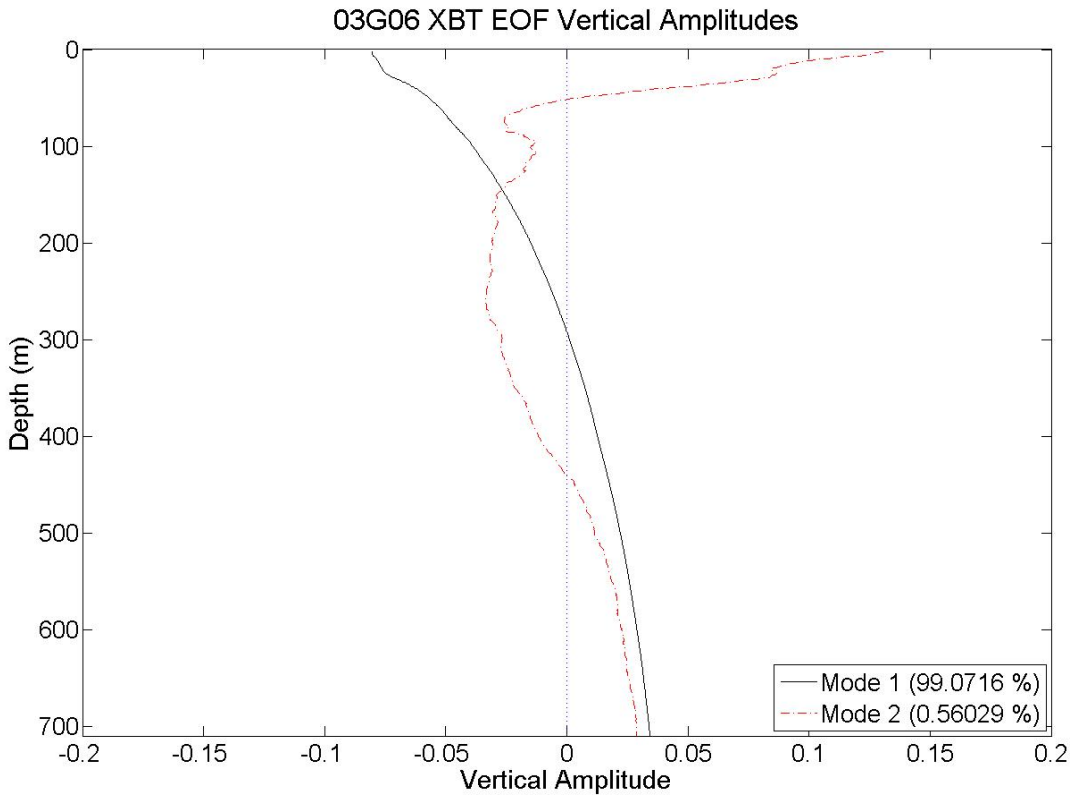

Figure 3.24 Vertical profile showing XBT EOF vertical mode amplitudes during 2003 cruise 03G06.

The results of the EOF analysis on the XBT data from this cruise were shown in Figures 3.24 and 3.25. The first two modes of the EOF analysis show similar patterns to those in 2002 (compare Figure 3.24 with Figure 3.11). The corresponding modal amplitudes were shown in Figure 3.25. Compared to the 2002 cruise, Mode 1 has about 0.5% less variance while mode 2 contains three times as much variance.

As was the case in 2002, the largest amplitudes in mode 1 occur near the surface and the amplitudes decay with depth. The conclusion that this mode represents the depth dependency of temperature was also reached for this data. Mode 2 contains more

vertical structure than mode 1 between the 100 m and 450 m depths. As Figure 3.25 shows, the modal amplitude was positive in mode 2 in the region associated with the Loop Current. Therefore, this mode was again believed to represent the variability of temperature between location and therefore, the variability between different processes occurring on the slope.

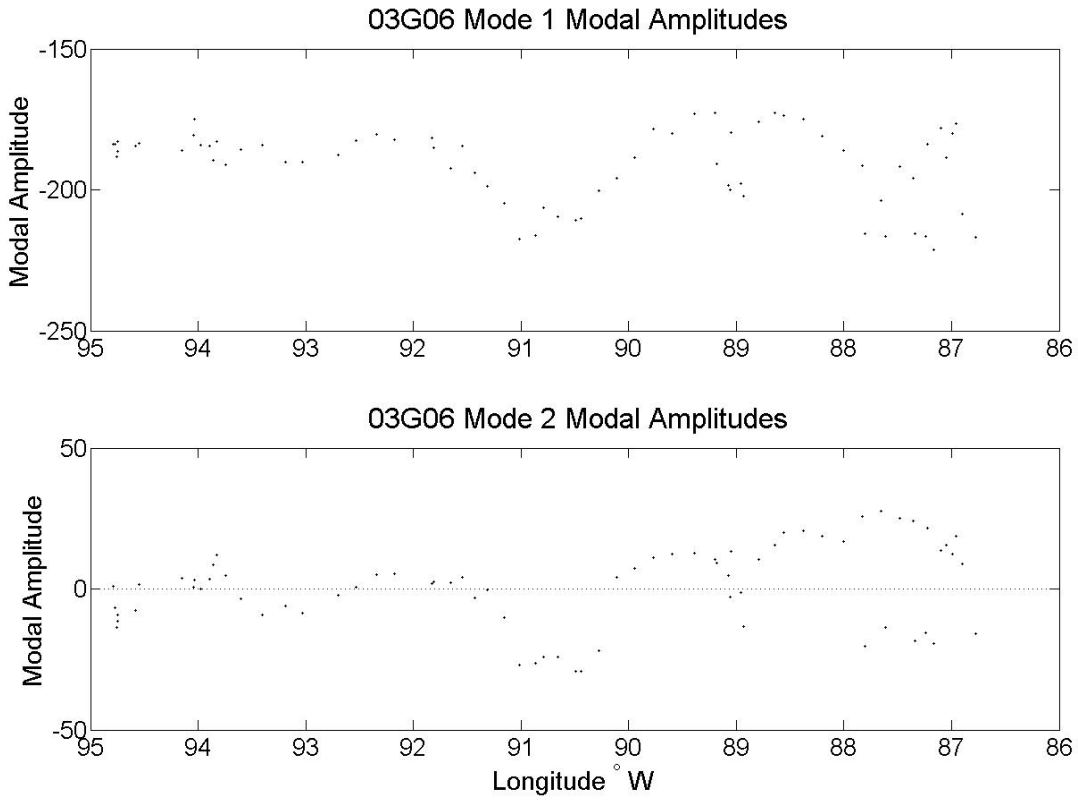

Figure 3.25 Modal amplitudes for XBT EOF calculation for 2003 cruise 03G06.

3.1.3 Summer 2003

During this cruise, the Loop Current continued to retreat towards the southeast. A Loop Current Eddy separated from the Loop Current in the last week of the cruise (Figure 3.26, Panel d). The pulling back of the Loop Current away from the escarpment began in the last week of the previous cruise. There were several cold slope eddies to the north and west of the Loop Current. In the western Gulf the LCE remnant remained but decreased in amplitude during this cruise (Figure 3.26, Panels a-d).

This cruise followed the previous cruise by about 5 days. There were several problems during the cruise that affected the area surveyed and prevented the ship from traveling east along the 1000 m isobath (Figure 3.27). This cruise was shortened due to the presence of a hurricane in the Gulf.

The cruise began by surveying in the western Gulf between 93ºW and 94ºW. However, the cruise ceased when, on June 29th, a tropical depression that had just moved into the Gulf to the northwest of the Yucatan peninsula became Tropical Storm Bill. Tropical Storm Bill traveled north across the Gulf and made landfall on June 30th in southwest Terrebonne Parish, LA. This storm interrupted the cruise, and the ship returned to Galveston for shelter. This required the rapid transit to the eastern Gulf after the storm passed.

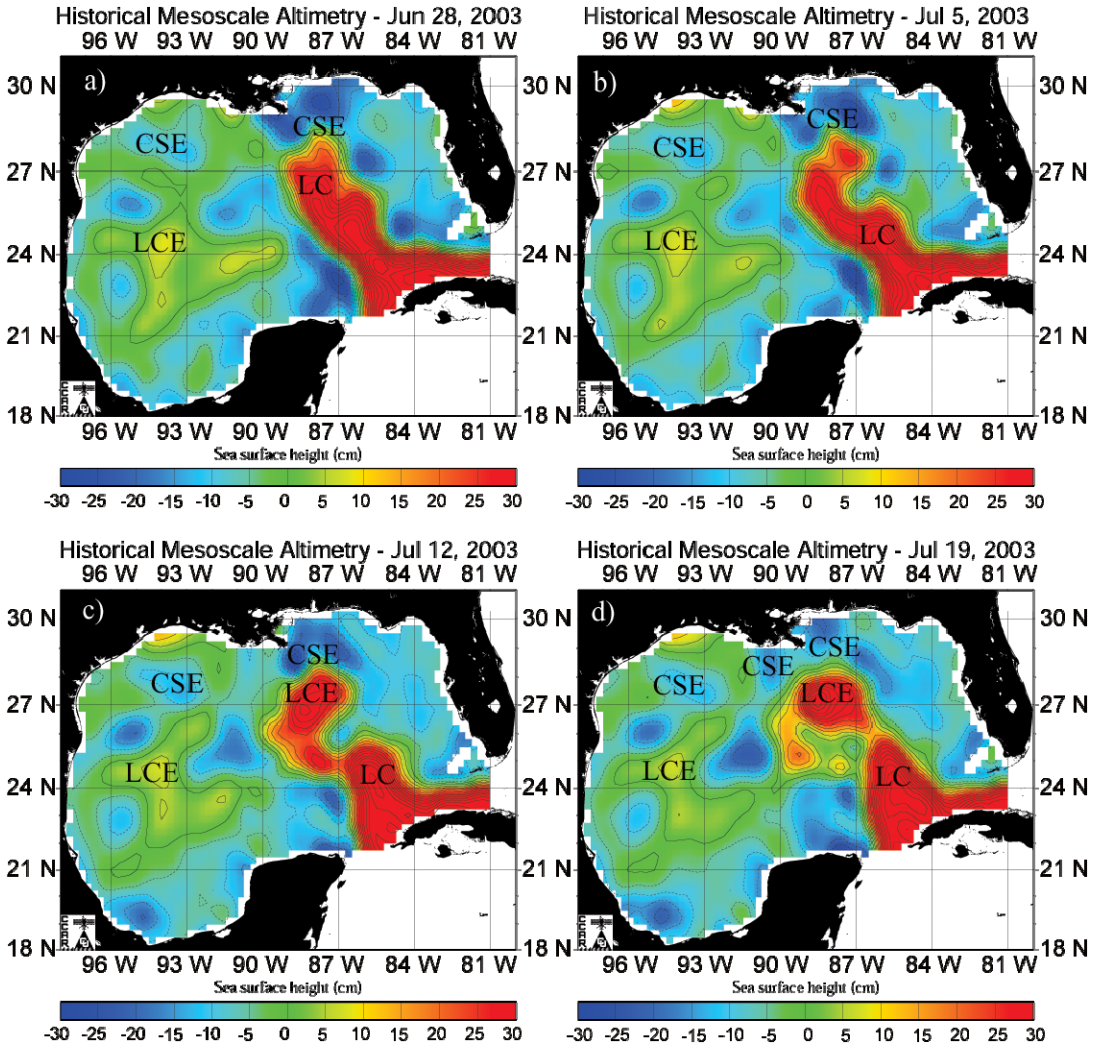

Figure 3.26 Weekly intervals of SSH during the SWSS S-tag cruise in 2003. Images downloaded from the Colorado Center for Astrodynamics Research. The SSH contour interval is 5 cm. (SSH Source: R. Leben, CCAR, Univ. of Colorado).

The *R/V Gyre* left Galveston on July 3rd and headed almost directly east across the shelf towards the 1000 m isobath near Mississippi canyon. The remainder of the cruise was spent in waters to the east of 90ºW. Tropical Storm Claudette entered the

Gulf on July 11th; becoming a hurricane and making landfall near Port O'Conner, TX on July 15th. Due to this storm the cruise was ended early, and the *R/V Gyre* made port in Pascagoula, MS (Figure 3.27).

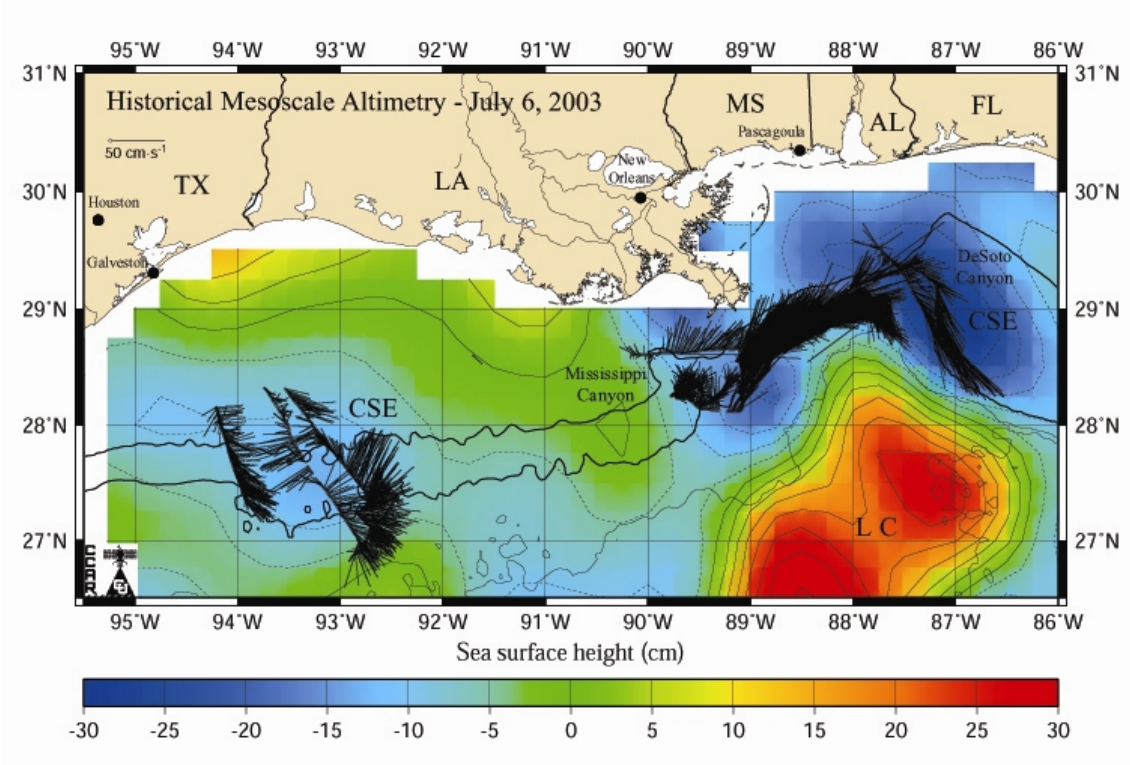

Figure 3.27 Velocity vectors during the second cruise of 2003 for the near surface (41 m) depth bin. Shown are the 200 m, 1000 m (in bold), 2000 m, and 3000 m contour lines. The SSH contour interval is 5 cm. (SSH Source: R. Leben, CCAR, Univ. of Colorado).

As the locations of the velocity vectors in Figure 3.27 indicate, the cruise track did not intersect the Loop Current or any major anticyclonic feature. On the western legs of the cruise, a CSE was centered near 28ºN, 93ºW. The velocity in this CSE reached almost 50 cm/s (Figure 3.28).

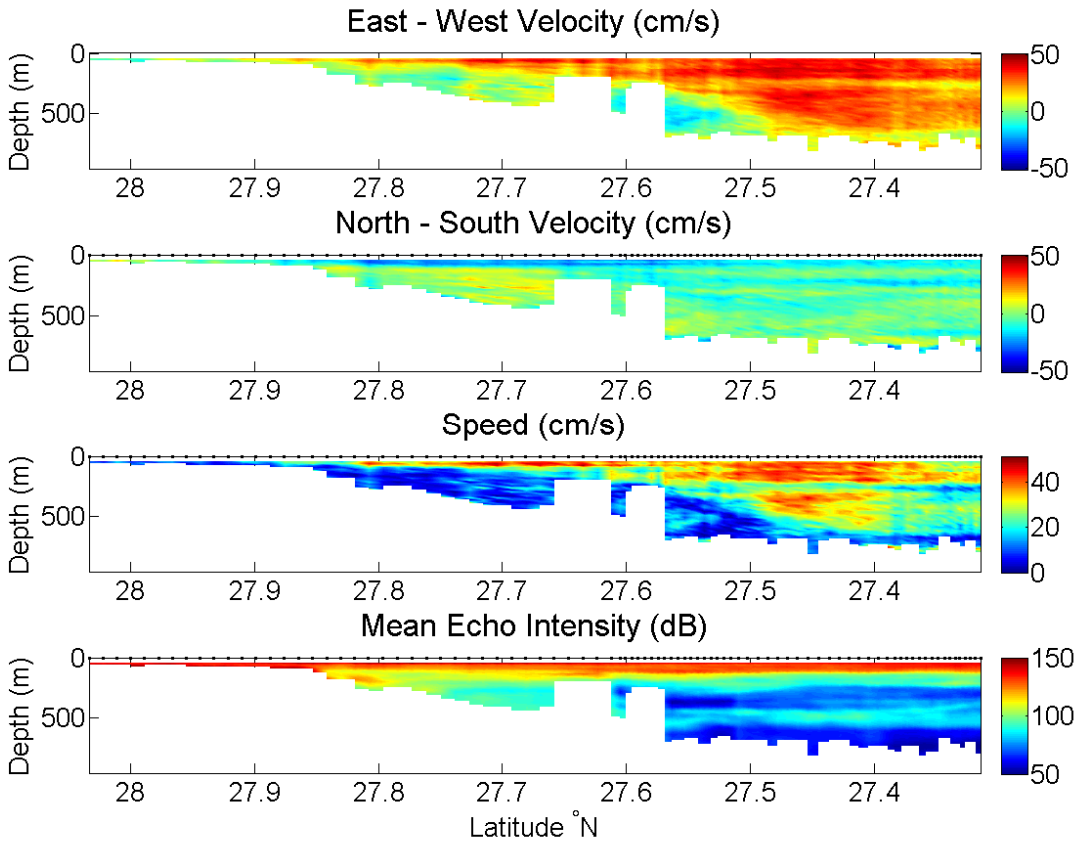

Figure 3.28 Vertical sections from the 38-kHz ADCP data for the segment straddling 94ºW in Figure 3.27. East and north component velocities are positive while west and south are negative in the upper two panels. The white space near the bottom of each panel indicates the bottom of the usable ADCP data.

The velocity section shown in Figure 3.28 reveals the presence of a cyclonic counter flow along the slope of the Sigsbee Escarpment. This section corresponds to the westernmost segment of the cruise, shown in Figure 3.27 crossing 94ºW. The counter flow appears as the northwest current velocities in the component panels and as the region of weaker flow in the speed panel (Figure 3.28). The velocity vectors in Figure

3.27 show that overlying the counter flow, and offshore from it to the depth of observation, as shown in Figure 3.28, the direction of flow was to the southeast at up to 50 cm/s. The velocity and speed exceeded 50 cm/s in this CSE across 93ºW (not shown).

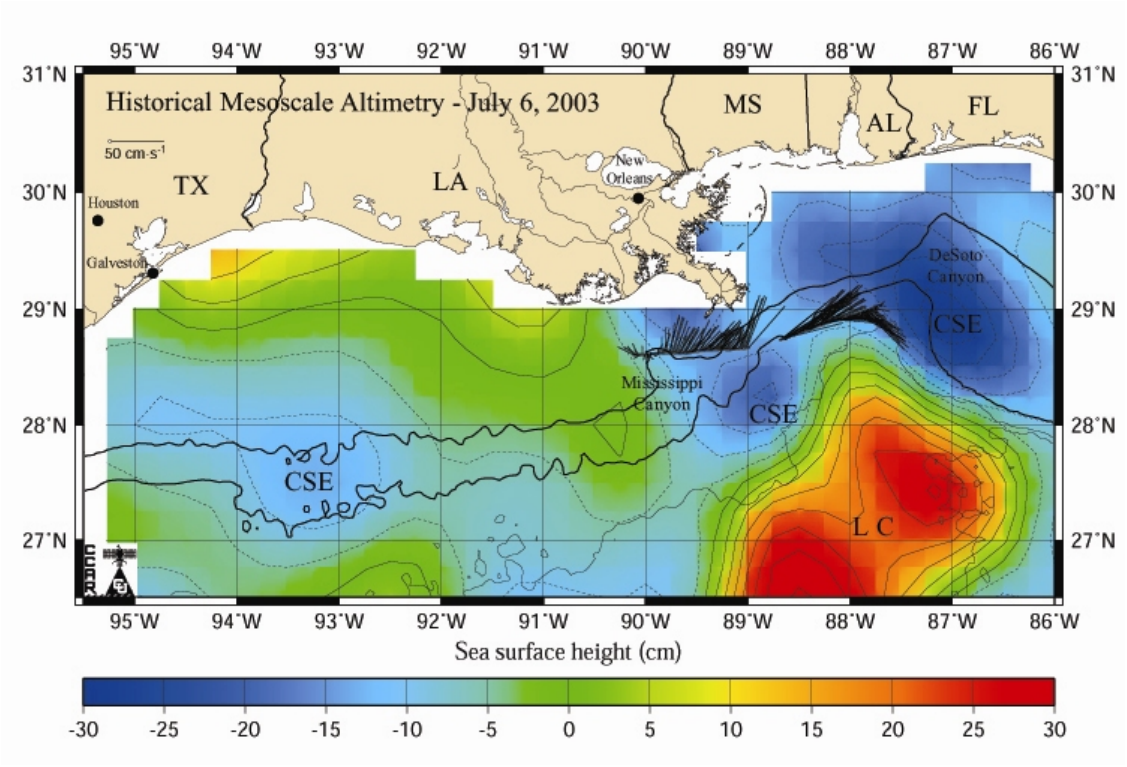

Figure 3.29 Velocity vectors after transiting across the shelf. Shown are the 200 m, 1000 m (in bold), 2000 m, and 3000 m contour lines. The SSH contour interval is 5 cm. (SSH Source: R. Leben, CCAR, Univ. of Colorado).

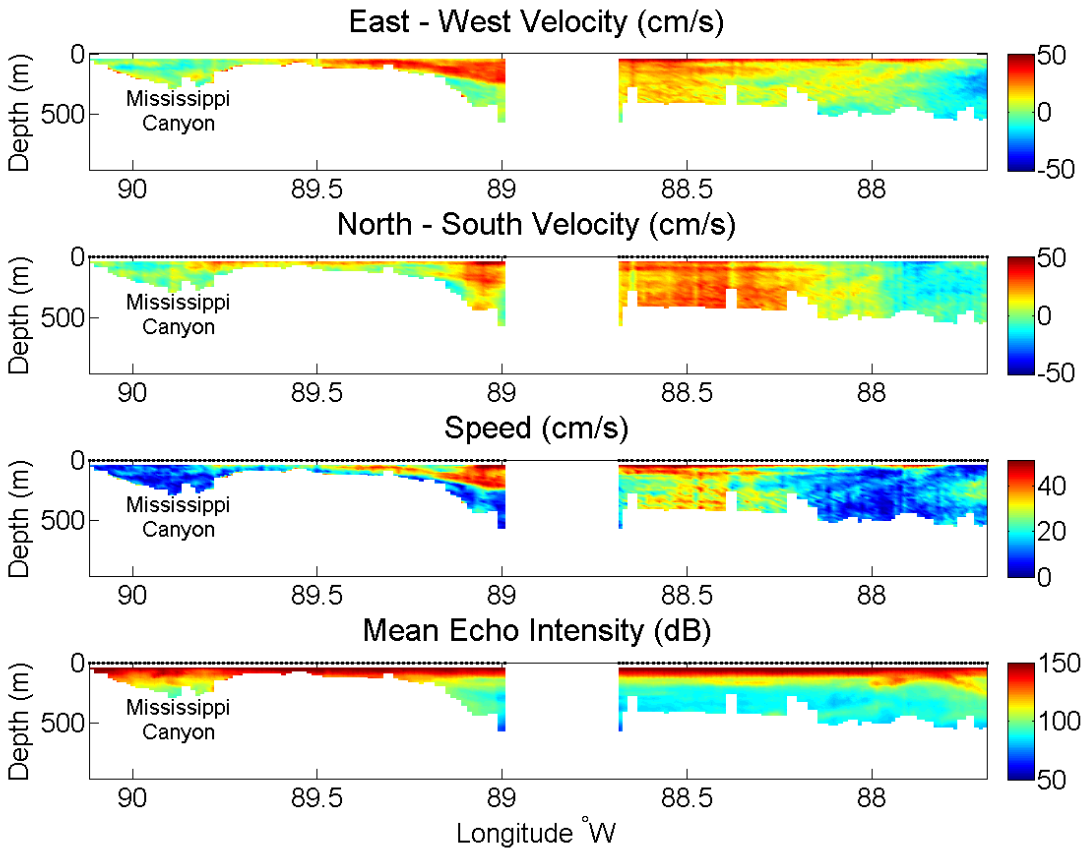

Figure 3.30 Vertical sections from the 38-kHz ADCP for the cruise track shown in Figure 3.29. East and north component velocities are positive while west and south are negative in the upper two panels. The white space near the bottom of each panel indicates the bottom of the usable ADCP data.

After the passage of Tropical Storm Bill, the *R/V Gyre* headed east across the shelf, crossing Mississippi Canyon before reaching the 1000 m isobath near 89ºW (Figure 3.29). In the CSEs observed in the eastern part of the study area between Mississippi Canyon and DeSoto Canyon, the velocity and speed were generally around 50 cm/s.

There was more evidence for the weak (~ 20 cm/s) cyclonic flow along the slope in Figure 3.30 just to the west of 89ºW. Flow in the surface waters was generally to the northeast, especially in the area north of the Loop Current. East of 88ºW the velocity vectors wrap around the Loop Current towards the southeast between the Loop Current and the CSE that was centered near 29ºN, 87ºW. The vertical section shows weaker speeds east of 88.3ºW throughout the observed depths where the velocity vectors show the change of direction. Figure 3.30 also shows the contrast between the surface-most currents and those at depth.

As can be seen in Figure 3.27 the ship spent most of the cruise between 87.5ºW and 89ºW. There were three transits across this region. The first was towards the east from July 3rd to the 6th (Figure 3.30). Not shown were a westward transit on July 7th and an eastward transit on the 11th. During the second transit, velocities were observed in excess of 50 cm/s. As the sequence in Figure 3.26 shows, the Loop Current was retreating during this cruise. The velocities for the third transit were about half of those observed in the second transit. The third transit was also farther north than the first two transits across the area.

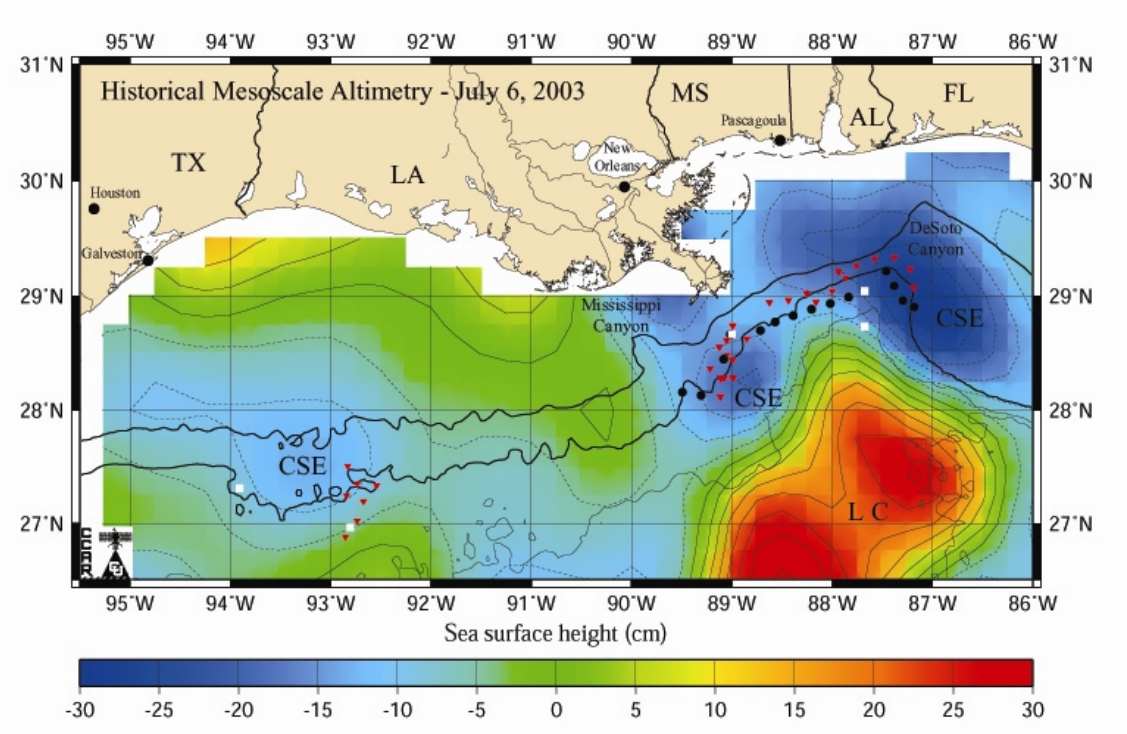

Figure 3.31 Locations of XBT and CTD stations during cruise 03G07. Black circles represent XBT stations used to create the vertical section. Red inverted triangles represent XBT stations not selected for use in the vertical section. White squares represent locations of CTD stations. Shown are the 200 m, 1000 m (in bold), 2000 m, and 3000 m contour lines. The SSH contour interval is 5 cm. (SSH Source: R. Leben, CCAR, Univ. of Colorado).

Two CTD stations and seven XBT stations were performed in the western part of the study area, but since they were so far from the main study area for this cruise they were left out of the XBT vertical section plot (Figure 3.31). Of the three CTD stations performed in the eastern part of the study area on this cruise two were suitable for geostrophic analysis. These were the eastern most stations; both were located along 87.7ºW and were separated by 31’ of latitude (Figure 3.31). The two stations proved

suitable because the station spacing was smaller than the SSH feature across which the relative velocity was calculated.

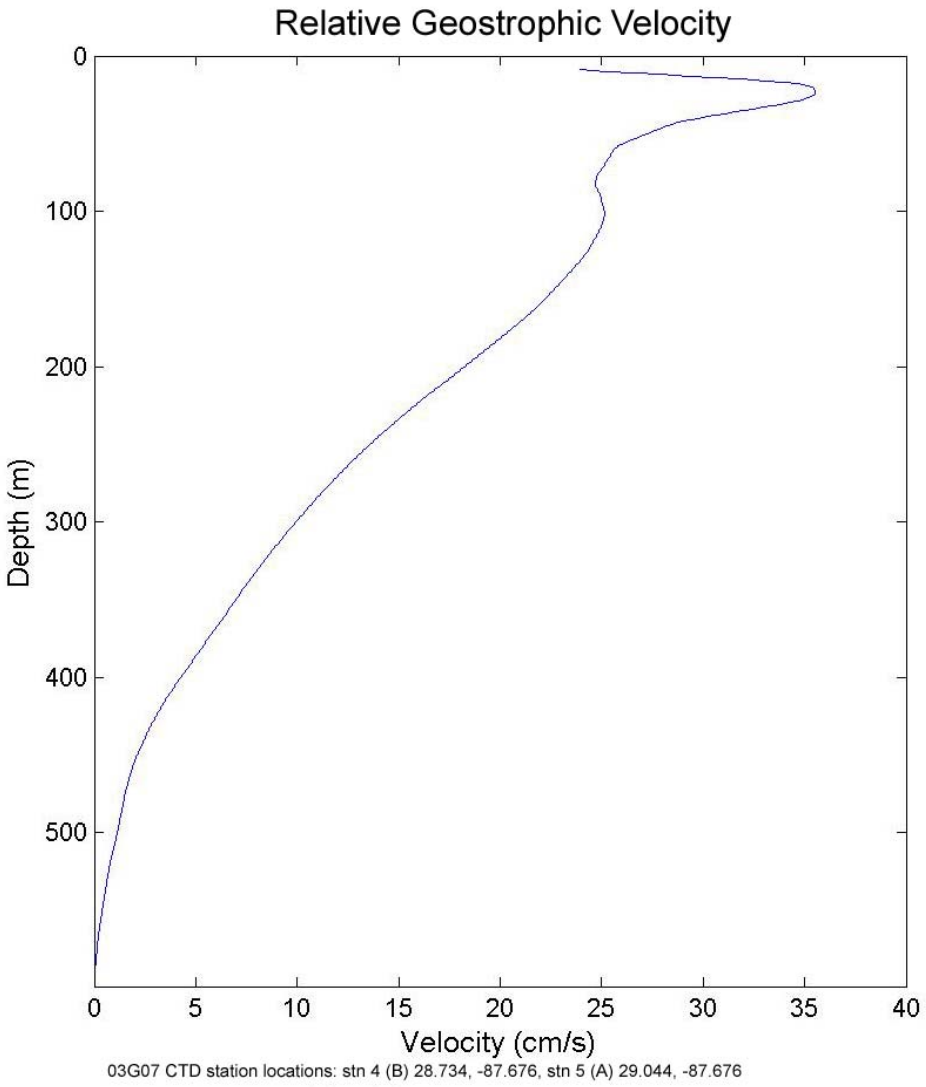

Figure 3.32 Geostrophic velocity profile for two stations during cruise 03G07.

The geostrophic velocity between these locations was a maximum of 36 cm/s at depths near 30 or 40 m. This compares well with the velocities in the east to west

component panel of Figure 3.30. Below this the velocity decreased except for a small increase at about 100 m. The zero velocity level was selected as the deepest common depth between the stations. This depth was chosen because the horizontal pressure gradient between the stations was assumed to be at the minimum there. This depth was located at about 600 m (Figure 3.32).

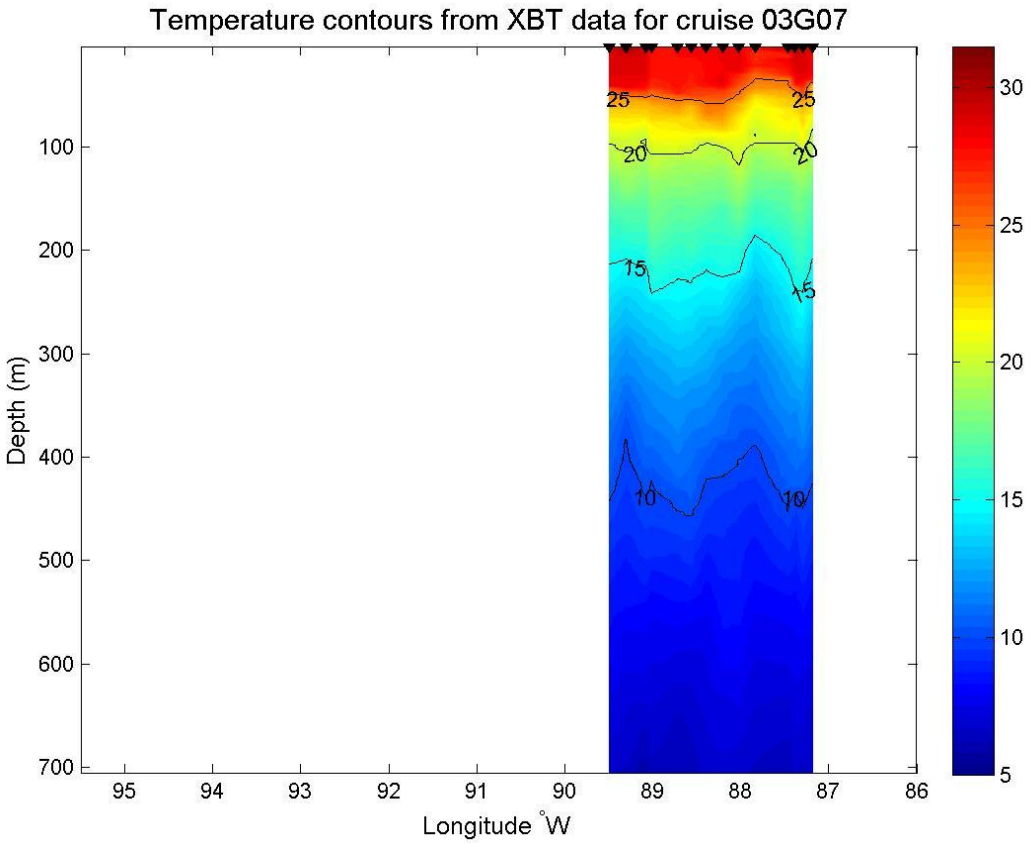

Figure 3.33 Vertical section of temperatures created from selected XBT stations shown in Figure 3.31. Black inverted triangles across the top edge represent the longitude of the XBT stations used. Temperatures are shown in Celsius. The white space on each side depicts that part of the study area not represented in the vertical section. The large area of white space in the western study area reflects the lack of data there due to curtailed operations relating from engine problems and storms.

An XBT temperature section was created for the region between 87ºW and 89.5ºW (Figure 3.33). This section shows some uplifting and some depression of isobaths related to features in the SSH field, but overall the isobaths were fairly horizontal due to the weak SSH gradients across the area. Compared to the earlier cruise that summer, the 15ºC and 10ºC isobaths were about 25-50 m deeper. This was in contrast to the previous cruise.

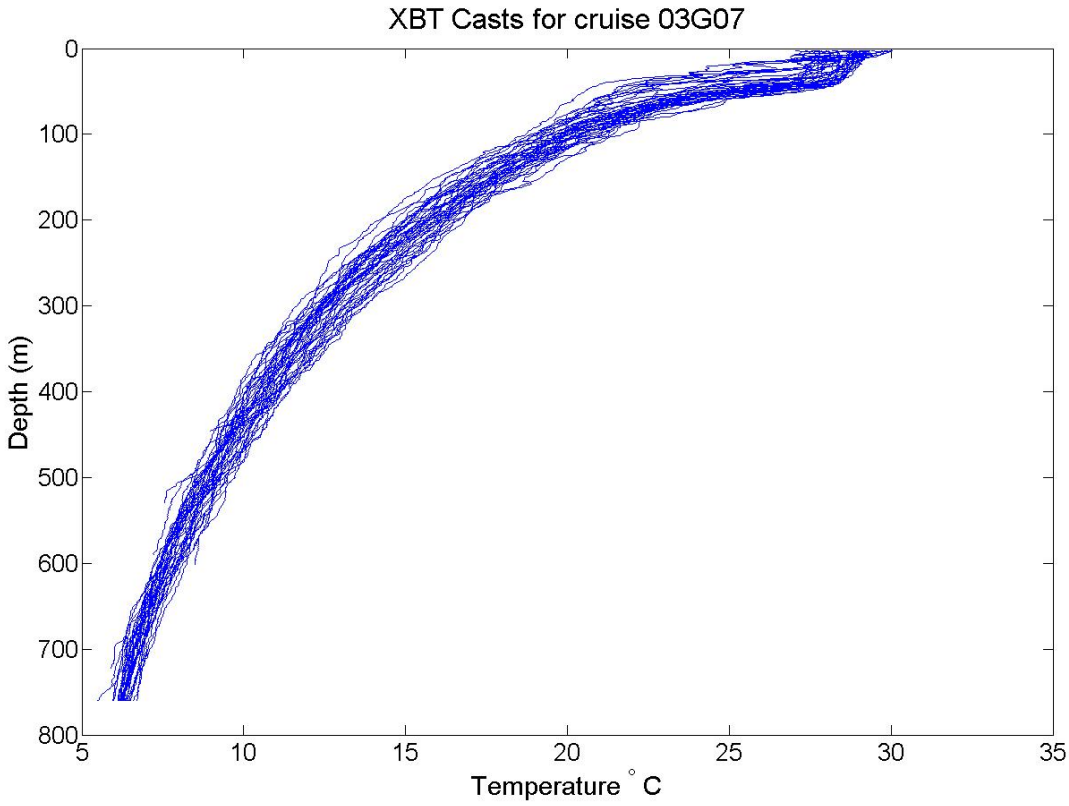

Figure 3.34 Cruise 03G07 vertical profiles of all XBT stations.

Vertical profiles for the XBT stations have less scatter in them than was previously observed. There was variability in temperature among the profiles located between 100 m and 450 m (Figure 3.34). Maximum surface temperatures were less than those of the previous cruise; however this cruise did not sample the Loop Current so this was not unexpected. The summer mixed layer was about 25 m, which was consistent with the previous cruises.

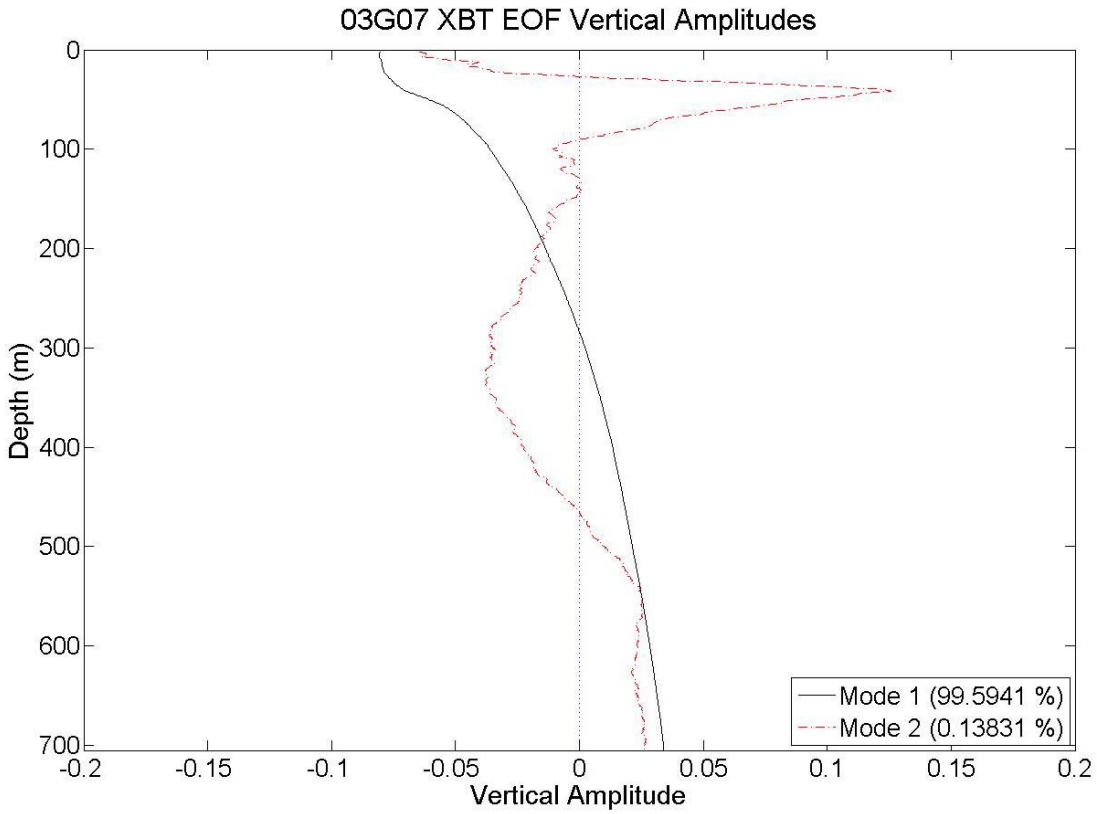

Figure 3.35 Vertical profile showing XBT EOF vertical mode amplitudes during 2003 cruise 03G07.

The results of the EOF analysis on the XBT data from this cruise were shown in Figures 3.35 and 3.36. The EOF vertical amplitudes (Figure 3.35) and modal amplitudes

(Figure 3.36) for the XBT stations from this cruise were similar to the previous cruises. The percent variances were more similar to the 2002 cruise than they were to the first 2003 cruise. Mode 1 contains over 99.5% of the variance, was surface intensified, and decays with depth. Mode 1 was very similar to both of the other cruises. Mode 2 contains structure at 50 m not seen in the previous cruises, as well as the variability previously seen between 100 m and 450 m.

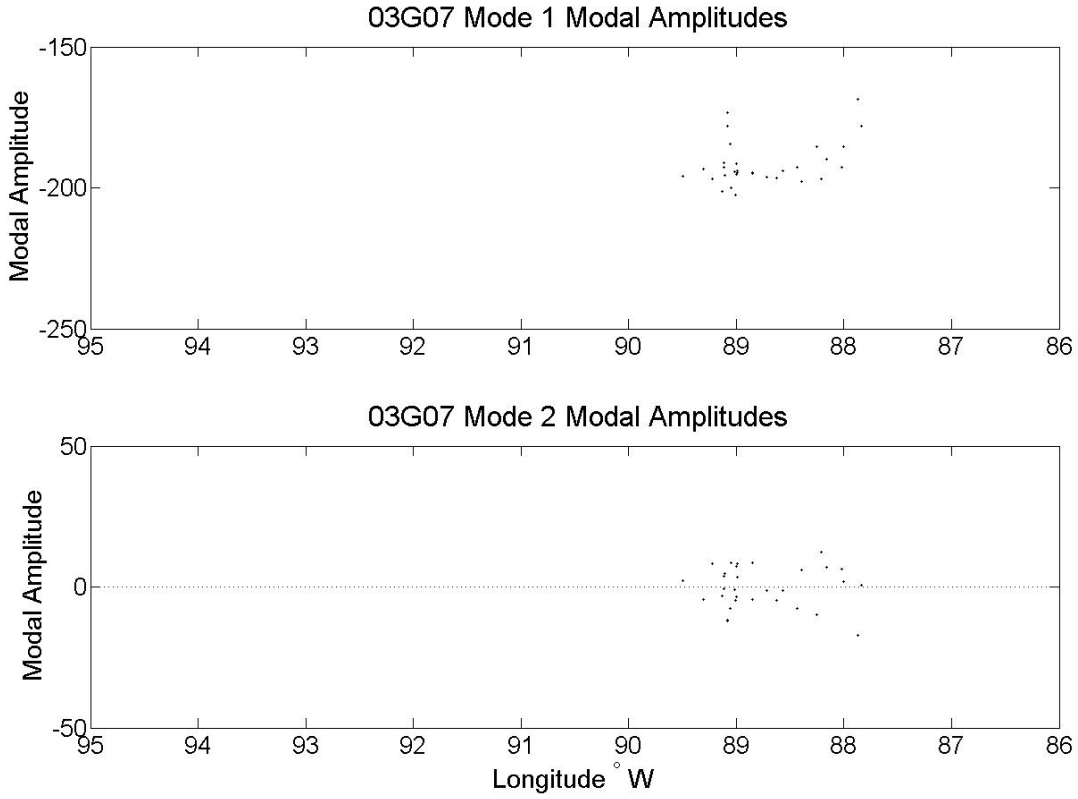

Figure 3.36 Modal amplitudes for XBT EOF calculation for 2003 cruise 03G07.

3.1.4 Summer 2004 Cruise 04G05, May 25 – June 18

A sequence of SSH images spanning the cruise appear in Figure 3.37. During the cruise the Loop Current remained south of 27ºN and east of 89ºW, therefore direct influence on the study area did not occur. Since the Loop Current was not present in the study area, the SSH field resembles the 2002 cruise more than either of the cruises in 2003. The Loop Current did not appreciably change appearance in the SSH sequence (Figure 3.37).

The sequence of SSH images shows a remnant LCE slowly moving westward centered southwest of 24ºN, 93ºW and slowly moving westward. There was a poorly resolved WSE to the northwest of this LCE. The SSH field suggests that this WSE might be connected to the LCE. This WSE became more defined by the end of the cruise and was centered near 26ºN, 95ºW, (Figure 3.37, Panel d).

In the study area, the SSH field was composed of cyclonic and anticyclonic features in a synclinal pattern with the anticyclonic features near shore and the cyclonic features arcing around them from Galveston to the Florida panhandle. This synclinal formation broke up during the cruise, as shown in the lower panels (c and d) of Figure 3.37. The CSE north of the Loop Current separated into two pieces during the cruise. The western CSE of this pair was observed during the cruise (Figure 3.38 and 3.39).

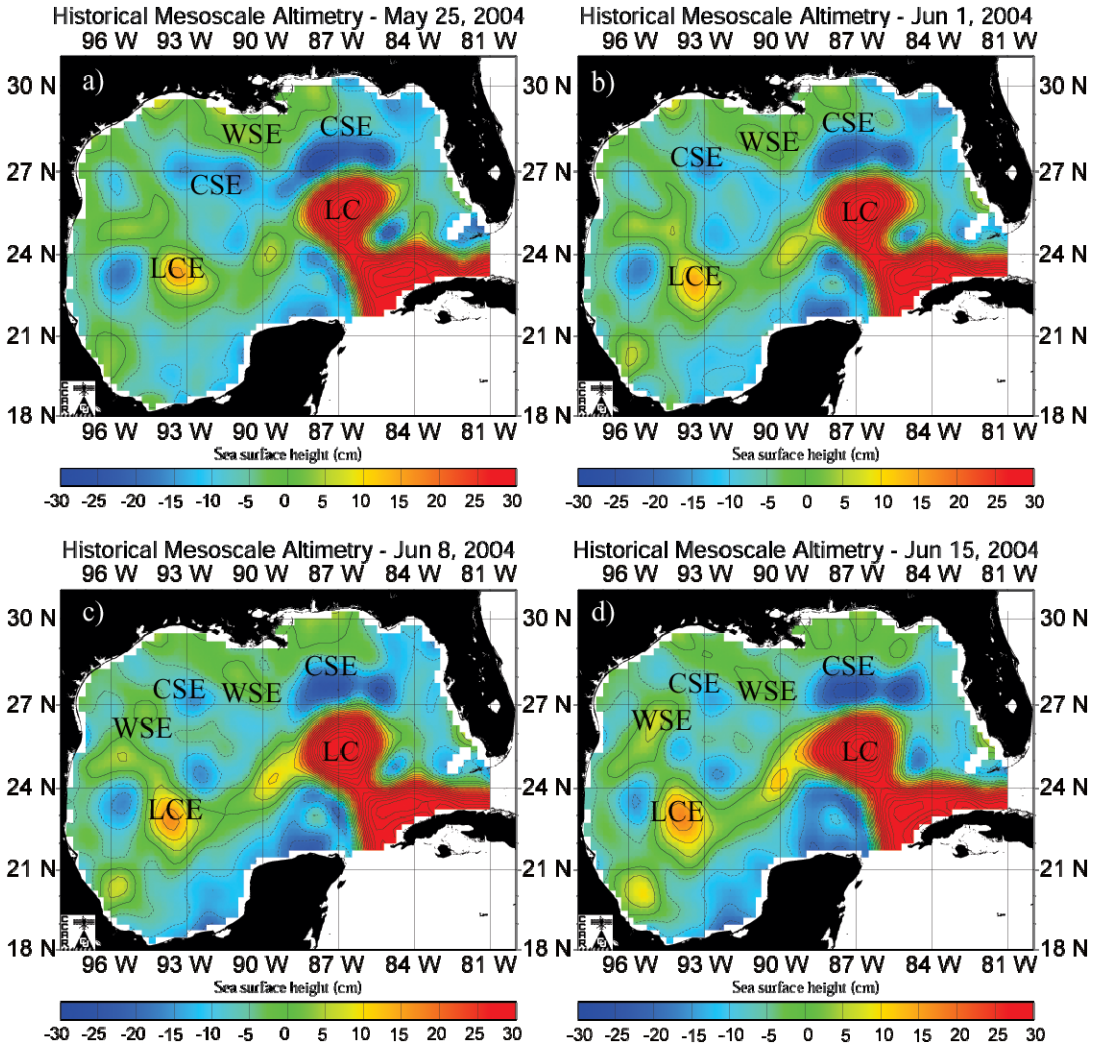

Figure 3.37 Weekly intervals of SSH during the SWSS S-tag cruise in 2004. Images downloaded from the Colorado Center for Astrodynamics Research. The SSH contour interval is 5 cm. (SSH Source: R. Leben, CCAR, Univ. of Colorado).

The western part of the study area did not begin as far west. The *R/V Gyre* traveled to 27.5ºN, 93.5ºW before tracking eastward along the 1000 m isobath. ADCP data for this cruise included both 150-kHz and 38-kHz frequencies.

Comparing Figures 3.38 (150-kHz) and 3.39 (38-kHz) with Figures 3.2, 3.14, and 3.27, it was clear that the velocities observed during this summer were, in general, weaker than during 2003 and more like those observed in 2002. The near surface velocity vectors from the 150-kHz (11 m) and 38-kHz (41 m) instruments showed similar patterns, but with slightly weaker magnitudes at the deeper level. The strongest velocities were associated with the WSE centered near 28ºN, 91ºW and with the edge of the CSE near 87ºW.

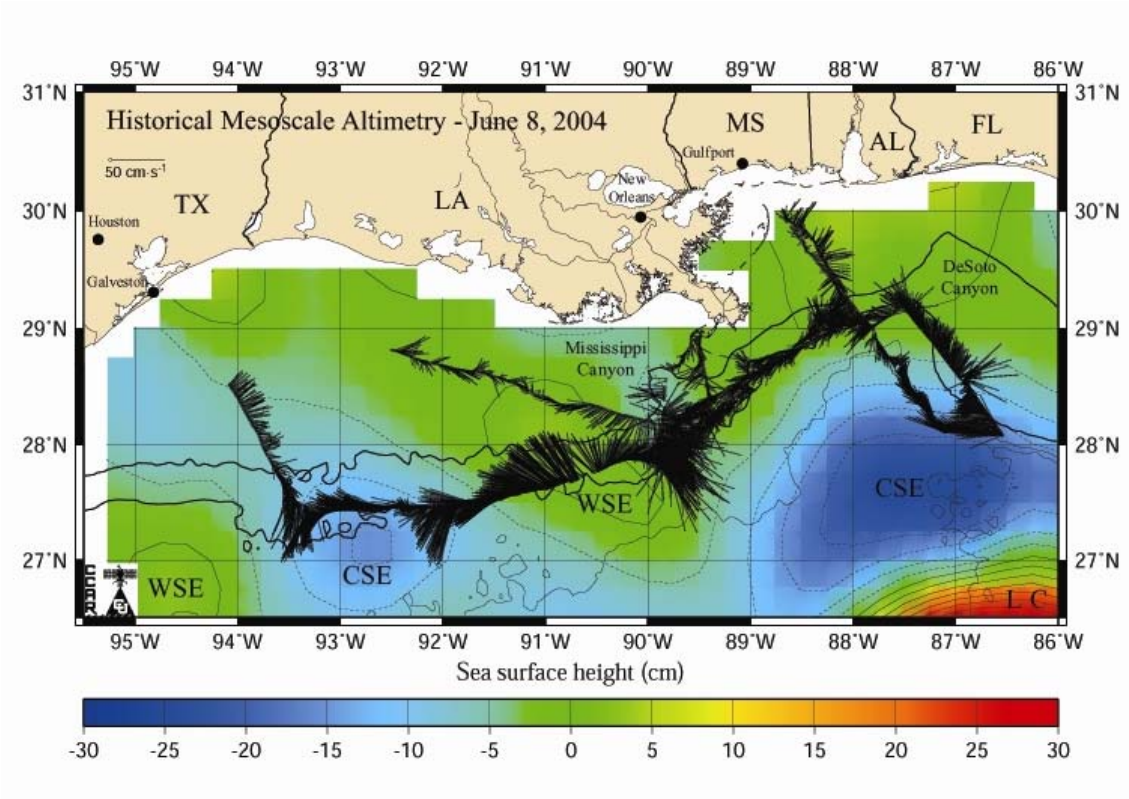

Figure 3.38 Velocity vectors during 2004 for the near surface 150-kHz (11m) depth bin. Shown are the 200 m, 1000 m (in bold), 2000 m, and 3000 m depth contours. The SSH contour interval is 5 cm. (SSH Source: R. Leben, CCAR, Univ. of Colorado).

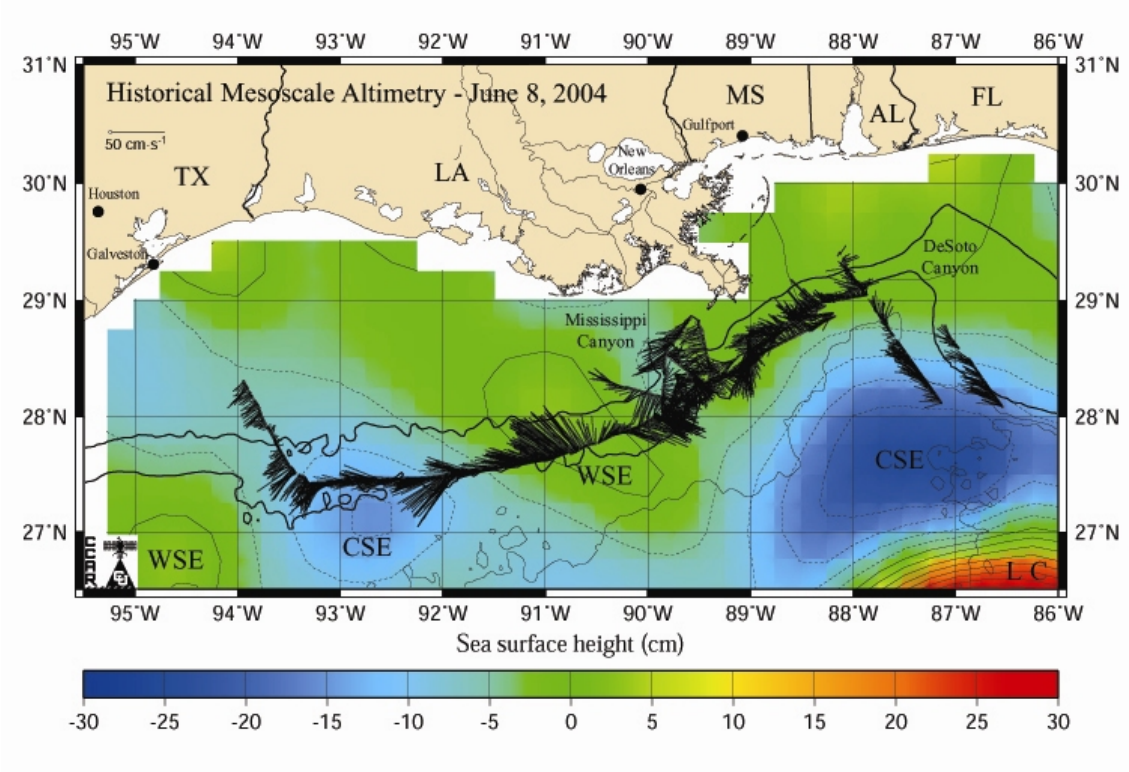

Figure 3.39 Velocity vectors during 2004 for the near surface 38-kHz (41m) depth bin. Shown are the 200 m, 1000 m (in bold), 2000 m, and 3000 m depth contours. The SSH contour interval is 5 cm. (SSH Source: R. Leben, CCAR, Univ. of Colorado).

The velocity vectors from the 150-kHz ADCP, during the eastward transit along the 1000 m isobath, show higher velocities west of 89.5ºW that were associated with the CSE and WSE. Weaker currents were observed to the east of 89.5ºW (Figure 3.40).

The 150-kHz ADCP vertical section shows that most of the flow was towards the west in the upper 250 m, except near the eastern edge of the WSE (Figure 3.41). The velocities exceeded 50 cm/s between the CSE and WSE near 92ºW and speeds were generally above 40 cm/s for much of the upper 200 m.

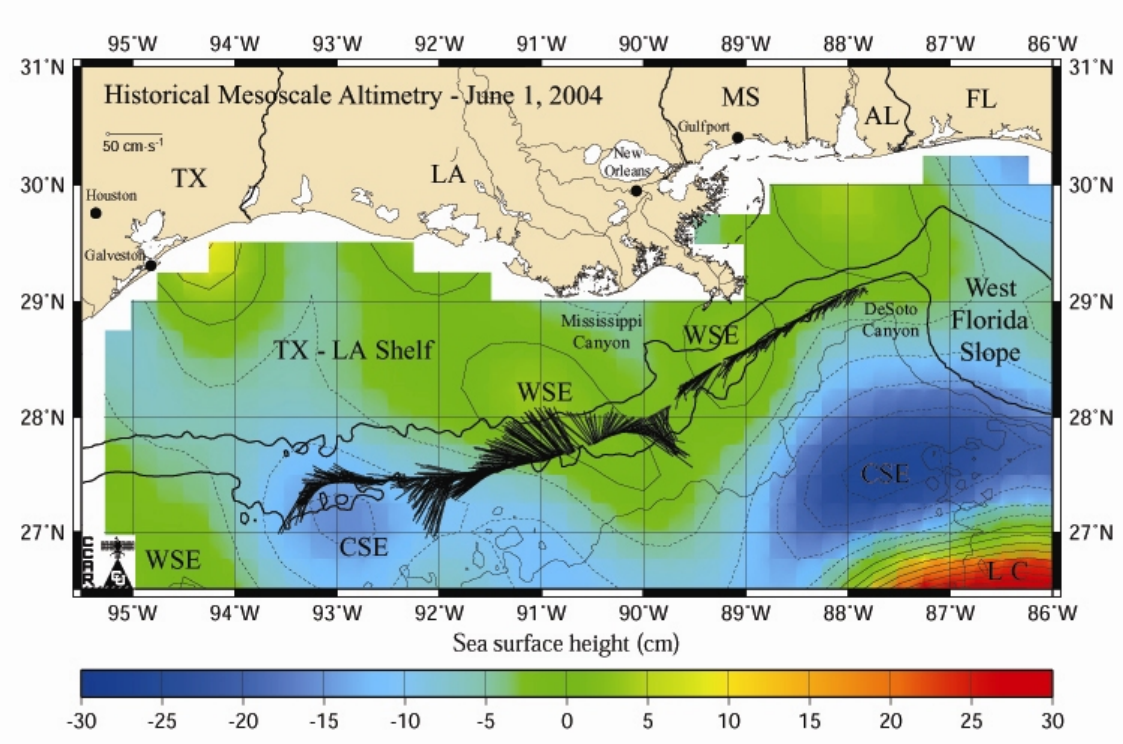

Figure 3.40 Location of transect for 150-kHz vertical section shown in Figure 3.41 showing velocity vectors m in cm/s at 10 m. Shown are the 200 m, 1000 m (in bold), 2000 m, and 3000 m depth contours. The SSH contour interval is 5 cm. (SSH Source: R. Leben, CCAR, Univ. of Colorado).

In the outer band of the WSE speeds over 50 cm/s were observed, but only in the upper 150 m. In the center of the WSE, just to the east of 90.5ºW, the observed speeds were less than 10 cm/s.

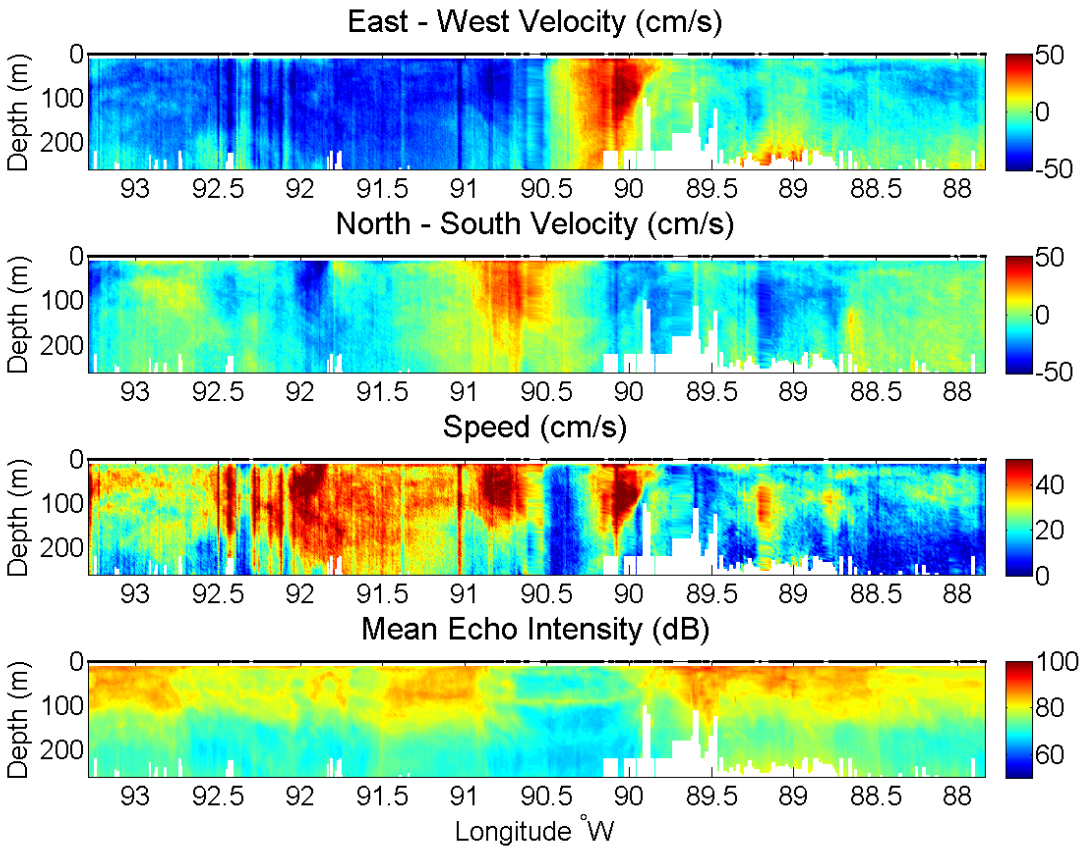

Figure 3.41 Vertical sections from the 150-kHz ADCP data for the segment shown in Figure 3.40. East and north component velocities are positive while west and south are negative in the upper two panels. The white space near the bottom of each panel indicates the bottom of the usable ADCP data.

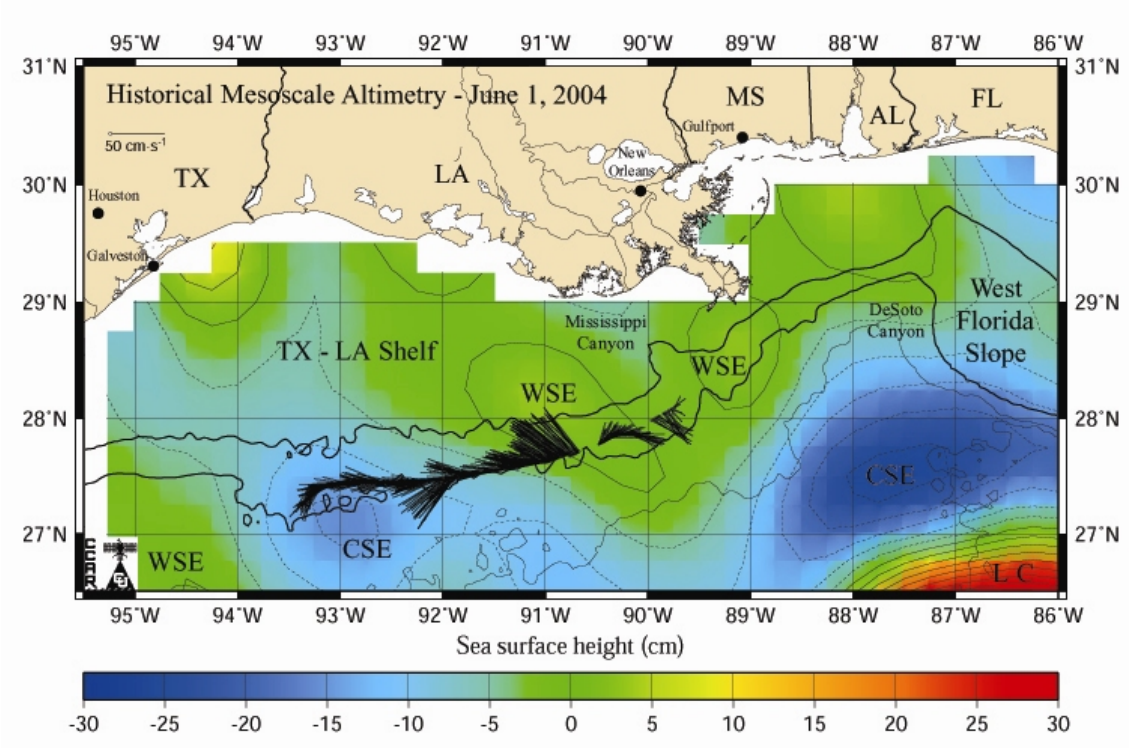

Figure 3.42 Location of transect for 38-kHz vertical section shown in Figure 3.43 showing vector velocity vectors in cm/s at 41 m. Shown are the 200 m, 1000 m (in bold), 2000 m, and 3000 m depth contours. The SSH contour interval is 5 cm. (SSH Source: R. Leben, CCAR, Univ. of Colorado).

The 38-kHz ADCP velocity vector transect does not extend as far as the 150-kHz transect. The directions of the 38-kHz velocity vectors agree with the 150-kHz velocity vectors except with slightly reduced magnitudes due to attenuation with depth (Figure 3.42). The vertical sections were also quite similar to those of the 150-kHz ADCP data, but extend to almost 800 m in some areas (Figure 3.43).

The flow was mostly westward in the upper 600 m and generally less than 50 cm/s except in the same areas as described for the 150-kHz data. There were more gaps in the 38-kHz data, but the WSE can still be identified by the low central speed

surrounded by the two regions of higher flow in the upper 150 m between 90ºW and 90.5ºW.

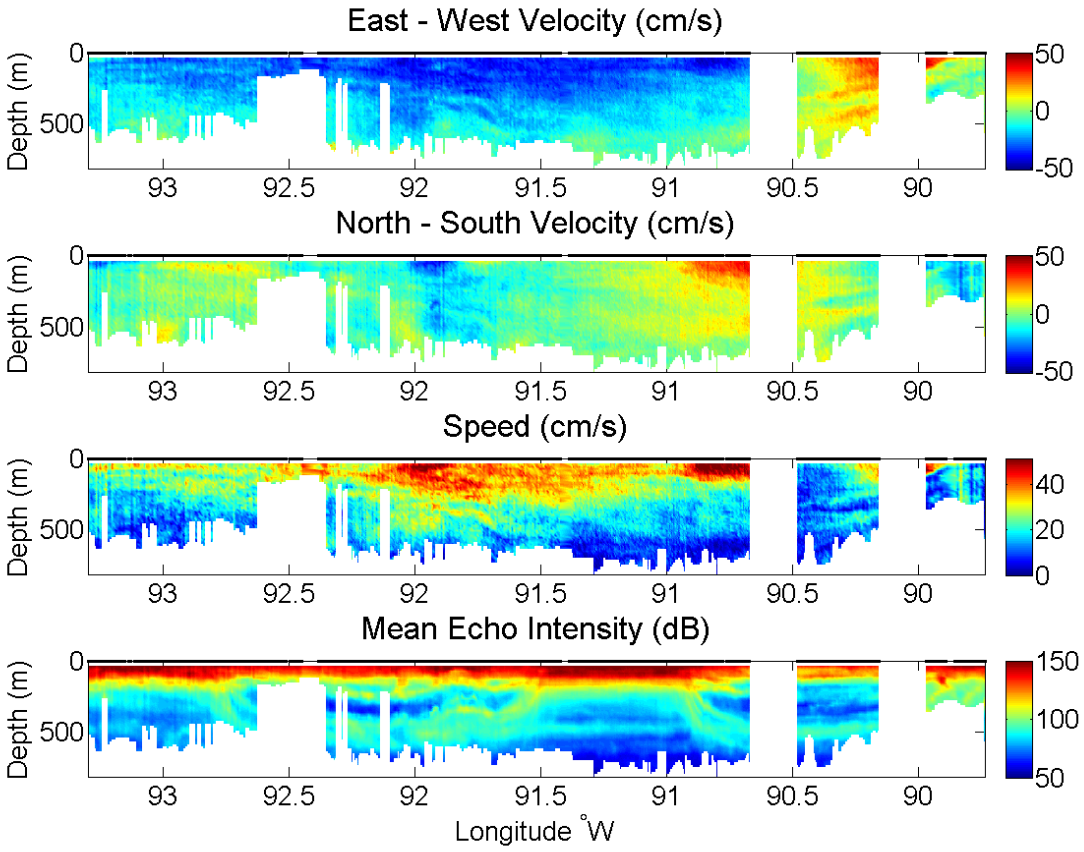

Figure 3.43 Vertical sections from the 38-kHz ADCP data for the segment shown in Figure 3.42. East and north component velocities are positive while west and south are negative in the upper two panels. The white space near the bottom of each panel indicates the bottom of the usable ADCP data.

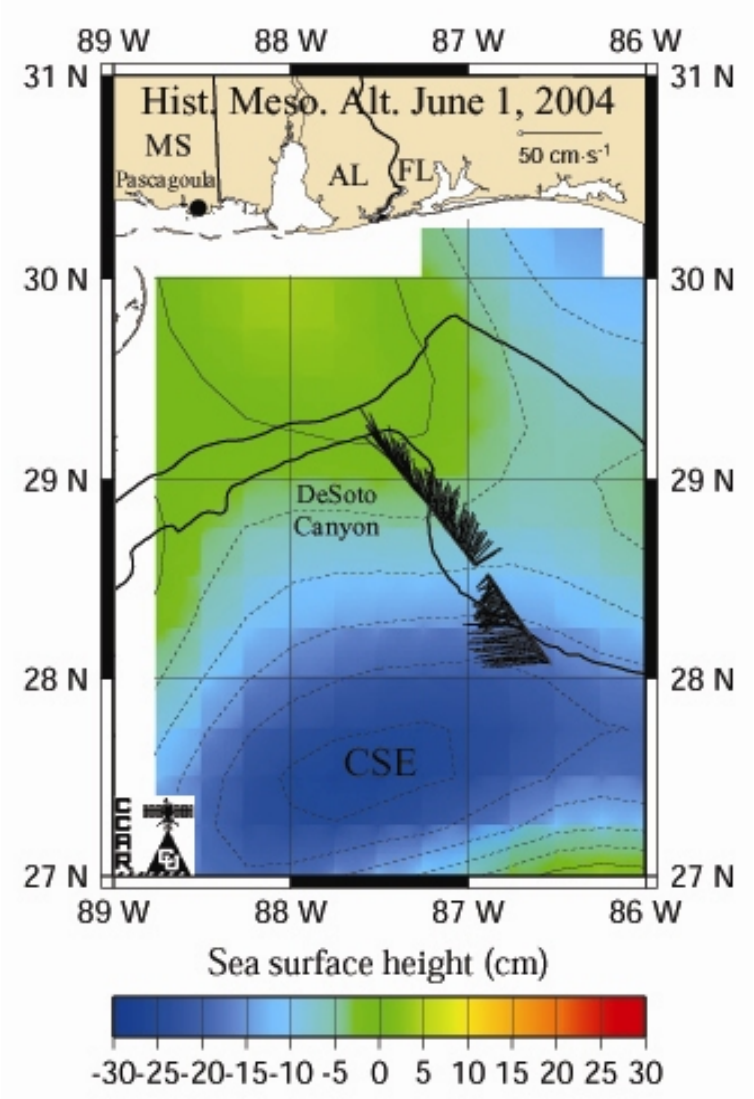

Figure 3.44 Location of transect for 150-kHz vertical section shown in Figure 3.45 showing velocity vectors in cm/s at 10 m. Shown are the 200 m, 1000 m (in bold), 2000 m, and 3000 m depth contours. The SSH contour interval is 5 cm. (SSH Source: R. Leben, CCAR, Univ. of Colorado).

The eastern end of the cruise passed through the CSE that was north of the Loop Current. This was shown in Figure 3.44 for data collected by the 150-kHz ADCP. The vertical section, shown in Figure 3.45, for this segment shows higher speeds, close to 50

cm/s, between 28.15ºN and 28.20ºN, at depths of 100 -200 m. This mid-depth velocity maximum was rather unusual since higher velocities were usually observed near the surface (Figure 3.45). The depth and magnitude of theses currents would qualify them as subsurface jets as defined by DiMarco et al. (2004). The 38-kHz ADCP data do not provide any additional information regarding this subsurface flow maximum and were not shown here.

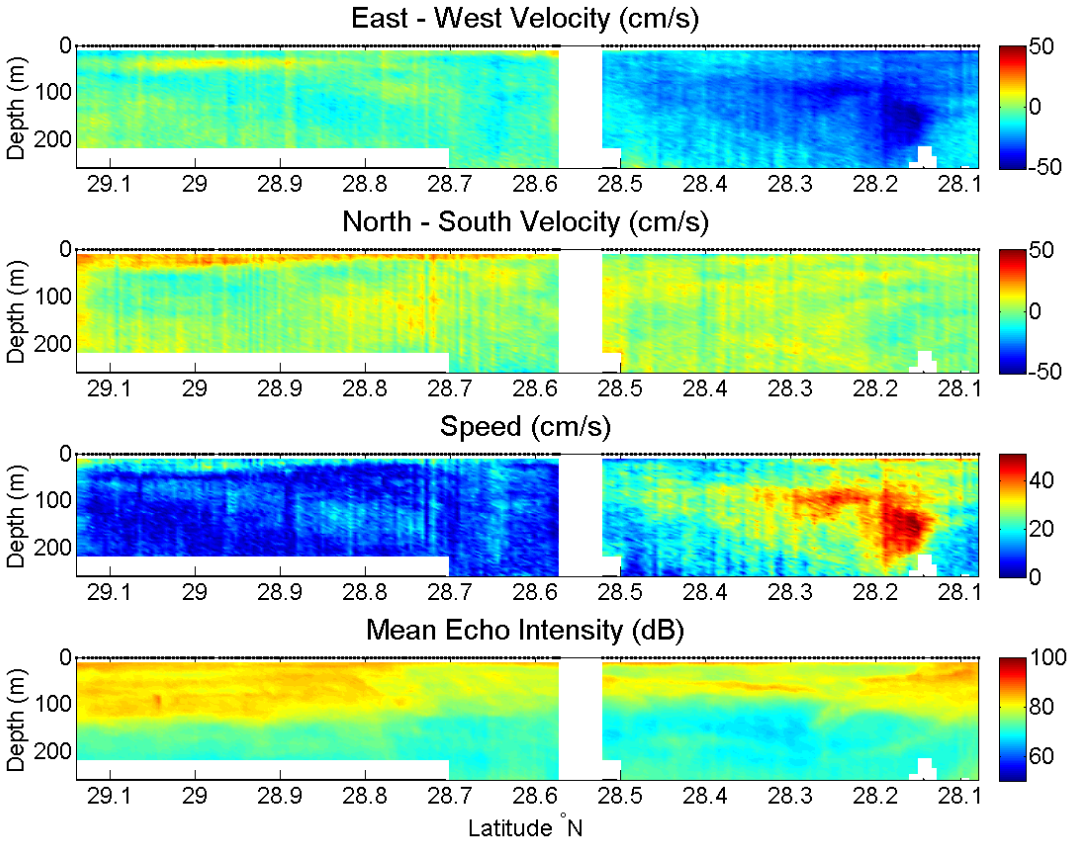

Figure 3.45 Vertical sections from the 150-kHz ADCP data for the segment shown in Figure 3.43. East and north component velocities are positive while west and south are negative in the upper two panels. The white space near the bottom of each panel indicates the bottom of the usable ADCP data.

Towards the end of the cruise the *R/V Gyre* traveled close to the southwest pass shipping channel of the Mississippi River. At this time in the cruise the SSH field had changed, and the track crossed a small CSE forming in the vicinity of Mississippi Canyon (Figure 3.46). Velocities near the southern end of this cruise track were close to 50 cm/s with the flow being primarily towards the east. The currents were less than 20 cm/s on the shelf close to the Mississippi River balize delta (Figures 3.46 - 3.49).

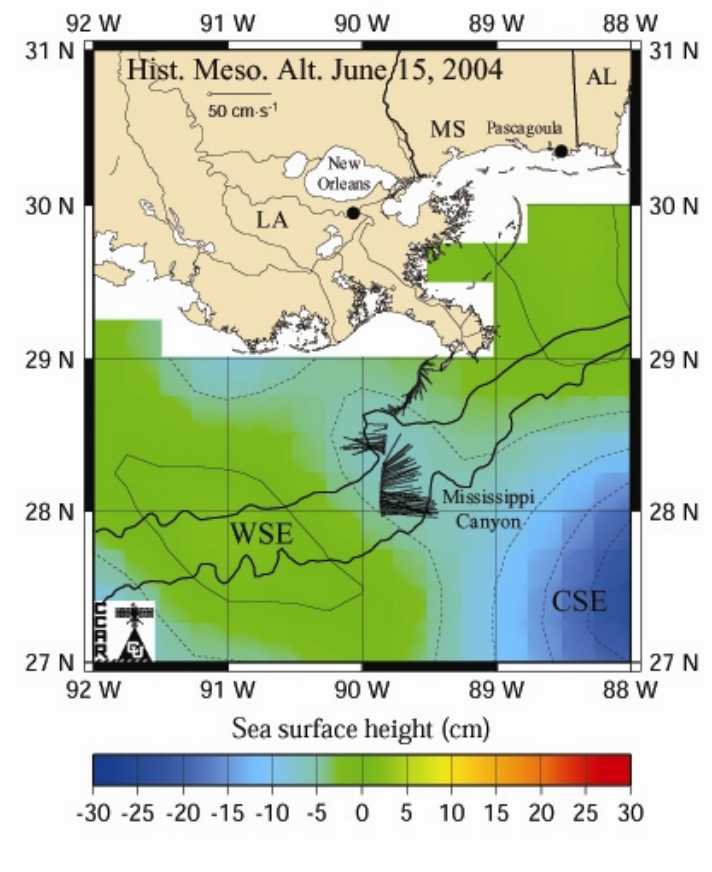

Figure 3.46 Location of transect for 150-kHz vertical section shown in Figure 3.47 showing velocity vectors in cm/s at 10 m. Shown are the 200 m, 1000 m (in bold), 2000 m, and 3000 m depth contours. The SSH contour interval is 5 cm. (SSH Source: R. Leben, CCAR, Univ. of Colorado).

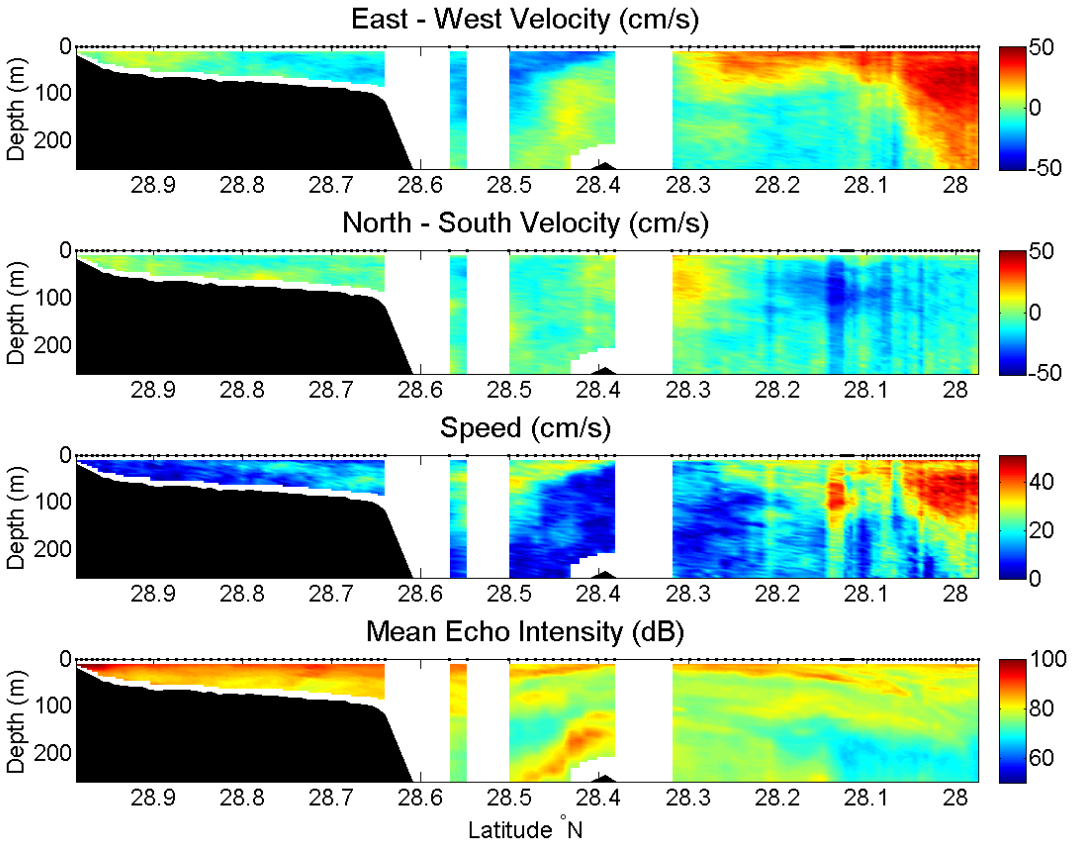

Figure 3.47 Vertical sections from the 150-kHz ADCP data for the segment shown in Figure 3.46. East and north component velocities are positive while west and south are negative in the upper two panels. The white space near the bottom of each panel indicates the bottom of the usable ADCP data.

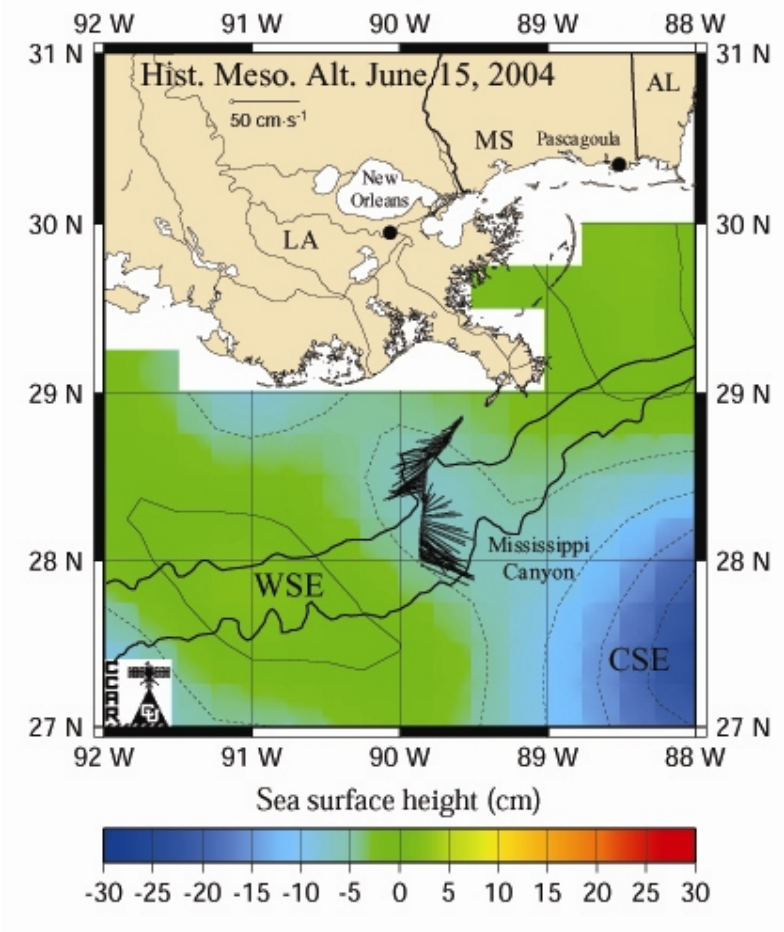

Figure 3.48 Location of transect for 38-kHz vertical section shown in Figure 3.49 showing velocity vectors in cm/s at 41 m. Shown are the 200 m, 1000 m (in bold), 2000 m, and 3000 m depth contours. The SSH contour interval is 5 cm. (SSH Source: R. Leben, CCAR, Univ. of Colorado).

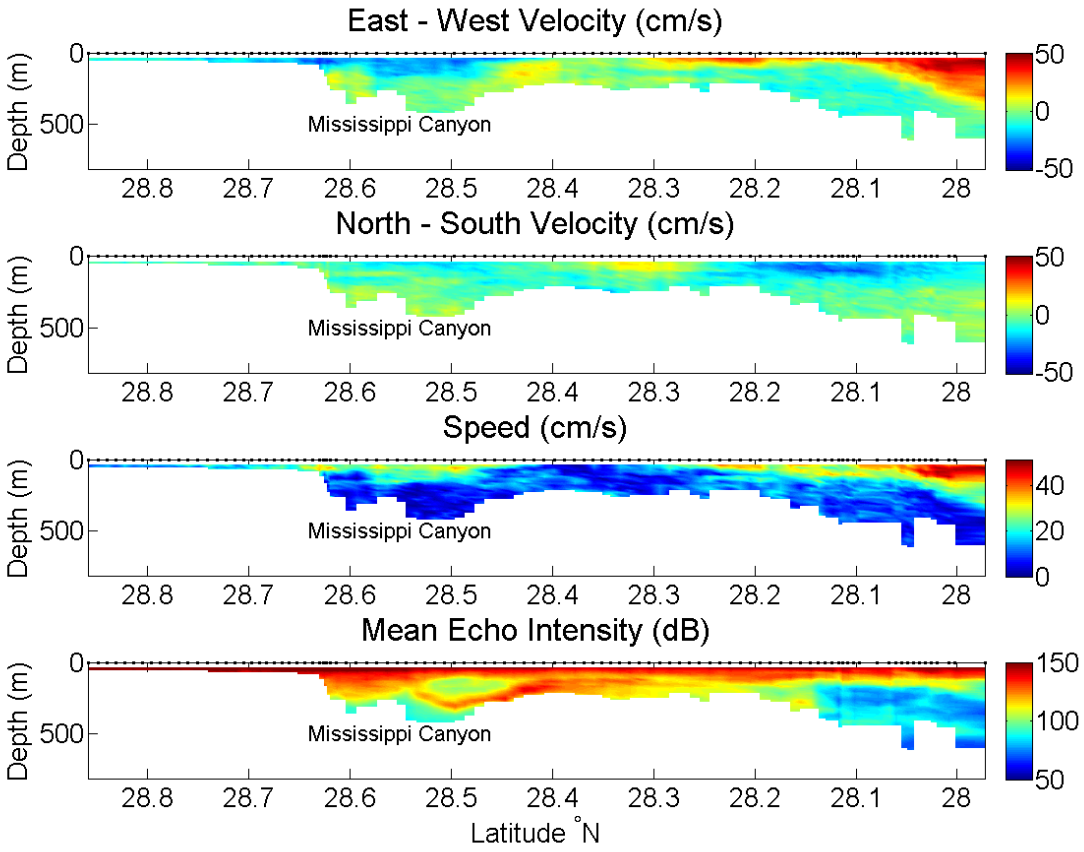

Figure 3.49 Vertical sections from the 38-kHz ADCP data for the segment shown in Figure 3.48. East and north component velocities are positive while west and south are negative in the upper two panels. The white space near the bottom of each panel indicates the bottom of the usable ADCP data.

Figure 3.50 shows the sites of the XBT and CTD stations that were carried out during the cruise. The CTD station spacing was larger than the SSH features, and therefore the geostrophic analysis did not yield useful results. A vertical section was created along the 1000 m isobath from the XBT stations to detail the temperature structure (Figure 3.51).

In Figure 3.51, the temperature structure does not show the presence of the CSE centered near 92.5ºW very well. A couple of stations were located in the edge of the CSE, but only some of the near-surface isotherms, west of 92ºW, slope upwards. The WSE was clearly represented by the downturned isotherms around 90.5ºW. Some of the isotherms appear to be depressed by almost 100 m.

The small CSE in Mississippi Canyon (Figures 3.46 and 3.48) was manifested in the temperature structure of Figure 3.51 by the uplifted 20ºC and 22ºC isotherms at 89.5ºW. To the east of this CSE, most stations were located across an area of almost constant SSH. The near-surface isotherms were essentially horizontal between 87ºW and 89ºW. The last four stations were located in the CSE, north of the Loop Current, and the isotherms were uplifted at all depths along the eastern edge of Figure 3.51.

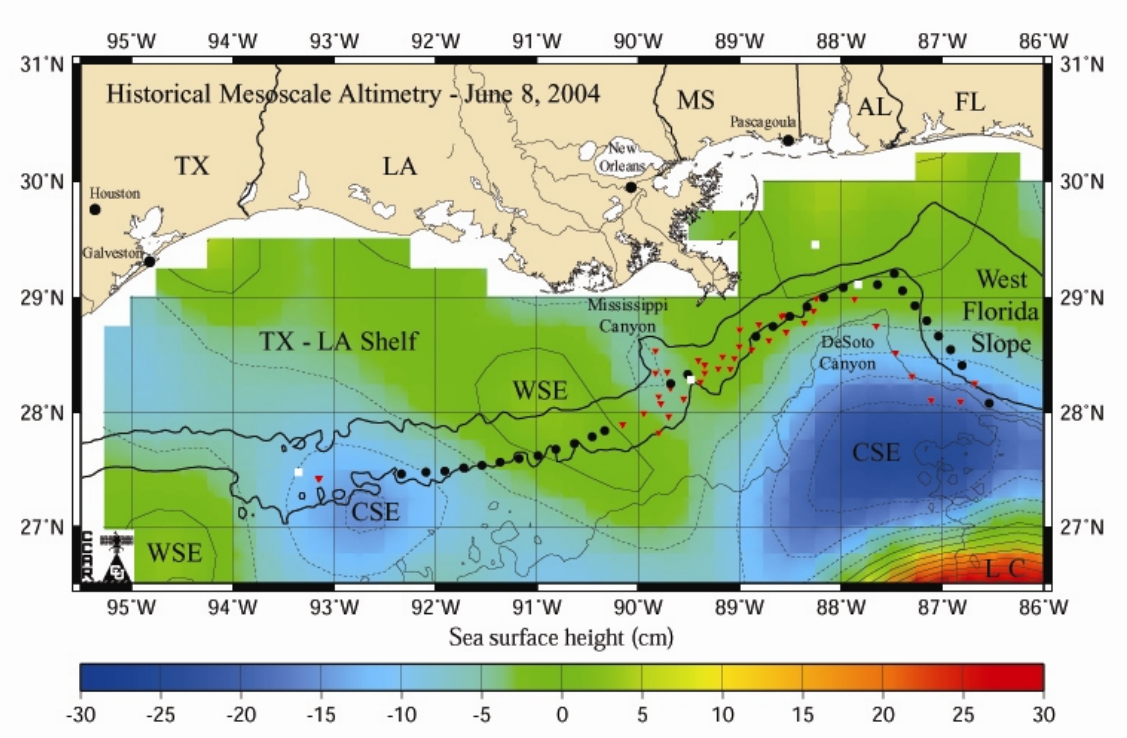

Figure 3.50 Locations of XBT and CTD stations during cruise 04G05. Black circles represent XBT stations used to create the vertical section. Red inverted triangles represent XBT stations not selected for use in the vertical section. White squares represent locations of CTD stations. Shown are the 200 m, 1000 m (in bold), 2000 m, and 3000 m contour lines. The SSH contour interval is 5 cm. (SSH Source: R. Leben, CCAR, Univ. of Colorado).

The vertical profiles produced from the XBT probes indicate surface temperatures were between 26ºC and 30ºC. There was some variability between stations at depths of 100 m and 450 m (Figure 3.52). There was less scatter between the stations of this cruise than either cruise 02G08 or cruise 03G06, and there was only slightly more scatter than the data from cruise 03G07.

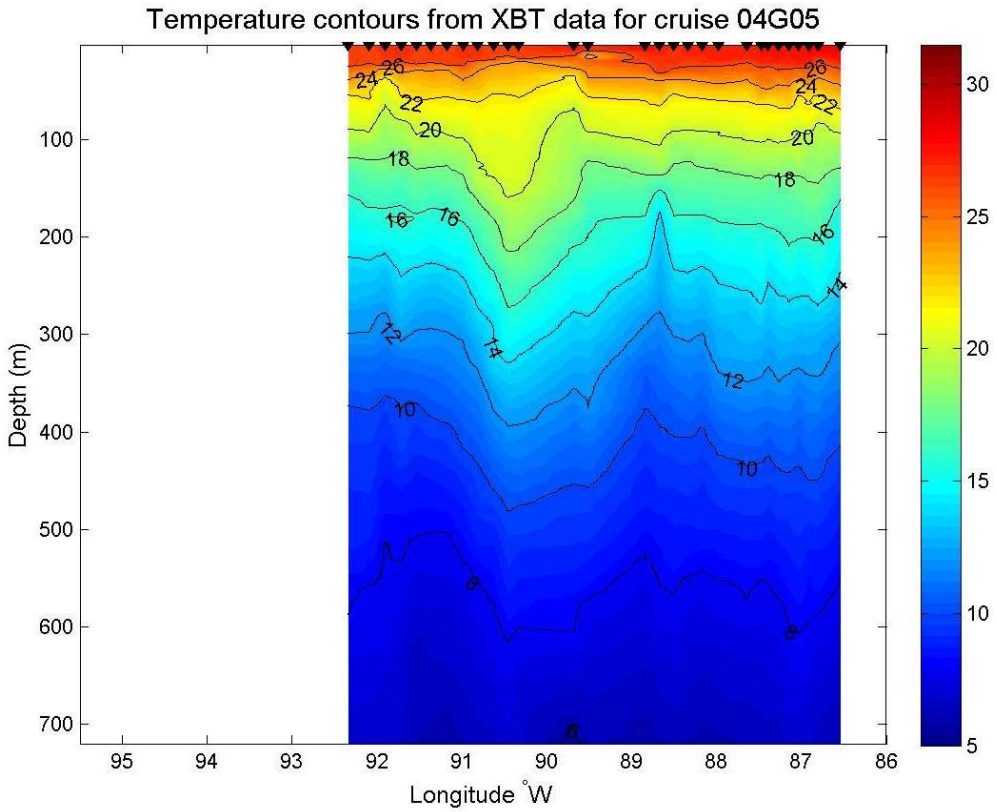

Figure 3.51 Vertical section of temperatures created from selected XBT stations shown in Figure 3.50. Black inverted triangles across the top edge represent the longitude of the XBT stations used. Temperatures are shown in Celsius. The white space on each side depicts that part of the study area not represented in the vertical section.

The EOF amplitudes calculated from the XBT data for this cruise were similar to the previous cruises (Figure 3.53). Mode 1 was surface amplified and decayed with depth. The summer mixed layer was visible in mode 1 and was about 25 m deep; similar to previous cruises. The structure in mode 2 was similar to cruise 20G08 and 03G06, but does not show the structure at 50 m that was seen in the 03G07 cruise data.

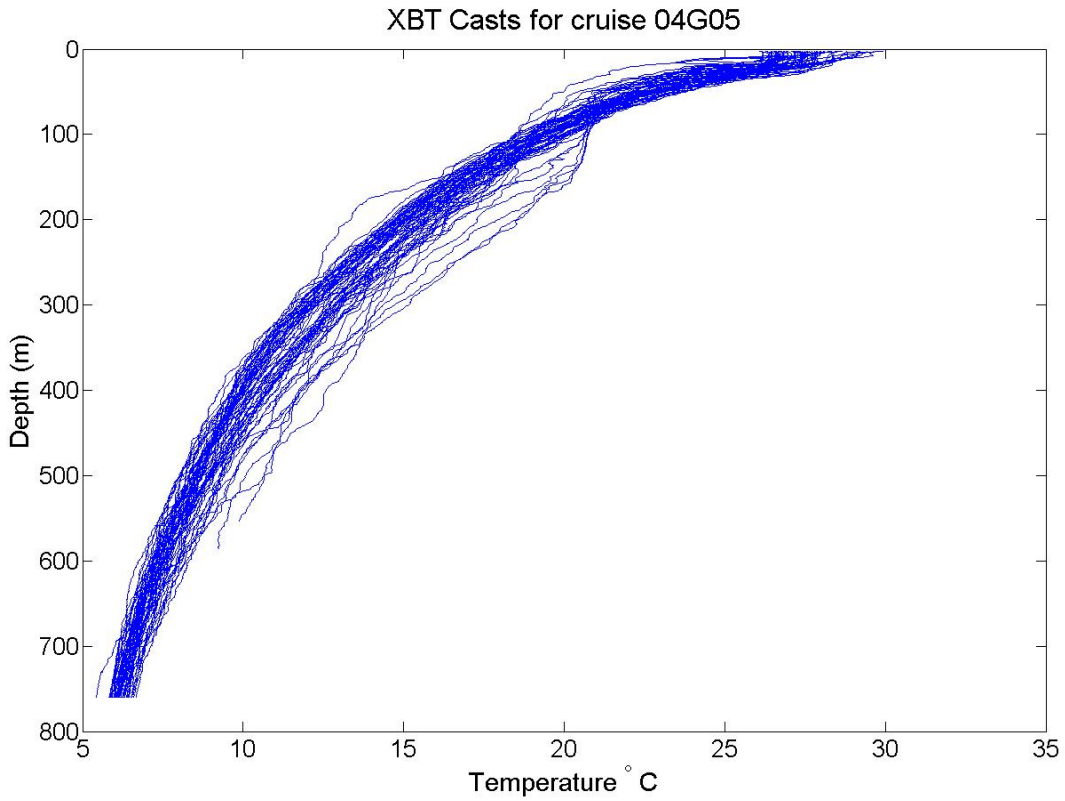

Figure 3.52 Cruise 04G05 vertical profiles of all XBT stations.

Mode 1 explains more variance than mode 1 from cruise 03G06 but less than the other two cruises. Mode 2 captures less variance than mode 2 in cruise 03G06 but more than in the other two cruises. The variance in mode 1 was most similar to mode 1 from cruise 03G07 and mode 2 was most similar to cruise 03G06. The EOF vertical amplitudes and modal amplitudes were shown in Figures 3.53 and 3.54.

The similarity of the vertical modes, in all four cruises, suggests that thermal structure during summer was stable over time. A surface mixed layer of about 25 m was apparent in mode 1 for all cruises. Mode 2 contains structure between 150 m and 450 m

that was also not present in mode 1. With the exception of cruise 03G07; mode 2 was similar between cruises. The modal amplitudes for mode 2 seem to show some relation to the SSH features and might represent variability between the mesoscale SSH processes (Figure 3.54).

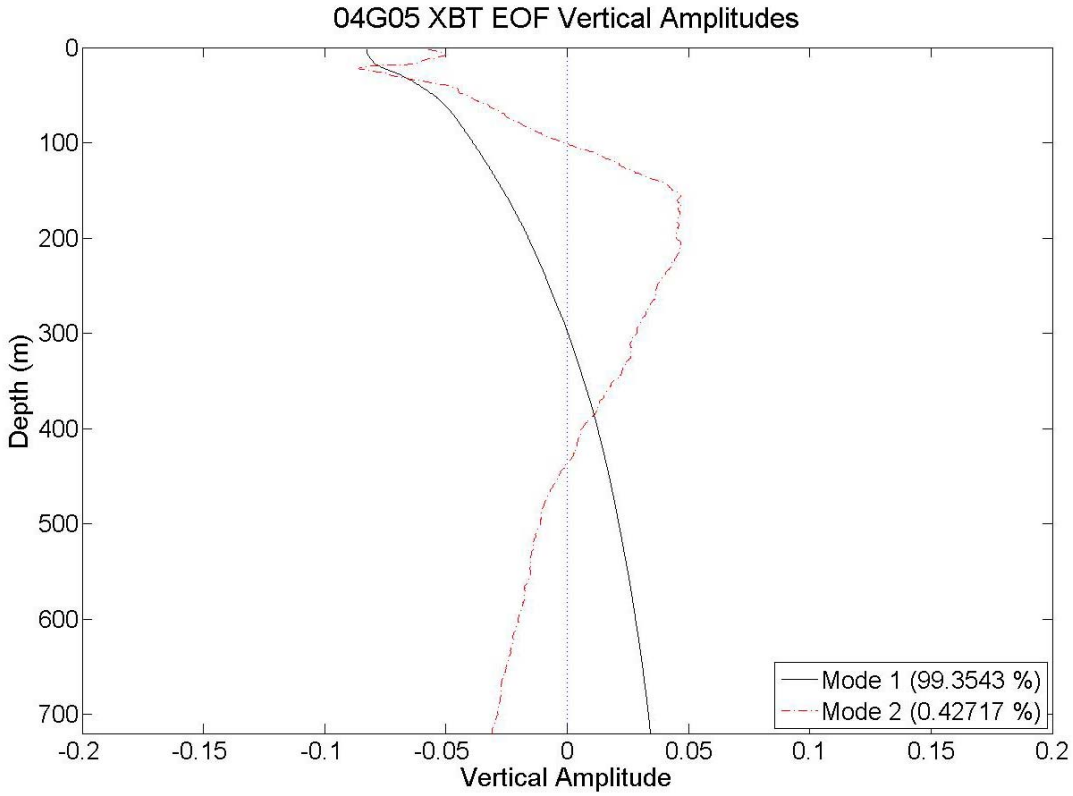

Figure 3.53 Vertical profile showing XBT EOF vertical mode amplitudes during 2004 cruise 04G05.

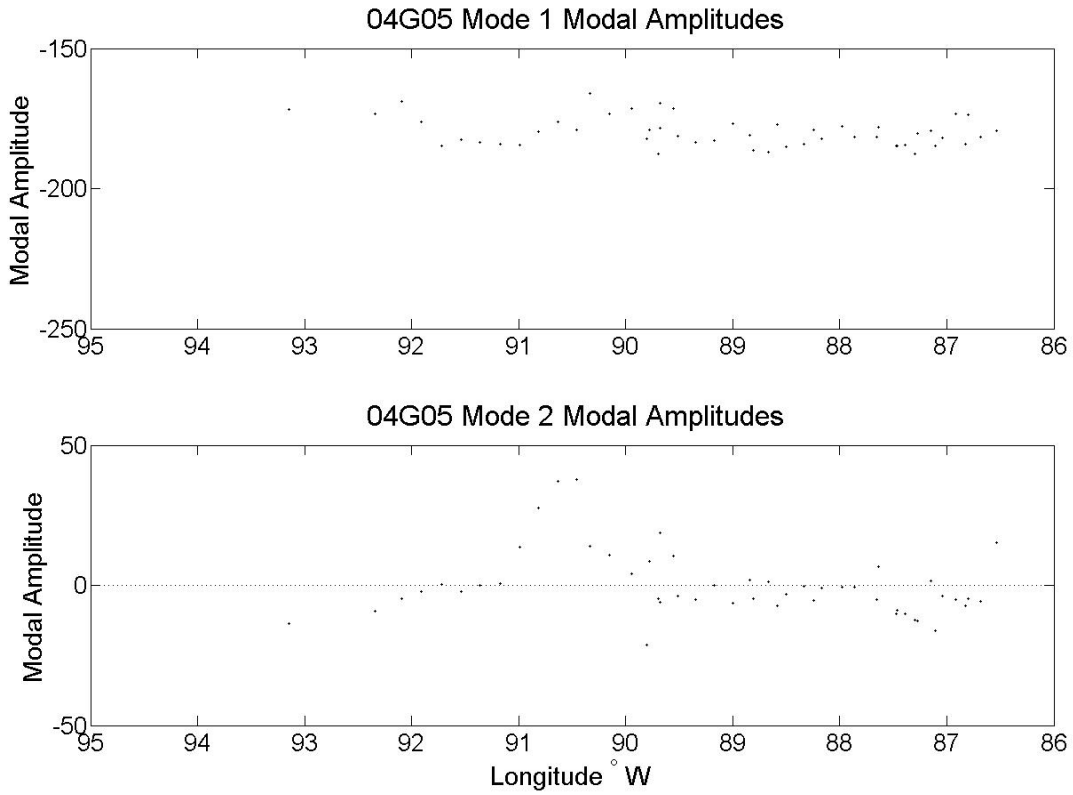

Figure 3.54 Modal amplitudes for XBT EOF calculation for 2004 cruise 04G05.

3.2 Platform-Mounted Data

3.2.1 Horizontal Velocity Time-Series

The upper panel of Figure 3.55 shows record length hourly wind velocity vectors, collected on the *Brutus* platform, at 122 m above the site elevation. The lower panel shows near-surface (51 m) hourly current velocity vectors, observed by the 38-kHz ADCP deployed on the *Ocean Star* mobile offshore drilling rig. The wind velocity

vectors clearly show a decrease in amplitude with the onset of summer. The direction of the wind vectors was evenly divided between north and south, while the current velocity vectors were primarily northeastward.

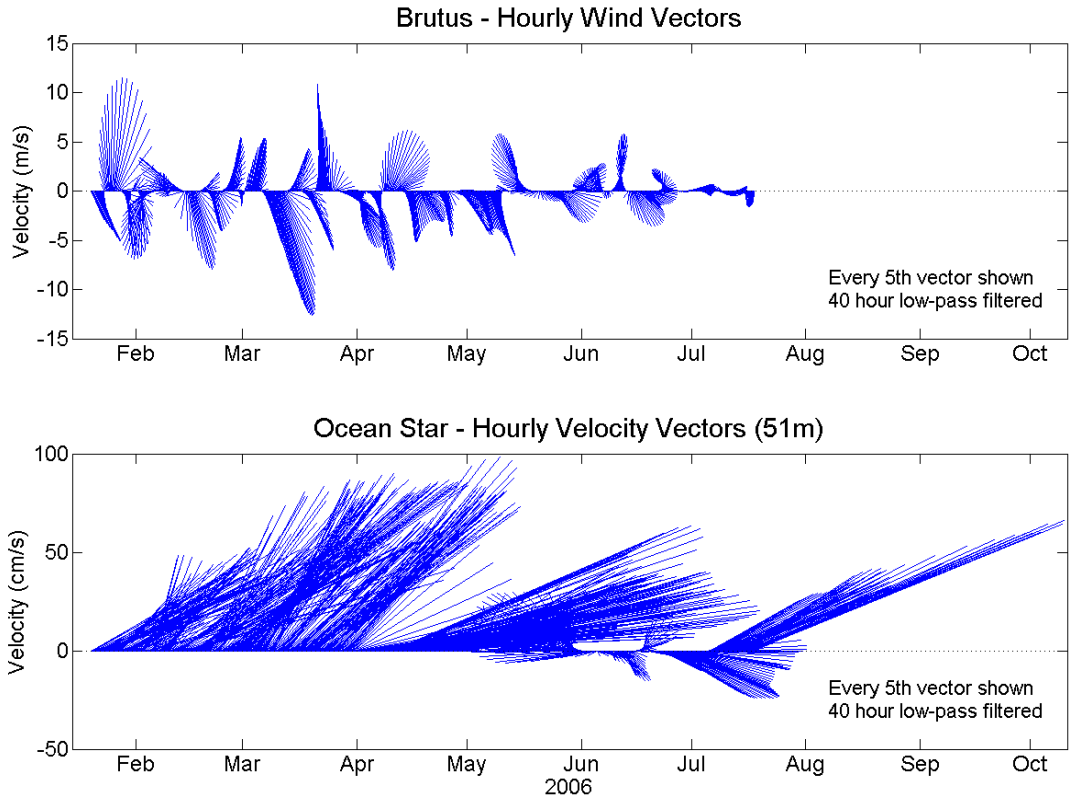

Figure 3.55 Record length velocity vectors of wind and the near-surface (51 m) 38-kHz ADCP depth bin. The wind data is collected 122 m above site elevation.

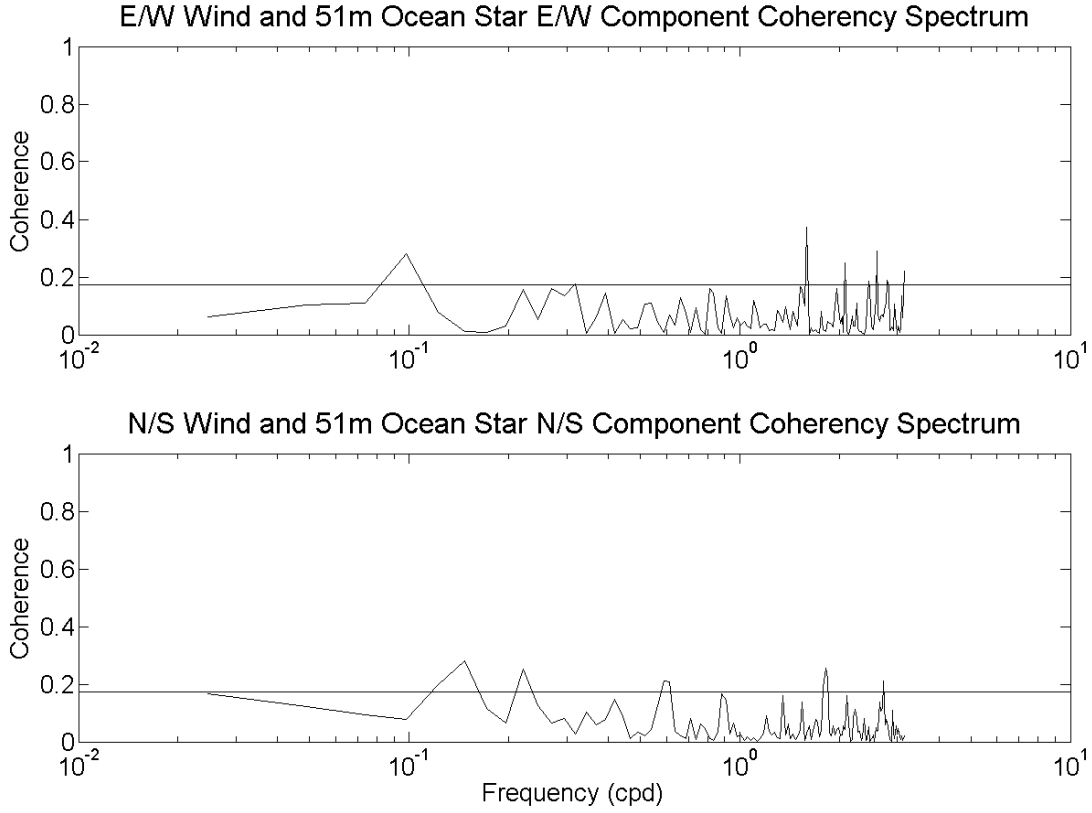

Figure 3.56 Results of the coherency analysis between the wind and near-surface 38-kHz ADCP velocity vectors. The solid horizontal line denotes the 95% significance level, which is 0.17.

The results of the coherency analysis were shown in Figure 3.56. The coherency analysis showed there was no significant correlation between the wind at 122 m and current velocity vectors at 51 m. As was reported above, the summer mixed layer was shown to be about 25 m deep. However, those data were collected during the summer months, and reveal nothing about the depth of the mixed layer during the winter and spring months. Since the mixed layer was shallower than 51 m during summer it follows that the winds would not be correlated with the current velocity vectors at 51 m.

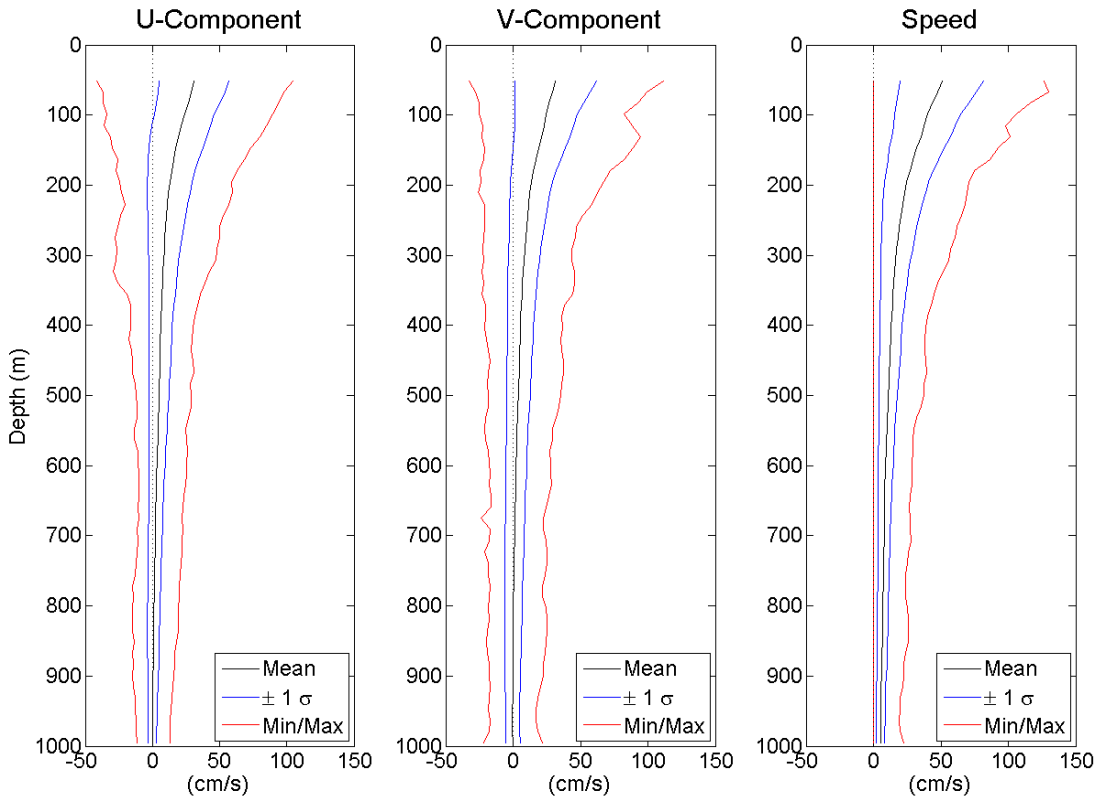

Figure 3.57 Record length statistics of 38-kHz ADCP velocity components and speed. Shown are the mean, plus and minus one standard deviation (STD), and the minimum and maximum values.

Record length statistics for the current velocity vectors were presented in Figure 3.57. This figure shows the means for each depth, plus and minus one standard deviation, and minimum and maximum curves for each depth. The minimum speed was very close to zero but generally not zero. The velocity components and speed were baroclinic above 800 m and barotropic below 800 m. Mean component velocities for all depths were less than 40 cm/s, but the mean speeds were about 50 cm/s in the near-surface depth bin. These results were consistent with those reported by Cole (2008) and Hamilton and Lugo-Fernandez (2001).

The mean component velocities were near zero below 800 m for both u- and v-components and the mean speeds were about 10 cm/s. Even though the mean of the components were near zero at the deepest depths the mean speed was not zero. This apparent paradox arises because both components, while weak (< 10 cm/s), were not zero. Inertial oscillations were clearly seen at these depths, and these oscillations average out to be near zero, but the speed was not zero, therefore, even though the mean velocity components was near zero the mean speed was not zero.

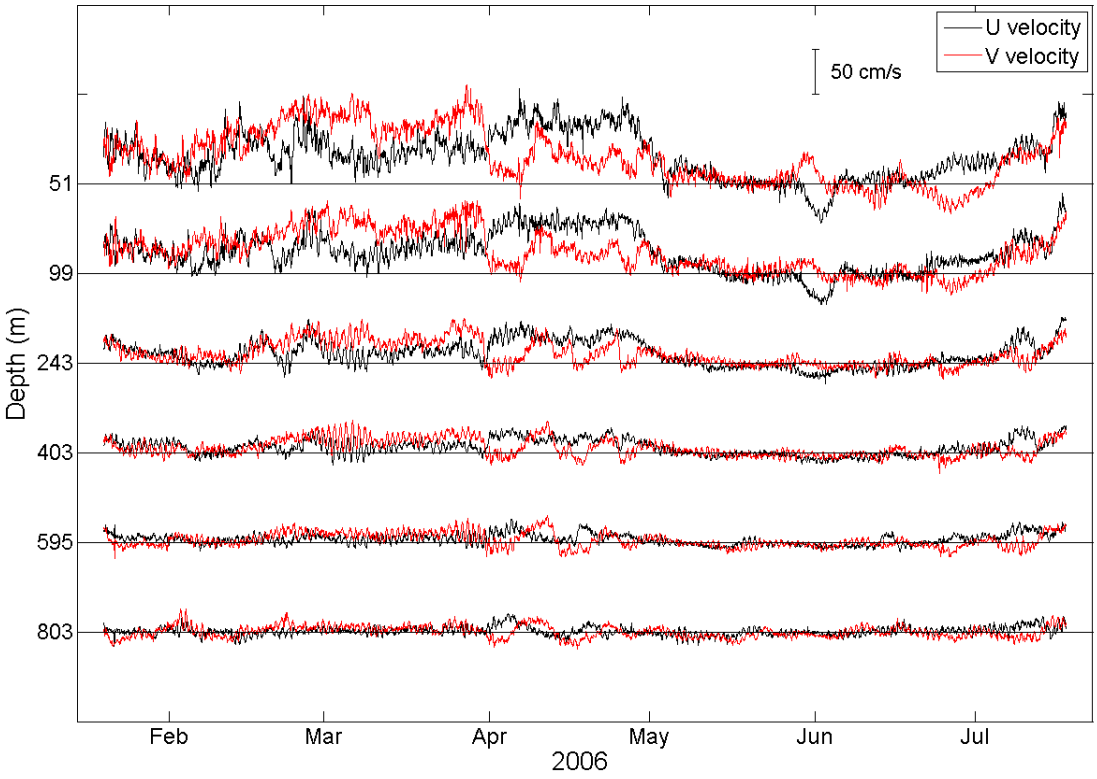

Figure 3.58 Gap-filled record length 38-kHz ADCP time-series showing the velocity components at six depths between 51 m and 803 m.

The velocity component time-series were presented in Figure 3.58 with the corresponding speed presented in Figure 3.59. Six depths were selected to span the range of observations. It was clear the two near-surface time-series were very similar. There was a slight reduction in magnitude at the 99 m depth. Inertial oscillations were visible throughout the record at all depths.

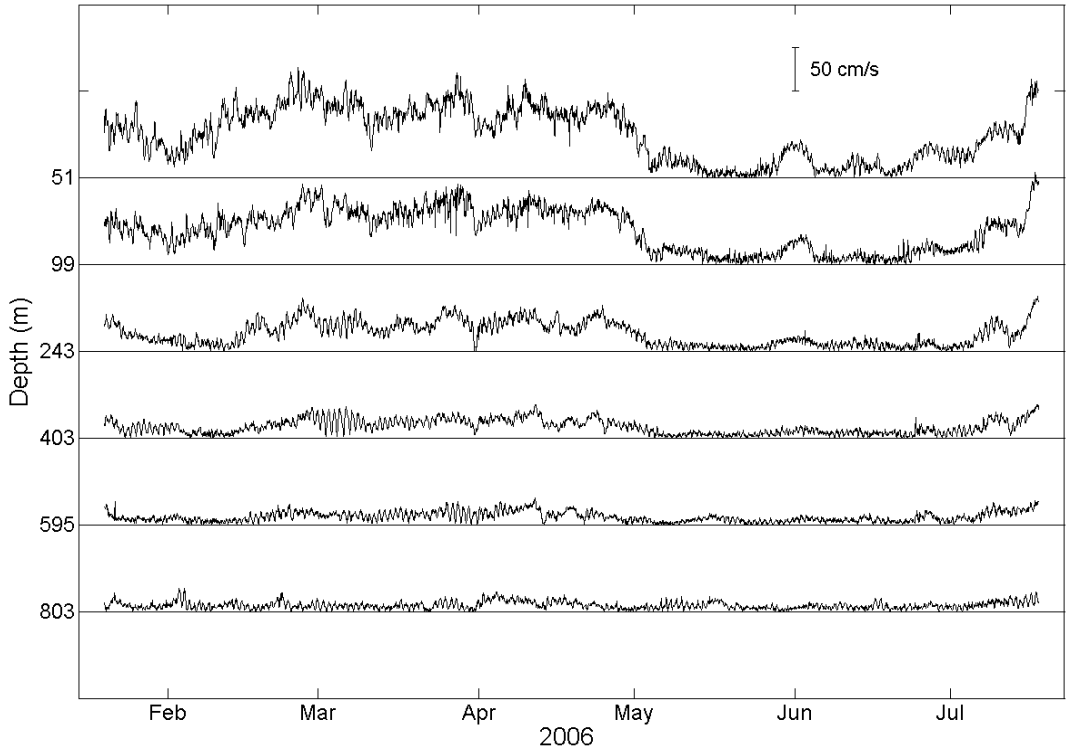

Figure 3.59 Gap-filled record length 38-kHz ADCP time-series showing the speed at six depths between 51 m and 803 m.

The record of observations can be divided in late April. From the beginning of the record until late April the velocities in the upper 100 m were generally greater than

50 cm/s and in the northeast direction (Figures 3.55 and 3.58). Starting in late April the velocities change direction, becoming mostly easterly, and the speed decreased dramatically to only a fraction of that seen during the first half of the record (Figure 3.59). The speed increased again in July near the end of the record.

The currents at the depths observed by the 38-kHz on the *Ocean Star* were not being forced by the overlying wind field; as was documented above. Therefore, a series of figures, showing the position of the *Ocean Star* in relation to the sea surface height field, was presented in Figures 3.60 through 3.68 (exclusive of Figure 3.62) because the SSH field was the only other mechanism that could influence the currents. Each figure shows the position of the offshore platforms and the relevant SSH features are labeled.

Figure 3.60 shows the SSH field near the beginning of the record. The *Ocean Star* was located to the north of the Loop Current and to the south of a CSE. The Loop Current was stretched westward along the escarpment almost to 93ºW. The horizontal portion was in the process of separating from the Loop Current.

The velocity components during this time were directed to the northeast (Figure 3.58). During this part of the record the speed was decreasing (Figure 3.59). This was possibly due to the separation of the small Loop Current eddy (~120 M, 220 km), centered near 27ºN, 92.5ºW (Figure 3.61). After this LCE separated, the Loop Current was oriented in a northwest to southeast direction. The CSE that was located directly north of the *Ocean Star* was also now oriented in a northwest to southeast direction. It appears to have weakened.

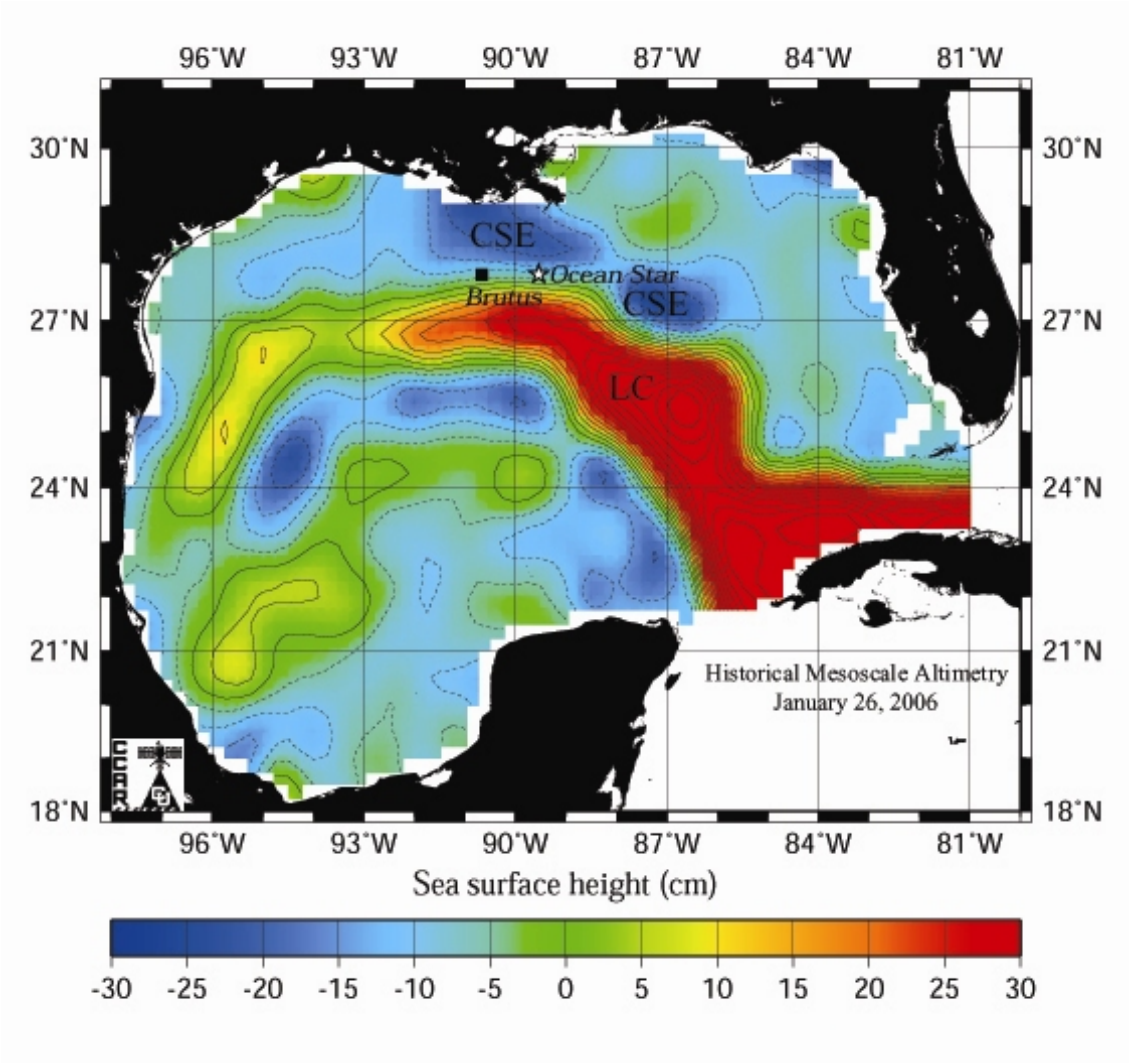

Figure 3.60 SSH field for late January, 2006. Shown are the locations of the *Ocean Star* mobile drilling rig, from which the ADCP current velocities were observed, and the *Brutus* fixed drilling platform, from which the wind velocity was observed. The contour interval is 5 cm. (SSH Source: R. Leben, CCAR, Univ. of Colorado).

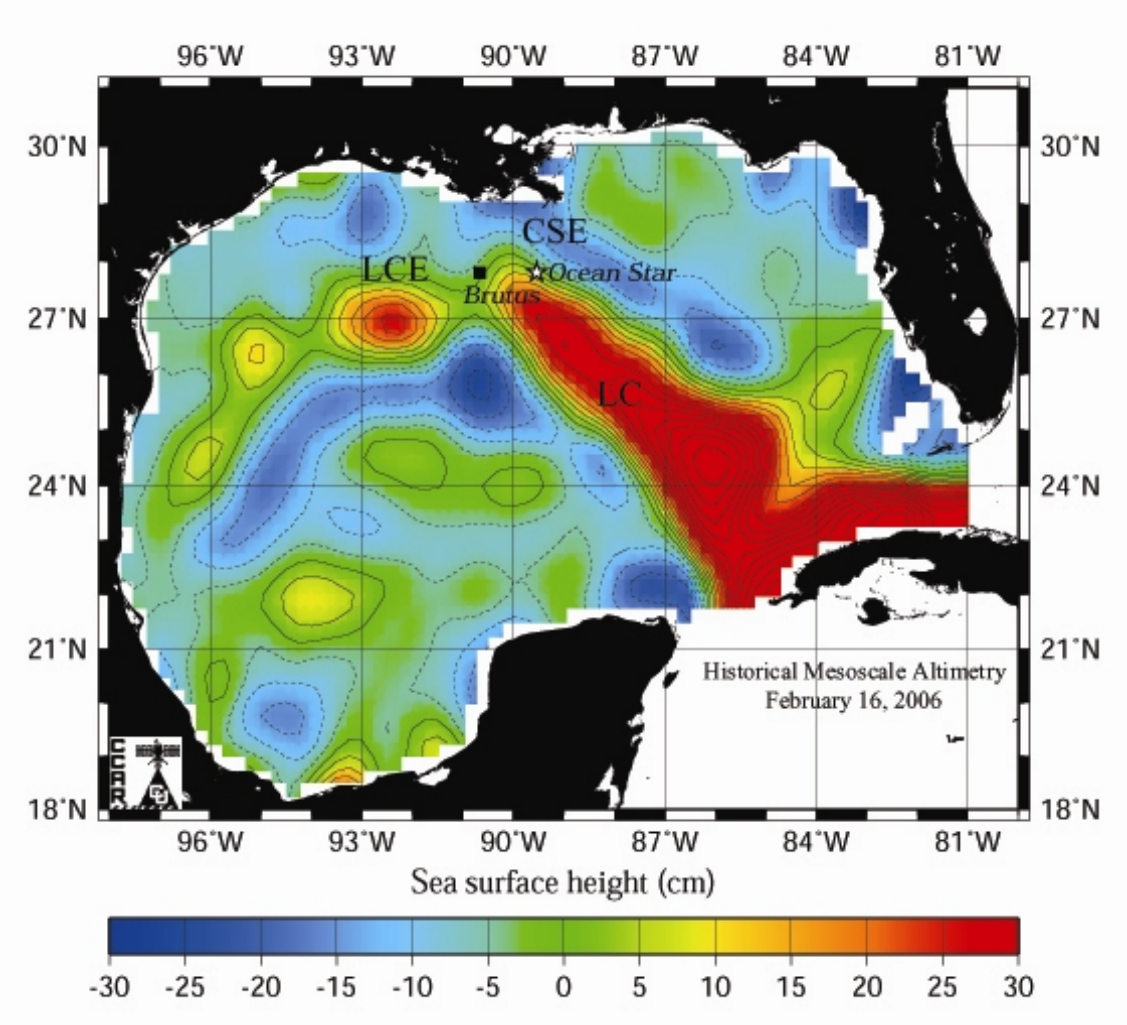

Figure 3.61 SSH field for mid February, 2006. Shown are the locations of the *Ocean Star* mobile drilling rig, from which the ADCP current velocities were observed, and the *Brutus* fixed drilling platform, from which the wind velocity was observed. The contour interval is 5 cm. (SSH Source: R. Leben, CCAR, Univ. of Colorado).

Based on the change in direction of the velocity components, shown in Figure 3.58, and the decrease in speed (Figure 3.59) the separation event probably occurred in very early February. A Hovmöller plot, which shows the speed at all depths along the y-

axis over time, represented along the x-axis, indicates the speed decreased to a minimum, below 20 cm/s, in early February (Figure 3.62).

The SSH field in mid February, a couple of weeks after the separation event, shows the *Ocean Star* was now located at the northeastern tip of the Loop Current (Figure 3.61). During February, the currents became more northerly as they flowed to the northeast (Figure 3.58). By March the speed was greater than 100 cm/s (Figure 3.59).

As Figure 3.63 shows, a second eddy separated from the Loop Current by mid March; this eddy was about 180 M or 330 km along the long axis. The first Loop Current eddy was now labeled LCE 1, and the newly formed eddy was labeled LCE 2. LCE 1 was now centered near 27ºN, 94ºW, and LCE 2 was centered near 26.5ºN, 89.5ºW. There was a decrease in speed that was coincident with a decrease in the v-component velocity in the second week of March (Figures 3.58 and 3.59). This decrease in speed was visible in the upper 150 m of the Hovmöller plot (Figure 3.62). There were strong inertial oscillations visible, at the 243 m and 403 m depths, just prior to the reduction in speed and the change in the v-velocity component. Since inertial oscillations faster with greater speed, it was not surprising that they diminished when the speed decreased.

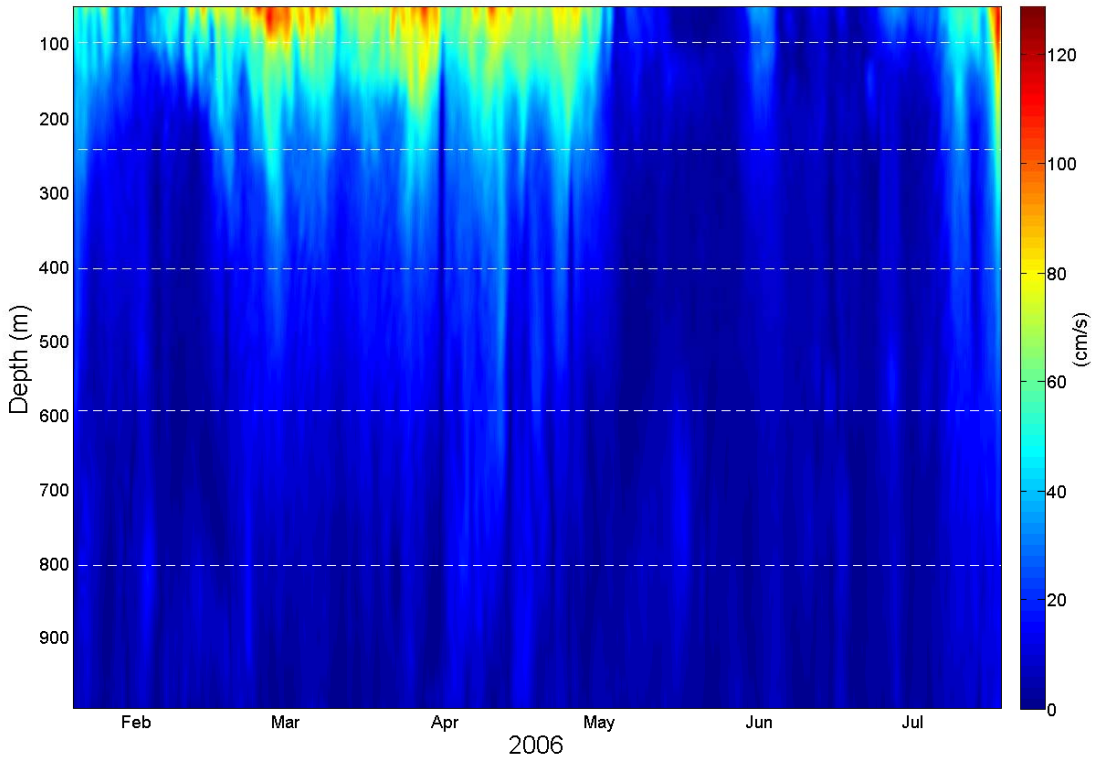

Figure 3.62 Hovmöller plot of speed (in cm/s) for the *Ocean Star* platform. The data were decimated to days and 40 hour low-pass filtered. Horizontal dashed lines correspond to the depths shown in the time-series plots for vector components and speed. The 51 m depth corresponds to the top edge of the plot and is not represented by a dashed line.

It was unknown if these events were connected with the separation of LCE 2. However, a change in inertial oscillations was also apparent in early February when the first LCE separated. Perhaps there was an increase in speed, and therefore in the inertial oscillations, as the LCE coalesces and the SSH contours close, just prior to separation from the Loop Current. Since LCE 1 (~120 M, 220 km) was not as large as LCE 2 (180 M, 330 km) at separation, maybe the inertial oscillations associated with it were smaller.

More likely wind events, shown in Figure 3.55 were responsible for the inertial oscillations.

LCE 2 was elliptical, with the long axis oriented in a southwest to northeast direction, and it was connected to a weak WSE at 29ºN, 87.5ºW (Figure 3.63). The *Ocean Star* was located just north of LCE 2 and south of the CSE, which was smaller than it was in the mid February SSH plot. The velocity vectors were to the northeast until the end of the month, when the v-component drops to near zero and the vectors were oriented primarily eastward (Figure 3.55). This was explained by the anticyclonic rotation of the long axis of LCE 2.

As Figure 3.64 shows, the long axis of LCE 2 was now slightly oriented in a northwest to southeast direction. The currents near the edge of the eddy, at the *Ocean Star*'s location, will be towards the east. The rotation of LCE 2 can explain the reduction in the v-velocity component, which was visible at all depths as April begins in Figure 3.58. The decrease in the v-component was particularly visible in the velocity vectors shown in the lower panel of Figure 3.55. As this occurred, the speed decreased from over 100 cm/s in late March to around 50 cm/s as the eddy rotated (Figure 3.59). The decrease in speed was apparent at all depths.

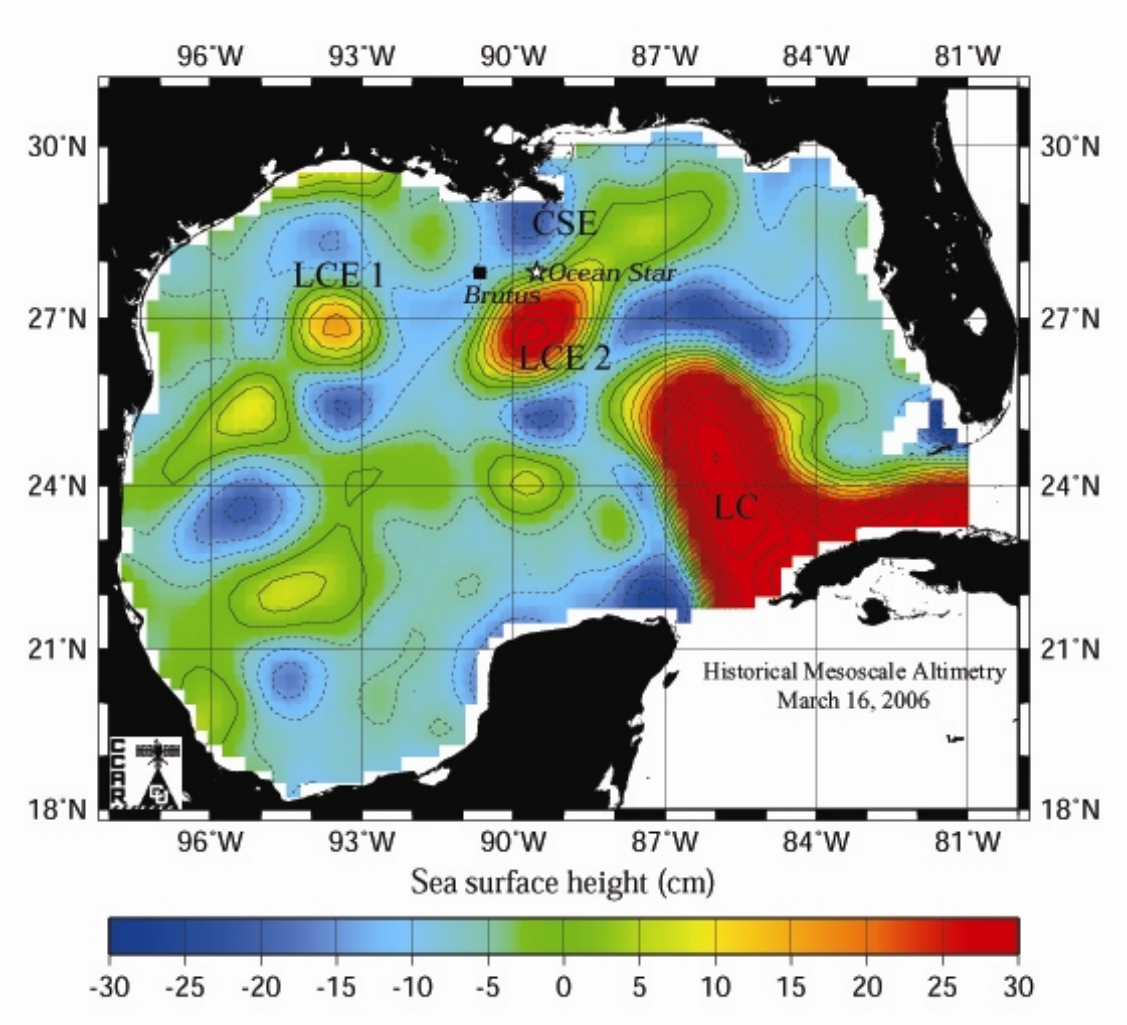

Figure 3.63 SSH field for mid March, 2006. Shown are the locations of the *Ocean Star* mobile drilling rig, from which the ADCP current velocities were observed, and the *Brutus* fixed drilling platform, from which the wind velocity was observed. The contour interval is 5 cm. (SSH Source: R. Leben, CCAR, Univ. of Colorado).

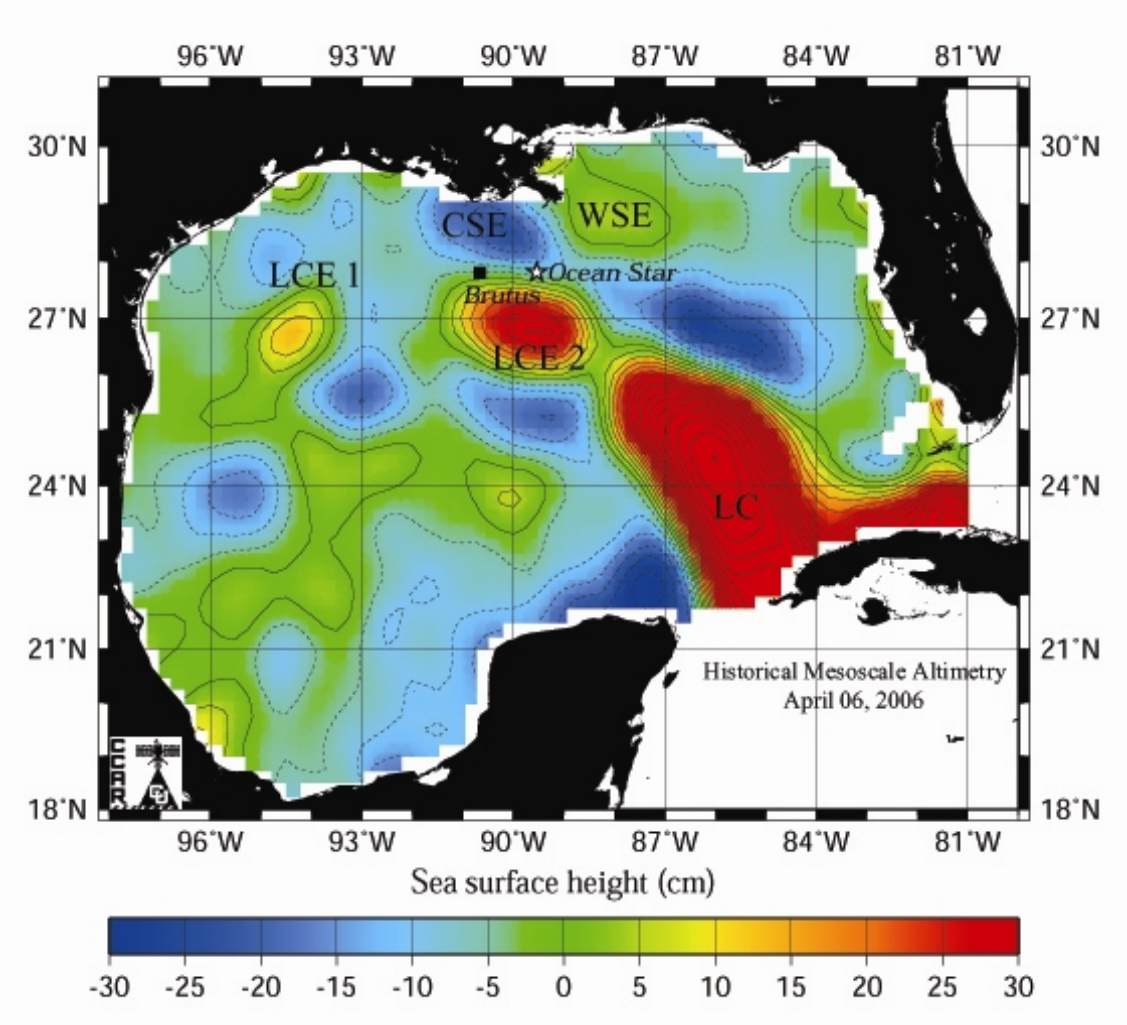

Figure 3.64 SSH field for early April, 2006. Shown are the locations of the *Ocean Star* mobile drilling rig, from which the ADCP current velocities were observed, and the *Brutus* fixed drilling platform, from which the wind velocity was observed. The contour interval is 5 cm. (SSH Source: R. Leben, CCAR, Univ. of Colorado).

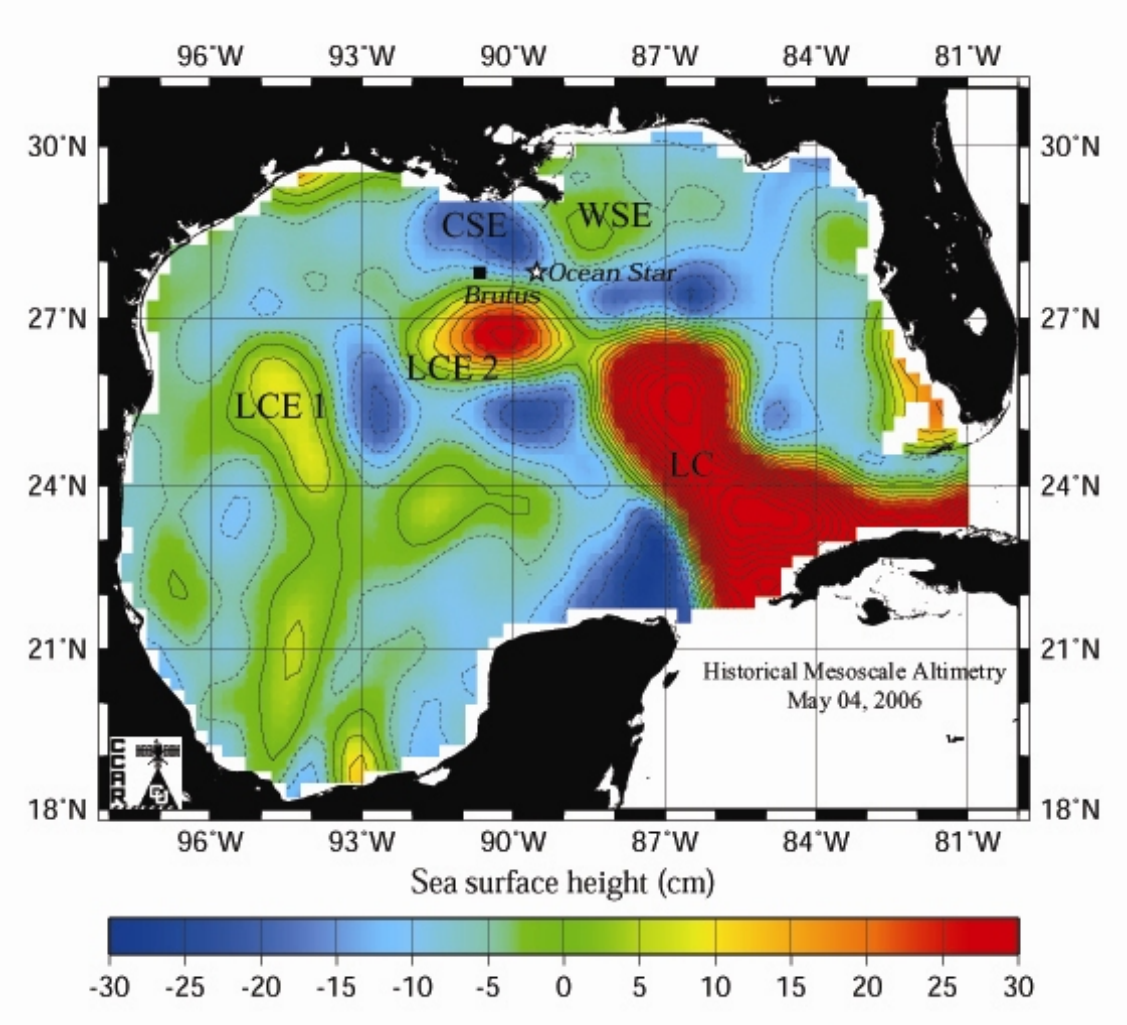

Figure 3.65 SSH field for early May, 2006. Shown are the locations of the *Ocean Star* mobile drilling rig, from which the ADCP current velocities were observed, and the *Brutus* fixed drilling platform, from which the wind velocity was observed. The contour interval is 5 cm. (SSH Source: R. Leben, CCAR, Univ. of Colorado).

The rotation of LCE 2 severed its connection to the WSE northeast of the *Ocean Star* but created an isthmus of positive SSH anomaly with the Loop Current. The CSE located northwest of the *Ocean Star* was connected to the CSE north of the Loop Current

by a ribbon of negative SSH anomaly (Figure 3.64). In Figure 3.59, the decrease in speed associated with the rotation of LCE 2 was probably the result of severing the connection between the eddy and the WSE and therefore reducing the flow past the *Ocean Star* as the path of the currents was altered towards the Loop Current.

During the month of April the current speed increased to 100 cm/s in the second week of the month, before starting to decrease steadily into May. A comparison of Figures 3.64 and 3.65 indicates that one explanation for this slow decrease in speed was the westward translation of LCE 2. As the eddy moved westward away from the *Ocean Star*, the speed decreased. Notice also that the CSE to the northwest of the *Ocean Star* was close enough that it could affect the velocity vectors. Since the CSE was located on the shelf, it will only affect velocities near the surface. This can help explain how the u-component velocities in the upper 250 m (upper three time-series in Figure 3.58) remain fairly consistent through April, while those deeper seem to decrease slightly as May approaches. Influence from the CSE could maintain the shallower velocities, while the deeper velocities, which were probably driven primarily by LCE 2, decrease as LCE 2 moves westward and away from the *Ocean Star*. Fluctuations in the v-component velocity could result from LCE 2 changing shape slightly as it moved westward, which would alter the direction of flow observed by the ADCP at the *Ocean Star*.

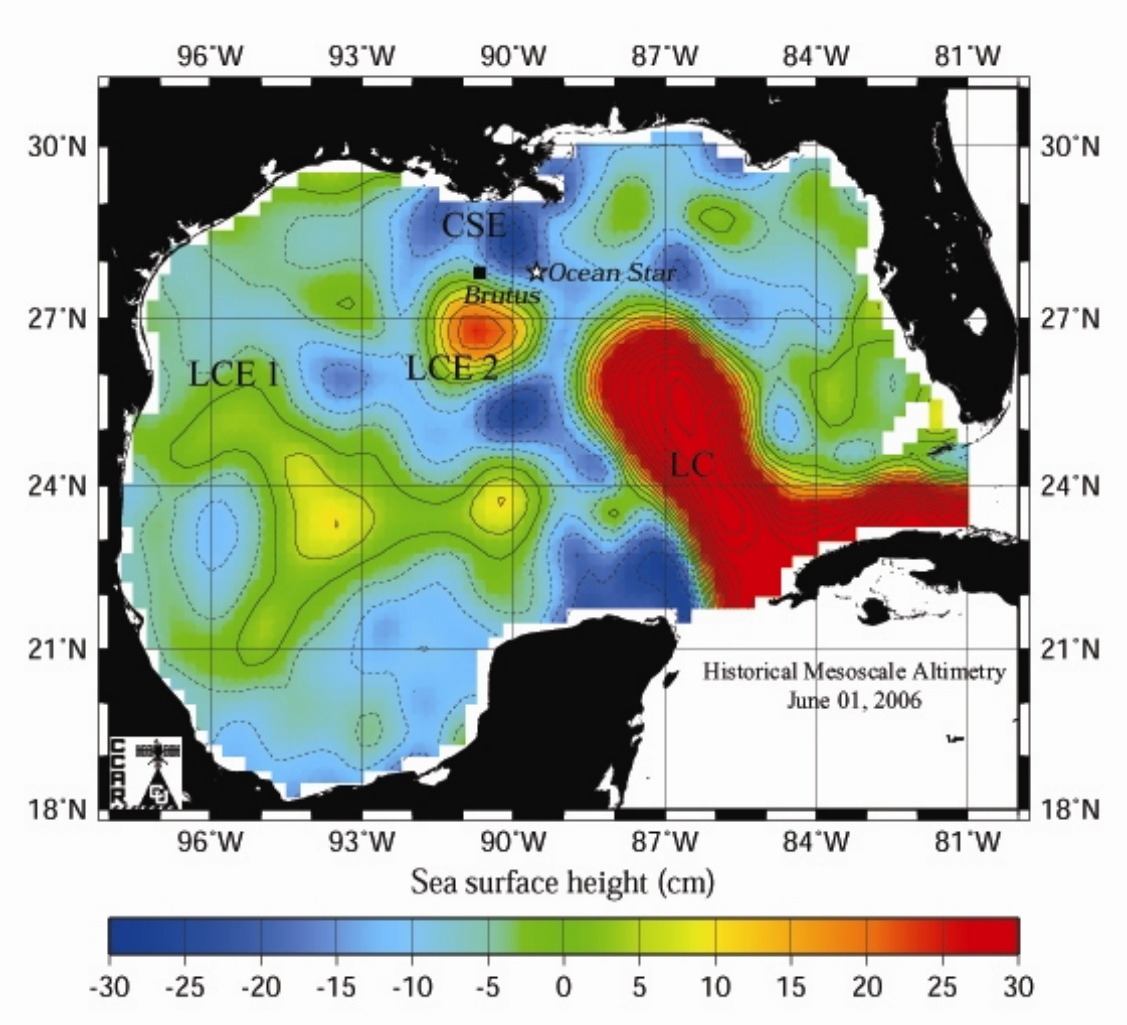

Figure 3.66 SSH field for early June, 2006. Shown are the locations of the *Ocean Star* mobile drilling rig, from which the ADCP current velocities were observed, and the *Brutus* fixed drilling platform, from which the wind velocity was observed. The contour interval is 5 cm. (SSH Source: R. Leben, CCAR, Univ. of Colorado).

A transition period occurred from the end of April to early May, in which the u- and v- velocity components, along with the speed, decreased to near zero (Figures 3.58 and 3.59). The reason for this was seen in Figure 3.65, the SSH plot for early May. This

figure indicates that the LCE 2 moved west to 26.5ºN, 90.5ºW and the *Ocean Star* was now located in an area of weak negative SSH anomaly.

The northeastward flow being observed at the *Ocean Star* was probably driven by the CSE to its northwest, which was situated to drive currents in a northwesterly direction. The time-series of speed in Figure 3.59 show speeds less than 25 cm/s near the surface associated with the northwest flow that diminished with depth. The northwest flow was not well defined below 250 m. The velocity components also diminish with depth to 250 m, below which the components were close to zero, except for a curious inertial oscillation, visible at 800 m, in the u-component (Figure 3.58). The speed and velocity components remain close to zero until the end of May.

From the end of May into early June, Figures 3.55 and 3.58 show that the flow was to the northwest in the upper 250 m. Figure 3.59 indicates the speed at this time in the near-surface bin was about 45 cm/s. This was caused by the CSE, which had been located to the northwest of the *Ocean Star*, moving to a position northeast of the *Ocean Star* where it displaced the WSE. As the CSE moved from a position northwest of the *Ocean Star* to a position northeast of it, there was a period of about a week, just prior to when it moved, where the position of the CSE relative to the rig drove velocities to the northwest (Figure 3.66).

As the June 1 SSH plot shows, LCE 2 has moved farther to the west and was now centered at 26.5ºN, 91ºW, and the shape was becoming circular (Figure 3.66). LCE 2 continued to move southwest and away from the *Ocean Star* for the remainder of the observational record; it no longer affected currents at the rig. The Loop Current has

begun to move northwest again and was now north of 27ºN. From early to mid June the near-surface velocity vectors were generally just south of east as the vectors in Figure 3.55 illustrate. The deeper velocity vectors were toward the east as the v-component in Figure 3.58 for these depths was very close to zero. Near surface speeds were not above 30 cm/s until the third week of June, when they increase to about 45 cm/s (Figure 3.59).

Stronger currents to the southeast appear in the third week of June and persisted to the end of the first week of July. There were two events taking place that could cause the southeasterly currents. First, the CSE, now located northeast of the *Ocean Star*, moved west, past the rig, and would be oriented in such a way as to drive southeast flow past the ADCP. Second, the Loop Current was approaching the *Ocean Star* from the southeast. Since the currents were present at all depths (Figure 3.58), this might be the more likely driving force behind the currents as it was shown earlier that the CSE might not be strong enough to influence currents at all observed depths.

As the Loop Current advances towards the *Ocean Star* the speed increased at all observed depths, eventually reaching about 120 cm/s by the end of the record at 51 m (Figure 3.59). The horizontal axis of Figure 3.55 was extended to accommodate the large northeasterly near-surface velocity vectors observed in mid July.

Figures 3.67 and 3.68 document the CSE as it moved past the *Ocean Star*, and the advance of the Loop Current. The last SSH figure shows that a third LCE has separated from the Loop Current in less than six months! This LCE was the largest of the three to separate during the period of observations and was over 200 M, or almost 400 km in diameter (Figure 3.68). The velocity vectors become oriented to the northeast

in mid July (Figure 3.58), coincident with the increase in speed to 2.5 knots (Figure 3.59). This was probably when LCE 3 edges past the *Ocean Star*.

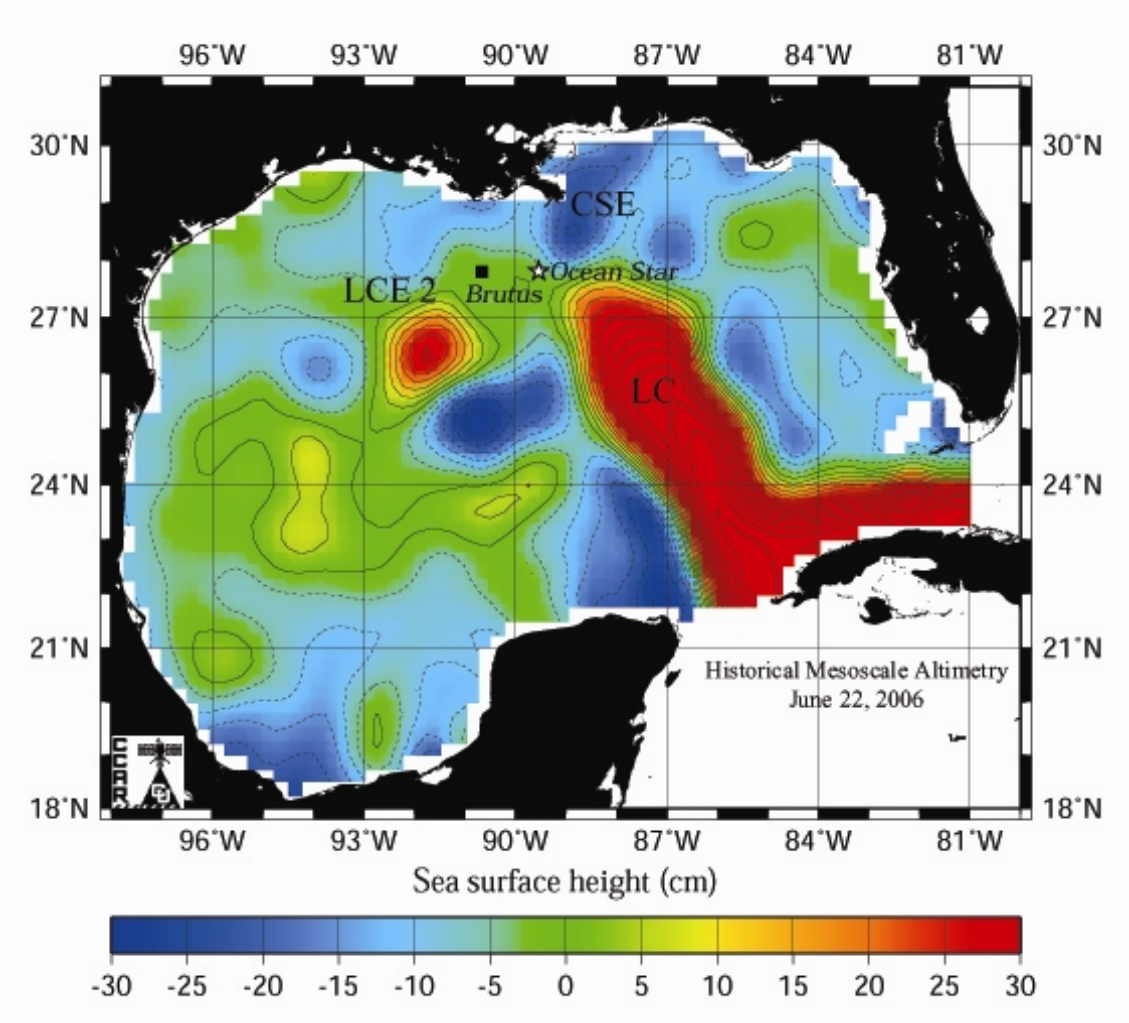

Figure 3.67 SSH field for the third week of June, 2006. Shown are the locations of the *Ocean Star* mobile drilling rig, from which the ADCP current velocities were observed, and the *Brutus* fixed drilling platform, from which the wind velocity was observed. The contour interval is 5 cm. (SSH Source: R. Leben, CCAR, Univ. of Colorado).

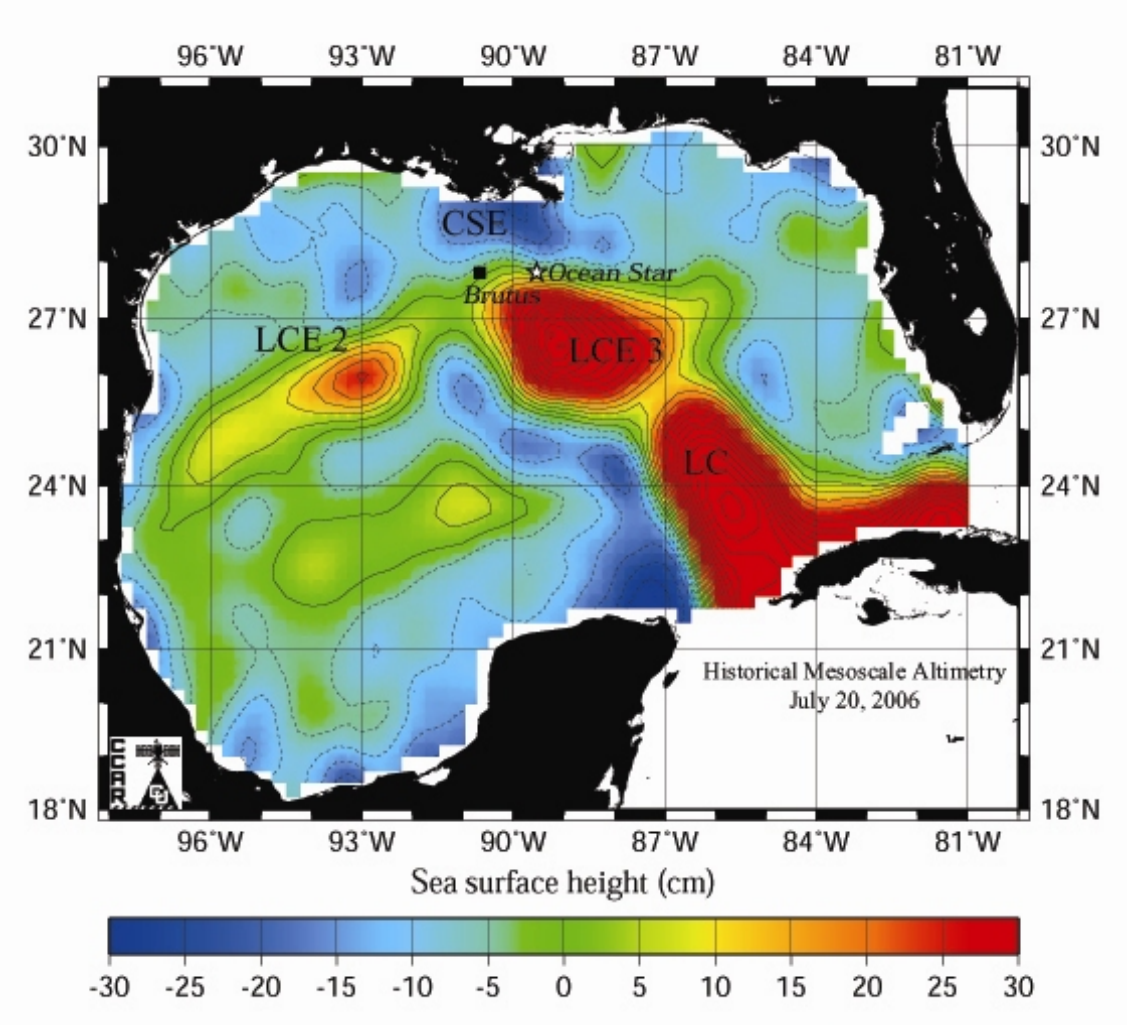

Figure 3.68 SSH field for the third week of July, 2006. Shown are the locations of the *Ocean Star* mobile drilling rig, from which the ADCP current velocities were observed, and the *Brutus* fixed drilling platform, from which the wind velocity was observed. The contour interval is 5 cm. (SSH Source: R. Leben, CCAR, Univ. of Colorado).

The first eight tidal constituents were removed from the data (Table 3.1) using the method of cyclic descent. The tides were very weak in the Gulf of Mexico and the calculated amplitudes were less than 4 cm/s. This was quite small.

Table 3.1. U-component tidal constituent amplitudes (cm/s) for the eight constituents removed from each time-series depth shown in Figure 3.58.

Constituent	51 m	99 m	243 m	403 m	595 m	803 m
M2	0.3	0.1	0.1	0.1	0.2	0.1
S2	0.3	0.2	0.0	0.0	0.1	0.1
N2	0.2	0.2	0.0	0.1	0.1	0.0
K2	0.2	0.3	0.1	0.1	0.0	0.1
K1	1.3	1.1	1.1	0.7	0.5	0.6
O1	0.6	0.3	0.7	0.5	0.6	0.7
P1	0.4	1.0	0.3	0.2	0.6	0.9
Q1	1.1	0.5	0.36	0.5	0.4	0.4

3.2.2 Horizontal Velocity Spectra

A frequency spectrum representation of the time-series described above was shown in Figure 3.69. The spectral structure was similar for both u- and v-components. The greatest amount of energy was present in frequencies lower than 0.1 cpd (> 10 days per cycle). This could be caused by mesoscale SSH features, such as the Loop Current or eddies that were located near the *Ocean Star* for periods longer than 10 days.

There was an obvious peak centered near 1 cycle per day, which was close to the inertial period (0.93 cpd) for this latitude; a smaller peak was noticeable at 2 cpd. Even

though the tides were removed prior to this analysis there could be some contribution to the 1 cpd and 2 cpd peaks (Figure 3.69). However, since inertial oscillations would impart the same energy at all depths, and the spectra indicate about the same energy for all depths, the 1 cpd peak most likely represents the inertial currents.

More visible in the v-component than in the u-component were peaks at 3, 4, and 5 cpd frequencies in the 99 m spectra. Less visible, but also present in this spectra, were peaks at 6, 7, 8, 9, and 10 cpd (Figure 3.69). It was unknown what caused these peaks.

The two near surface spectra (51 m and 99 m), in both components, possess very similar structure and there was a perceptible gap between these lines and the deeper lines. This gap could reflect the influence of the thermocline on isolating the deeper waters from those of the surface waters, by reducing the amount of energy transferred out of the surface into the deeper layers. Any of the vertical profile plots from the XBT data, such as Figure 3.10 for example, clearly show that temperatures decrease more rapidly below about 100 m. The thermocline could keep the higher energy of the surface waters near the surface and impede the transfer of energy to deeper waters. A fairly depth-dependent energy distribution was found between the 1.43 – 11.1 dpc band. This coincides with the band of frequencies (2 – 15 dpc) associated with weather patterns. Energy from weather phenomenon would naturally be larger near the surface and decrease with depth.

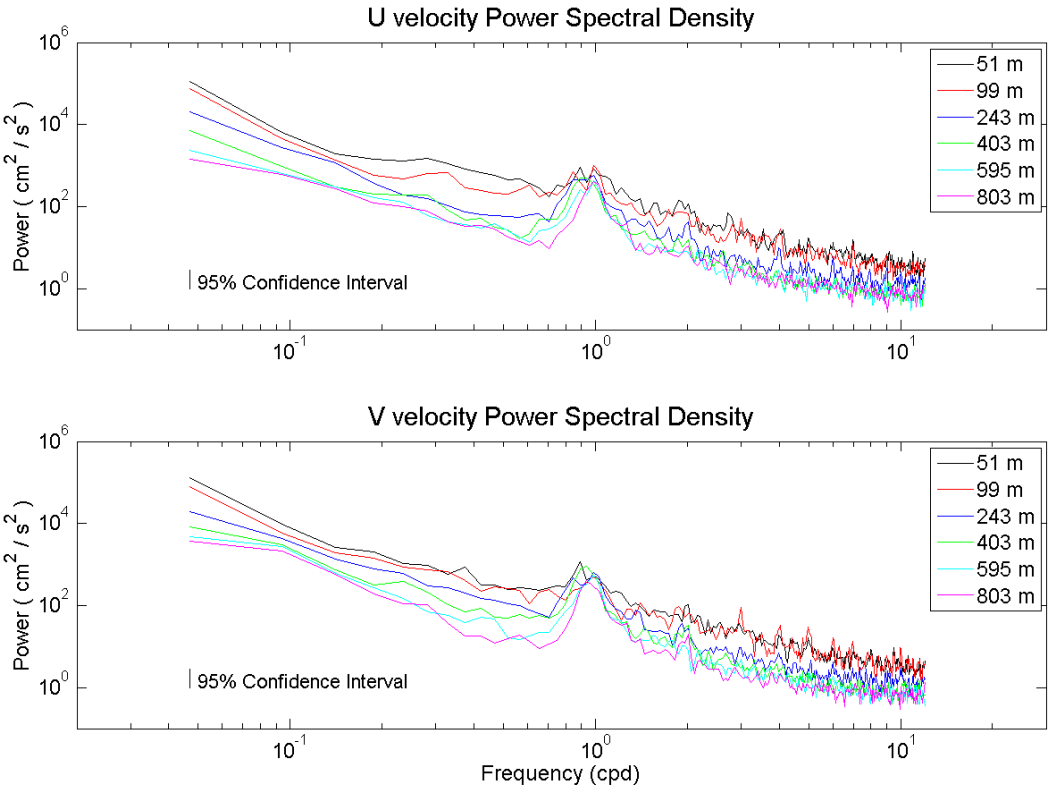

Figure 3.69 Power spectral densities for each velocity component computed at each of the depths used in the horizontal velocity time-series presented in log-log format. The tides were removed prior to this calculation, and each component was windowed with a 512 point Kaiser-Bessel window, with 50% overlap.

3.2.3 Empirical Orthogonal Function Analysis

Empirical orthogonal function (EOF) analysis as described in Emery and Thomson, (2001) was used to classify variance in the horizontal velocity data. Figure 3.70 shows the EOF vertical modes associated with the east/west velocity component. Figure 3.71 shows the modal amplitudes associated with the modes shown in figure 3.70. Figure 3.72 shows the north/south EOF vertical modes and Figure 3.73 shows the modal amplitudes associated with the north/south vertical modes.

The first three modes captured over 90% of the variance for both u- and v-components. Mode 1 was surface intensified in both components and approached zero near 1000 m (Figures 3.70 and 3.72). This mode was baroclinic at the depths observed. Mode 1 contains over 86% of the variance for the u-component velocity and over 77% for the v-component velocity. This was very similar to other results of EOF analysis in the Gulf of Mexico (Nowlin et al. 2001; Cole 2008).

The second mode represents about 5% of the u-component velocity variance and almost 11% for the v-component velocity; quite a bit less than the variance in mode 1. This mode has one zero crossing, which was just shallower than 200 m in the u-component and just deeper than 200 m in the v-component velocities. This mode intensified for both velocity components as depth increased. In Figure 3.70, this mode was baroclinic to about 500 m and then remained essentially barotropic to 900 m where it started to decrease again with depth. In Figure 3.72, mode 2 increased to a maximum at about 700 m but then decreased at depths deeper than 700 m without becoming

barotropic. Earlier studies agree with these findings, in that this mode typically shows intensification with depth and contains a zero-crossing in the upper 500 m (Nowlin et al. 2001).

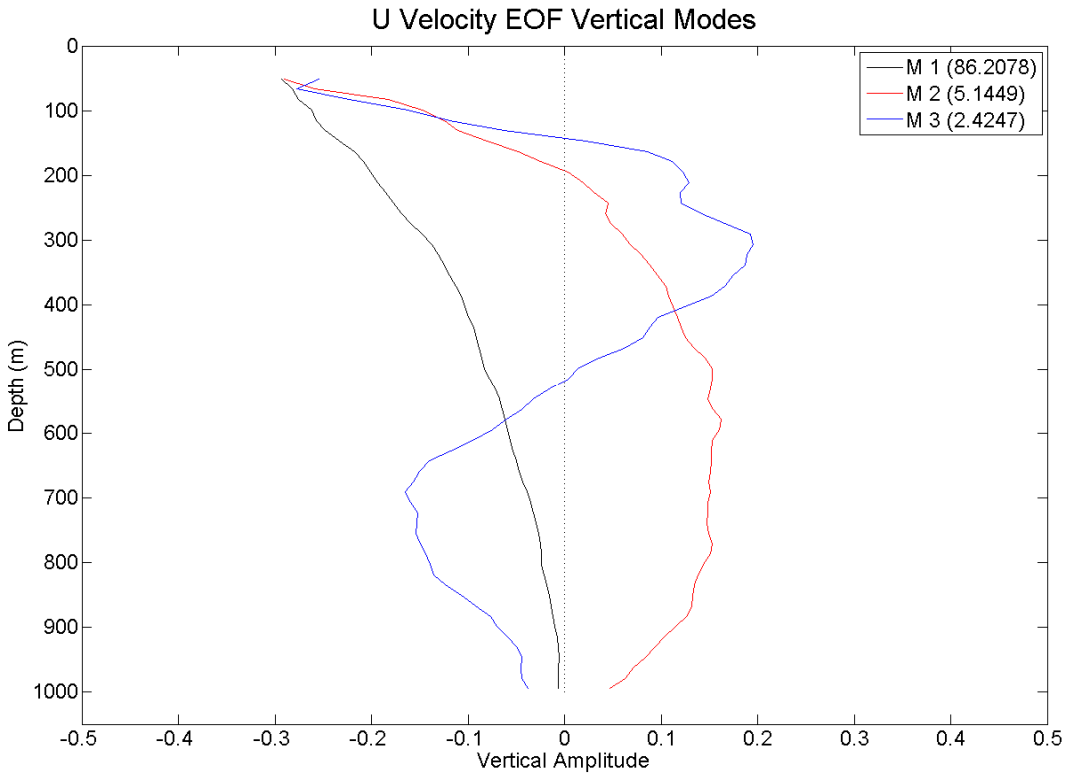

Figure 3.70 Vertical profiles of the u-component EOF vertical mode amplitudes.

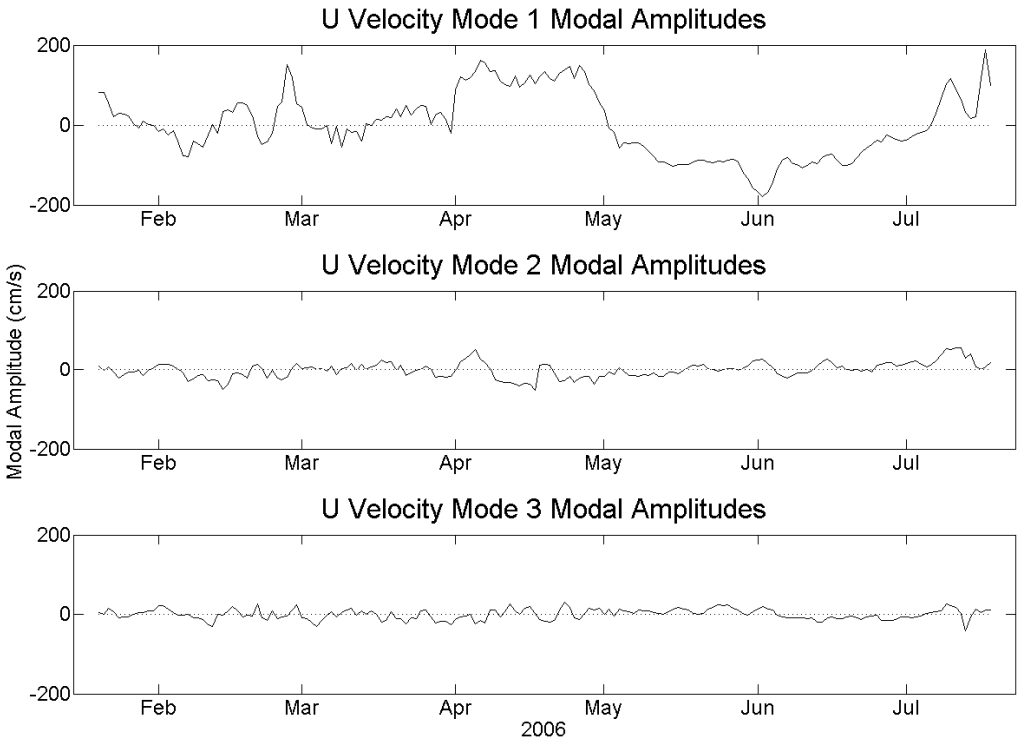

Figure 3.71 Time-series showing the u-component modal amplitudes.

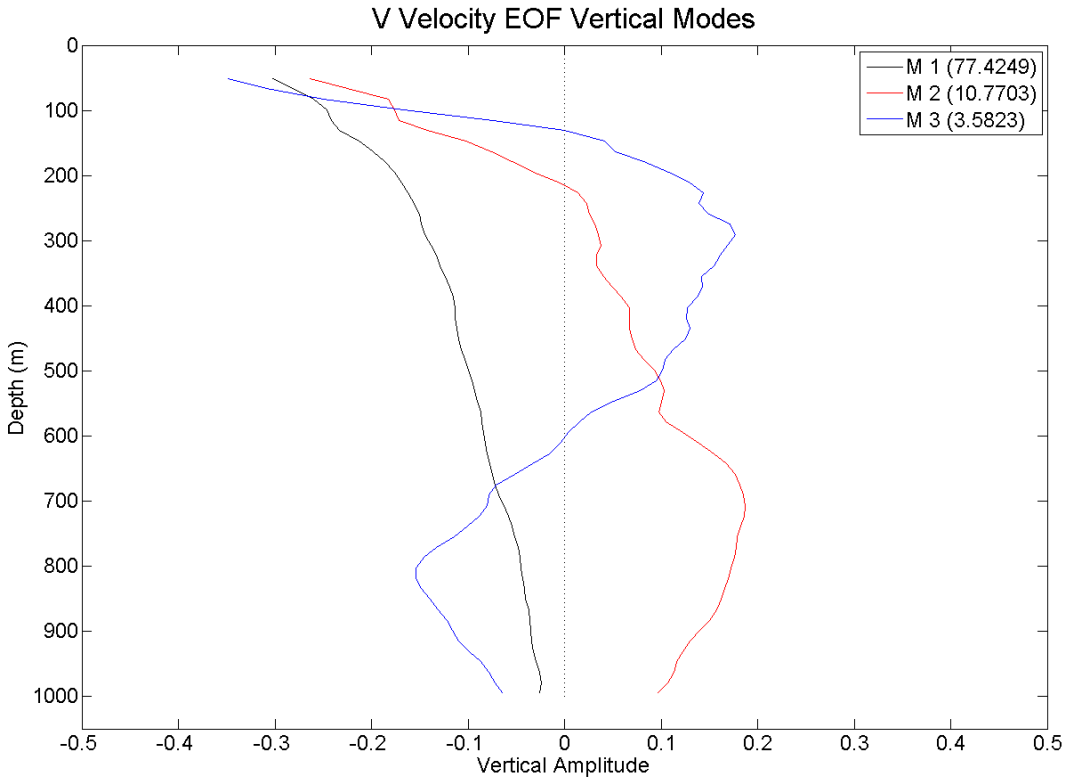

Figure 3.72 Vertical profiles of the v-component EOF vertical mode amplitudes.

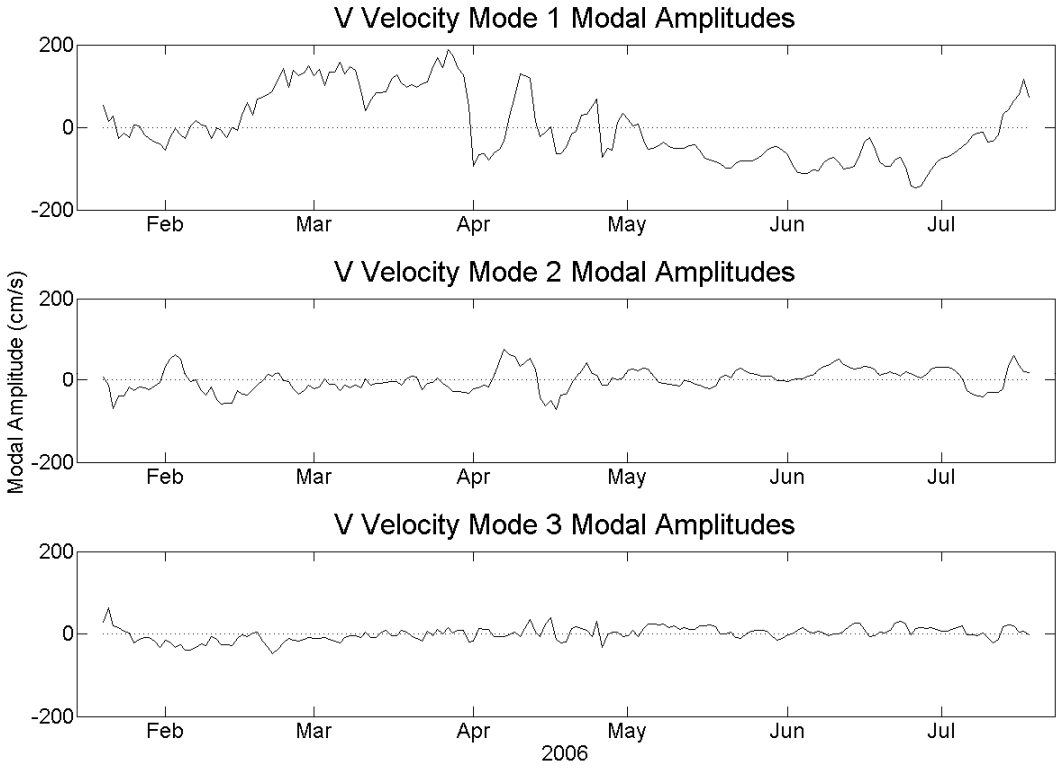

Figure 3.73 Time-series showing the v-component modal amplitudes.

The variance in mode 3 was only one-third to one-half the variance in mode 2. This mode has two zero crossings. The shallowest zero crossing occurs at about 125 m for both u- and v-velocity components, but was slightly deeper for the u-component. The deeper zero crossing was located at about 500 m in the u-component, and near 600 m in the v-component. Both u- and v-components reach maxima at about the same depths, but the second maximum was shallower for the u-component. The shallower maximum lies at about 300 m for both components. The deeper maximum was located near 700 m in the u-component and near 800 m in the v-component plots. Finding two

zero-crossings, in the upper 1000 m, in mode 3, was consistent with the analysis by Nowlin et al. 2001.

Comparing the results of the EOF analysis from the *Ocean Star* horizontal velocity data (Figure 3.70) to those from the SWSS XBT data (Figure 3.11 for example) shows some similarities. Mode 1 from the XBT analysis more closely resembles mode 2 from the horizontal velocity components because both have one zero-crossing and have similar shapes. The zero-crossing for the XBT data (~300 m) occurred about 100 m deeper than it did for the horizontal velocity component data.

Mode 2 from the XBT data and mode 3 from the horizontal velocity data both have two zero-crossings. Both zero-crossings were located slightly deeper in the horizontal velocity data than they were in the XBT data.

4. SUMMARY AND CONCLUSIONS

The current velocities observed during the 2002 and 2004 were similar in magnitude (~ 50 cm/s) and displayed more variability in direction than the currents observed during 2003 when the influence of the Loop Current was dominating the study area east of 90.5ºW. The direction of the near-surface velocity vectors reflect the mesoscale features nearby.

Stronger currents were observed in proximity to the features, such as the WSEs present during 2002 and 2004 or the Loop Current in 2003. In regions where there were no dominant SSH features present the velocity vectors tended to be more variable in direction and reduced in magnitude (50 cm/s or less).

The strongest current vectors (> 100 cm/s) recorded for all three summers were observed during the first cruise of 2003. These velocities coincided with the greatest extension of the Loop Current into the study area, and therefore its greatest influence on the currents. The strong velocities were observed as the ship transited across the Loop Current.

Throughout the second cruise of the summer in 2003, the Loop Current was retreating, and the observed currents were weaker because the Loop Current was not sampled, as it was during the first cruise of the summer when the cruise track crossed the northwestern edge of the Loop Current. The velocity vectors observed to the west of 90.5ºW, during the first cruise of 2003, were similar in magnitude and just as non-uniform in direction as the vectors observed in 2002 and 2004. The uniformity of

magnitude and direction of the vectors to the east of 90.5ºW was entirely due to the presence of the Loop Current.

A counter-current flowing along the slope was observed in several vertical velocity sections. This current was generally observed to be traveling in a down coast direction (westward or cyclonically). This current was observed in all three summers during each cruise, when the ship transited onto or off of the shelf. It was recorded in both 150-kHz and 38-kHz vertical sections and was present at all observed depths of the slope with speeds generally around 20 cm/s or less.

Vertical profiles from the XBT stations were very similar for all cruises. There was a surface summer mixed layer of about 25 m, below which the temperatures decreased with depth to about 6ºC at 760 m. Surface mixed layer temperatures were generally around 28ºC – 29ºC; the warmest surface temperatures (> 31ºC) were recorded during cruise 03G06. This wasn't surprising since this was the cruise that traversed part of the Loop Current. The similarity of temperatures observed for all three summers was evident in Figure 4.1, which shows the mean XBT temperature profiles for each cruise.

Notice that all four mean profiles intersect near 300 m. This was the approximate depth of the mean temperature for each of the mean profiles for each cruise. Mean temperatures for these mean profiles were about 13ºC. This was the same depth in the XBT EOF vertical amplitude plots at which the zero-crossing in mode 1 was to be found.

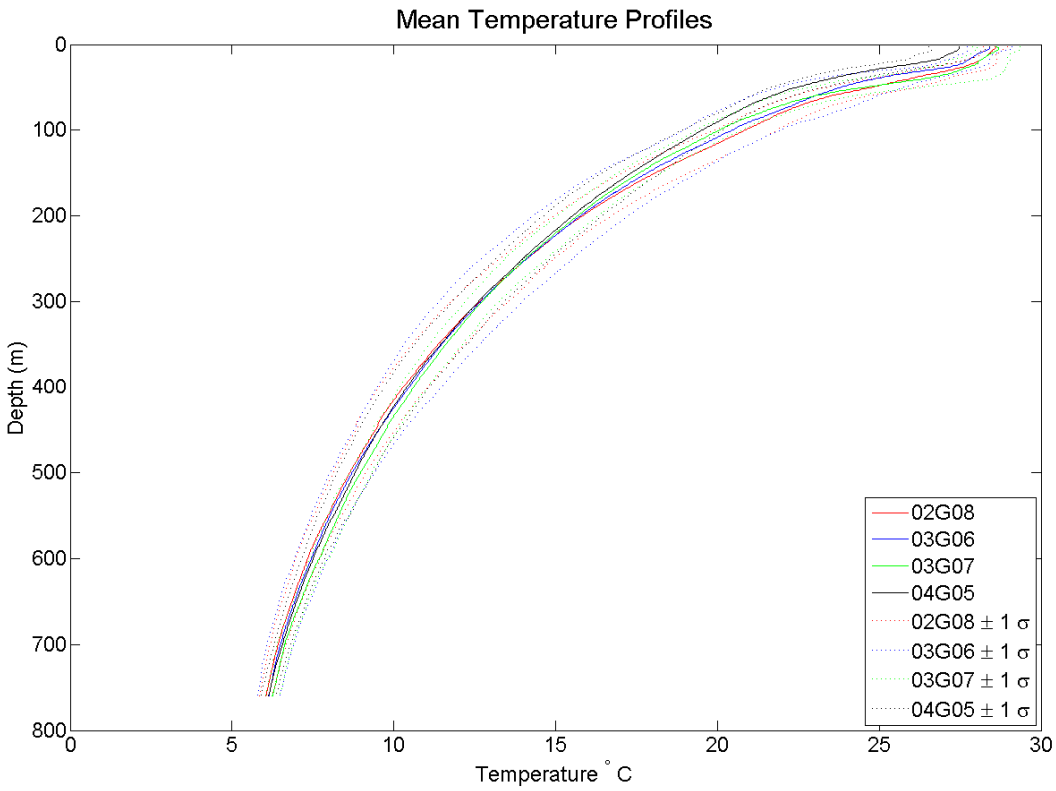

Figure 4.1 Mean temperatures calculated for all XBT stations and depths for each cruise.

The EOF vertical modes were very similar between the four cruises because the XBT temperature profiles were similar for the cruises. The greatest variance was attributed to the change of temperature with depth, and was associated with mode 1, which explained over 99% of the variance during all cruises. The temperature structure across the study area, although variable from location to location, was quite stable from year-to-year. Mode 1 was surface intensified because the temperatures there were more different from the mean temperature than those deeper, which were less variable than surface temperatures over time and from one location to another. A glance at any of the

EOF vertical mode 1 profiles will show increased variance with distance away from the zero-crossing, and the larger difference was located near the surface.

The variance captured in the second vertical mode was believed to be associated with the variability observed at different locations and was related to the different processes found at different locations. These processes were the elevation of isotherms caused by the cyclonic rotation of CSEs or the depression of isotherms caused by the anticyclonic rotation of WSEs. The displacement of isotherms (up to about 100 m) was apparent in the vertical sections of temperature and can be related to specific mesoscale features from the figures showing the locations of the XBT stations relative to the SSH field.

Because temperatures near the surface (less than 100 m) and those at depth (deeper than 450 m) were less variable with depth than those in the thermocline (between 100 m and 450 m), they will be less affected by elevation or depression of isotherms. As was clearly seen in the XBT vertical profiles, variability between individual profiles occurred between 100 m and 450 m. EOF vertical mode 2 contains variance in this depth range and the modal amplitudes for mode 2 appear to coincide with various SSH features. This could explain why the EOF vertical mode 2 zero-crossings occurred at these depths.

The few CTD profiles performed during each cruise provided evidence that Cruise 03G06 likely transited across the Loop Current as the TS-diagram plotted in Figure 3.20 for that cruise shows. The summer of 2003 was the only summer to have observed a salinity maximum greater than 36.7, which was the indicator for subtropical

underwater present in the Loop Current waters but not found in the Gulf waters. Therefore, this was an indication that cruise 03G06 likely observed the Loop Current. The few observations of salinity values higher than 36.7 during cruise 03G07 were probably residual traces as the Loop Current retreated.

Data collected from the platform-mounted instruments showed that the winds at the *Brutus* were not correlated with the currents at depths of 51 m or deeper at location of the *Ocean Star*. There was only incidental coherence between the wind current data. Velocity vectors of wind data compared to velocity vectors from the 51 m (near-surface) depth current data reinforce this result. Southerly directed winds were not reflected by southerly directed currents. This was in contrast to the hypothesis that the winds would be a determining factor on the currents, but as the data do not back that up for these depths that idea was rejected. It was possible that the influence of the wind was restricted to areas with no strong mesoscale feature present or to depths shallower than 51 m.

Record length statistics reveal that surface currents were more variable than deeper currents. As depth increased, velocities decreased to near zero below 800 m. This was about the depth as the sill in the Straits of Florida.

The importance of a local mesoscale feature on the speed and direction of the velocity vectors observed in the SWSS program data was also apparent in the time-series data. From January to May the platforms were located near the Loop Current or Loop Current eddies. Consequently, the velocity vectors and speeds were greater than they were from May through mid June when there were no strong SSH feature present at the

platform location. The influence of a shelf CSE was seen at the beginning of June but this feature was not strong enough to influence the entire water column like the Loop Current. Rather, velocity vectors showed that this influence was mostly confined to the upper 400 m, but they also show that when the Loop Current was present it influenced the velocity vectors and speed at all observed depths.

Inertial oscillations were very common in the time-series record and were particularly noticeable at depths between 250 m and 800 m. The signature of inertial currents at shallower depths might be obscured by the presence of stronger currents at those depths. Between May and mid June, when the currents were relatively weak, due to the lack of a strong mesoscale feature nearby, inertial oscillations were visible in the shallower velocity vector series.

The spectral analysis showed that most of the energy was contained in frequencies greater than fifteen days per cycle (0.05 – 0.07 cpd). There was a large peak at one cycle per day, which was associated with the inertial oscillations. This was supported by the equal energy for all depths observed for this peak.

The EOF analysis was consistent with the past work of Nowlin et al. (2001). Mode 1 was a surface intensified mode that decreased to near zero at 1000 m. Mode 2 was baroclinic above 500 m, contained a zero-crossing in the upper 500 m, and was barotropic below 500 m. Mode 3 has two zero-crossings, one near 125 m and one near 550 m, with maximum variance at 300 m and 750 m.

So the environment along the 1000 m isobath was highly variable. The depth of influence of various SSH features extend several hundred meters and these features were

not stationary with longitude. The vertical structure associated with the SSH features was different depending on the feature. Finally the fixed platform data were not wind correlated.

REFERENCES

Bunge, L., J. Ochoa, A. Badan, J. Candela, and J. Sheinbaum, 2002: Deep flows in the Yucatan Channel and their relation to changes in the Loop Current extension. *J. Geophys. Res.*, **107**(12), 1-7.

Cochrane, J. D., and F. J. Kelly, 1986: Low-frequency circulation on the Texas-Louisiana continental shelf. *J. Geophys. Res.*, **91**(C9), 10645-10659.

Cole, K. L., 2008: Low-frequency variability of currents in the deepwater eastern Gulf of Mexico. M.S. thesis, Texas A&M University, 102 pp. plus appendices.

Cox, J., C. Coomes, S. F. DiMarco, K. Donohue, G. Z. Forristall, P. Hamilton, R. R. Leben, and D. R. Watts, 2010: Technical report, exploratory study of deepwater currents in the eastern Gulf of Mexico. Gulf of Mexico OCS Region, Minerals Management Service, U.S. Dept. of the Interior, New Orleans, LA, in press.

DiMarco, S. F., M. K. Howard, W. D. Nowlin Jr., and R. O. Reid, 2004: Subsurface high-speed current jets in the deep water region of the Gulf of Mexico. OCS Study MMS 2004-022, Gulf of Mexico OCS Region, Minerals Management Service, U.S. Dept. of the Interior, New Orleans, LA, 97 pp.

Dinnel, S. P., and W. J. Wiseman, Jr., 1986: Fresh water on the Louisiana and Texas shelf. *J. Cont. Shelf Res.*, **6**, 765-784.

Donohue, K., P. Hamilton, K. Leaman, R. Leben, M. Prater, D. R. Watts, and E. Waddell, 2006: Exploratory study of deepwater currents in the Gulf of Mexico. Volume I: Executive summary. OCS Study MMS 2006-073, Gulf of Mexico OCS

Region, Minerals Management Service, U.S. Dept. of the Interior, New Orleans, LA, 186 pp.

Elliot, B. A., 1982: Anticyclonic rings in the Gulf of Mexico. *J. Phys. Oceanogr*., **12**, 1292-1309.

Emery, W. J., and R. E. Thomson, 2001: *Data analysis methods in physical oceanography*. Elsevier Science B. V., 638 pp.

Etter, P. C., 1983: Heat and freshwater budgets of the Gulf of Mexico. *J. Phys. Oceanogr*., **13**, 2058-2069.

——, M. K. Howard, and J. D. Cochrane, 2004: Heat and freshwater budgets on the Texas-Louisiana shelf. *J. Geophys. Res*., **109**(C02024), 1-23.

Gordon, R. L. 1996: *Acoustic doppler current profilers principles of operation: A practical primer.* RD Instruments, 52 pp.

Hamilton, P., 1990: Deep currents in the Gulf of Mexico. *J. Phys. Oceanogr.*, **20**, 1087-1104.

——, 1992: Lower continental slope cyclonic eddies in the central Gulf of Mexico. *J. Geophys. Res*., **97**(C2), 2185-2200.

——, 2007: Deep-current variability near the Sigsbee Escarpment in the Gulf of Mexico. *J. Phys. Oceanogr.*, **37**, 708-726.

——, A. Lugo-Fernandez, 2001: Observations of high speed deep currents in the northern Gulf of Mexico. *Geophys. Res. Lett.*, **28**(14), 2867-2870.

——, T. J. Berger, and W. Johnson, 2002: On the structure and motions of cyclones in the northern Gulf of Mexico. *J. Geophys. Res*., **107**(C12), 1-18.

Jochens, A. E., and D. C. Biggs, Eds., 2003: Sperm whale seismic study in the Gulf of Mexico; Annual report: year 1. OCS Study MMS 2003-069, Gulf of Mexico OCS Region, Minerals Management Service, U.S. Dept. of the Interior, New Orleans, LA, 139 pp.

——, ——, Eds., 2004: Sperm whale seismic study in the Gulf of Mexico; Annual report: year 2. OCS Study MMS 2004-067, Gulf of Mexico OCS Region, Minerals Management Service, U.S. Dept. of the Interior, New Orleans, LA, 167 pp.

——, ——, Eds., 2006: Sperm whale seismic study in the Gulf of Mexico; Annual report: years 3 and 4. OCS Study MMS 2006-067, Gulf of Mexico OCS Region, Minerals Management Service, U.S. Dept. of the Interior, New Orleans, LA, 111 pp.

——, and S. F. DiMarco, 2008: Physical oceanographic conditions in the deepwater Gulf of Mexico in summer 2000-2002. *J. Deep-Sea Res. II*, **55**, 2541-2554.

——, ——, D. Engelhaupt, J. Gordon, N. Jaquet, M. Johnson, R. Leben, B. Mate, P. Miller, J. Ortega-Ortiz, A. Thode, P. Tyack, J. Wormuth, and B. Würsig, 2006: Sperm whale seismic study in the Gulf of Mexico; Summary report, 2002-2004. OCS Study MMS 2006-034, Gulf of Mexico OCS Region, Minerals Management Service, U.S. Dept. of the Interior, New Orleans, LA. 352 pp.

Joyce, T. M., 1989: On in situ “calibration” of shipboard ADCPs. *J. Atmos. Oceanic Technol.*, **6**, 169-172.

Leben, R. R., G. H. Born, and B. R. Engebreth, 2002: Operational altimeter data processing for mesoscale monitoring. *Marine Geodesy*, **25**, 3-18.

Leipper, D. F., 1970: A sequence of current patterns in the Gulf of Mexico. *J. Geophys. Res*., **75**(3), 637-657.

Maul, G. A., 1977: The annual cycle of the Gulf Loop Current, part I, Observations during a one-year time series. *J. Mar. Res*., **35**, 29-47.

——, D. A. Mayer, and S. R. Baig, 1985: Comparisons between a continuous 3-year current-meter observation at the sill of the Yucatan Strait, satellite measurements of Gulf Loop Current area, and regional sea level. *J. Geophys. Res*., **90**(C5), 9089-9096.

Molinari, R. L., 1978: The relationship of the curl of the local wind stress to the circulation of the cayman sea and the Gulf of Mexico. *J. Phys. Oceanogr.*, **8**, 779-784.

——, and D. A. Mayer, 1982: Current meter observations on the continental slope at two sites in the eastern Gulf of Mexico. *J. Phys. Oceanogr.*, **12**, 1480-1492.

——, J. F. Festa, and D. W. Behringer, 1978: The circulation in the Gulf of Mexico derived from estimated dynamic height fields. *J. Phys. Oceanogr*., **8**, 987-996.

Morey, S. L., W. W. Schroeder, J. J. O'Brien, and J. Zavala-Hidalgo, 2003: The annual cycle of riverine influence in the eastern Gulf of Mexico basin. *Geophys. Res. Lett.*, **30**(16), 1867, doi:10.1029/2003Gl017348.

Morrison, J. M., and W. D. Nowlin, Jr., 1977: Repeated nutrient, oxygen and density sections though the Loop Current. *J. Mar. Res.*, **35**, 105-128.

——, W. J. Merrell, Jr., R. M. Key, and T. C. Key, 1983: Property distributions and deep chemical measurements within the western Gulf of Mexico. *J. Geophys. Res*., **88**(C4), 2601-2608.

Murphy, D. J., D. C. Biggs, and M. L. Cooke, 1992: Mounting and calibrating an acoustic doppler current profiler, *MTS Journal*, **26**, 34-38.

NDBC, cited 2009: Technical document 09-02, handbook of automated data quality control checks and procedures. [Available online at http://www.ndbc.noaa.gov/handbook.pdf.]

NDBC, cited Feb., 2010: Photograph of *Brutus* tension leg platform. [Available online at http://www.ndbc.noaa.gov/station_page.php?station=42362.]

Nowlin, W. D., Jr., A. E. Jochens, S. F. DiMarco, R. O. Reid, and M. K. Howard, 2001: *Deepwater physical oceanography reanalysis and synthesis of historical data: synthesis report*. OCS Study MMS 2001-064, Gulf of Mexico OCS Region, Minerals Management Service, U.S. Dept. of the Interior, New Orleans, LA. 528 pp.

——, ——, ——, ——, ——, 2005: Low-frequency circulation over the Texas-Louisiana continental shelf. *Circulation in the Gulf of Mexico: Observations and models, Geophys. Monogr*., Vol. 161, Amer. Geophys. Union, 219-240.

——, D. F. Paskausky, and H. J. McLellan, 1969: Recent dissolved-oxygen measurements in the Gulf of Mexico deep waters. *J. Mar. Res.*, **27**, 39-44.

Ohlmann, J. C., P. P. Niiler, C. A. Fox, and R. R. Leben, 2001: Eddy energy and shelf interactions in the Gulf of Mexico. *J. Geophys. Res*., **106**(C2), 2605-2620.

——, ——, 2005: Circulation over the continental shelf in the northern Gulf of Mexico. *Progress in Oceanography*, **64**, 54-81.

Pond, S., and G. L. Pickard, 2000: *Introductory Dynamical Oceanography*. Pergamon Press Ltd, 329 pp.

Rigzone, cited Feb., 2010: Photograph of *Ocean Star* mobile offshore drilling unit. [Available online at http://www.rigzone.com/data/rig_detail.asp?rig_id=601.]

Shay, L. K., A. J. Mariano, S. D. Jacob, and E. H. Ryan, 1998: Mean and near-inertial ocean current response to hurricane Gilbert. *J. Phys. Occeanogr*., **28**, 858-889.

Sheinbaum, J., J. Candela, A. Badan, and J. Ochoa, 2002: Flow structure and transport in the Yucatan Channel. *Geophys. Res. Lett.*, **29**(3), 1-4.

Sturges, W., 1993: The annual cycle of the western boundary current in the Gulf of Mexico. *J. Geophys. Res*., **98**(C10), 18053-18068.

——, and R. Leben, 2000: Frequency of ring separations from the Loop Current in the Gulf of Mexico: A revised estimate. *J. Phys. Oceanogr.*, **30**, 1814-1819.

Vukovich, F. M., 1986: Aspects of the behavior of cold perturbations in the eastern Gulf of Mexico: A case study. *J. Phys. Oceanogr.*, **16**, 175-188.

——, and G. A. Maul, 1985: Cyclonic eddies in the eastern Gulf of Mexico. *J. Phys. Oceanogr.*, **15**, 105-117.

Wessel, P. and W. H. F. Smith, 1998: New, improved version of the Generic Mapping Tools released, EOS Trans. AGU, 79, 579.

Wiseman, W. J. Jr., and S. P. Dinnel, 1988: Shelf currents near the mouth of the Mississippi River. *J. Phys. Oceanogr.*, **18**, 1287-1291.

Zavala-Hidalgo, J., S. L. Morey, and J. J. O'Brien, 2003: Cyclonic eddies northeast of the Campeche Bank from altimetry data. *J. Phys. Oceanogr.*, **33**, 623-629.

VITA

Name: Michael Alan Lalime

Address: Department of Oceanography
Texas A&M University
College Station, TX 77843-3146

Education: B.S., Oceanography, Hawaii Pacific University, 1999
M.S., Oceanography, Texas A&M University, 2010